18th YGES2026

18TH YOUNG GEOTECHNICAL ENGINEERS SYMPOSIUM

22-23 June 2026

Imperial College London



IMPERIAL

BGA
• THE BRITISH •
GEOTECHNICAL
ASSOCIATION

Proceedings of the
18th Young Geotechnical Engineers Symposium

YGES2026

22-23 June 2026

Imperial College London

London, UK

Edited by

Katerina Tsiampousi,

Francesca Palmieri,

Dariel Hernández Delfin,

Hao Wang, and

Si Suo

IMPERIAL

BGA
• THE BRITISH •
GEOTECHNICAL
ASSOCIATION

How to Cite:

Tsiampousi, K., Palmieri, F., Hernández-Delfin, D., Wang, H. & Suo, S. (eds.) (2026) *Proceedings of the 18th Young Geotechnical Engineers Symposium (YGES2026), 22-23 June 2026, London, UK*. London: Imperial College London.

DOI: https://doi.org/10.25560/131150

Organising Committee

Katerina Tsiampousi, Imperial College London

Francesca Palmieri, Imperial College London

Dariel Hernández Delfin, Imperial College London

Hao Wang, Imperial College London

Si Suo, Imperial College London

Session Chairs

Angela Casarella, Imperial College London

Catherine O'Sullivan, Imperial College London

Domniki Asimaki, Imperial College London

Marcelo Sanchez, Imperial College London

Pishun Tantivangphaisal, Imperial College London

Richard Jardine, Imperial College London

Invited Keynote Speakers

Dr. Natalie Wride

Mott MacDonald

Keynote Lecture: Back to Basics for not so Basic Cases

Dr. Ken Vinck

Imperial College London

Keynote Lecture: Chalk Characterisation for Driven Pile Behaviour at Chalk Sites

The Organising Committee would like to thank our colleagues for chairing the technical sessions, our keynote speakers for delivering their inspiring keynote lectures, and our volunteers, Dr Maryam Sadat Maddah Sadatieh and Mr Pedja Tosovic, for their invaluable assistance.

Foreword

The extended abstracts in these proceedings were presented at the 18th British Geotechnical Association Young Geotechnical Engineers' Symposium (YGES2026), held at Imperial College London from 22-23 June 2026.

The BGA Young Geotechnical Engineers Symposia provide an excellent opportunity for postgraduate students, researchers and early-career geotechnical engineers to present their latest research and discuss current challenges in geotechnical engineering. The symposium offers a welcoming forum in which participants can exchange ideas, receive constructive feedback and build professional relationships in an informal and collaborative atmosphere. For many delegates, YGES represents their first major conference and an important milestone in their research careers.

The contributions presented at YGES2026 demonstrate the breadth and quality of contemporary geotechnical engineering research and practice. The proceedings include studies covering laboratory testing, field investigations, numerical modelling, analytical methods and data-driven approaches, addressing topics such as soil behaviour, foundations, geoenvironmental engineering, transportation infrastructure, offshore geotechnics and sustainable engineering solutions. Together, these contributions highlight the innovation, diversity and enthusiasm of the next generation of geotechnical engineers and their commitment to advancing both research and professional practice.

The organising committee was delighted to recognise outstanding contributions through the symposium awards. The Best Presentation Award was presented to Sarah Irvine, and the Outstanding Presentation Awards were presented to Benedek Nagy, Rayn Chia, and Javier Sánchez Fernández. We warmly congratulate the award recipients for their excellent work.

The organising committee was honoured to host the 18th YGES at Imperial College London. The success of the symposium is owed to all delegates for their enthusiastic participation and engaging technical discussions. We are sincerely grateful to our session chairs for their professionalism in facilitating the technical sessions, and to our keynote speakers, Dr Natalie Wride and Dr Ken Vinck, for delivering inspiring lectures that greatly enriched the symposium.

Finally, we would like to thank the British Geotechnical Association for its continued support of the Young Geotechnical Engineers' Symposium series, volunteers and colleagues whose dedication and hard work made the event possible. We hope that these proceedings will serve as a valuable record of the symposium and encourage continued collaboration and innovation within the geotechnical engineering community.

Katerina Tsiampousi, Francesca Palmieri, Dariel Hernández Delfin, Hao Wang, and Si Suo

London, June 2026

Table of Contents

Fundamentals of Soil Behaviour

Exploring the stability of granular metamaterials for soil stabilisation applications
S. Irvine, V. Angelidakis 3

Rate of primary consolidation behaviour of kaolinite under chemically active pore fluids
K. Adebayo, K. Vinck, A. Casarella, and C. O' Sullivan 5

Thermal volumetric behaviour of clays
A. Khare, T. Le, T. A. V. Gaspar and L. Zdravković 7

Rethinking glacial till: brittle and contractive response under critical state testing
L. Souza, F. W. Barra and Tom Shire 9

Simulating the water retention curves for hydrophobic granular soils
T. Zhao, M. Sutman and C. Beckett 11

A low-cost automated apparatus for measuring water entry pressure
Q. Zhang and G. El Mountassir 13

Offshore Geotechnics

Drilled and grouted pile/anchor design for offshore renewable energy: interface shear behaviour from direct shear box tests
O. Deniz, H. Burd 17

Numerical modelling of shared anchor piles for floating offshore wind turbines
A.R. Bin Bahri, L. Cui and S. Bhattacharya 19

Monotonic lateral loading of monopiles in sandy soils, considering drainage effects
R.W.L Chia, C.M. Martin, O. Adamidis, H.J. Burd 21

Development of practical geotechnical design tools for offshore wind turbine foundations subject to cyclic loads
C. Hin, Chin. and P. Tantivangphaisal. 23

Calibration of Low-Cost Soil Moisture Sensors for Accurate Measurement of Water Content in High Plasticity Clay
X. Z. Wu, Joel A. Smethurst and K. M. Briggs 25

Long-term deformation mechanisms of monopile foundation in sand under cyclic lateral loading of different symmetries
L.L.K. Hung-Lo-Sang, J. Wang, C.M. Heron, A. Pettey and A.M. Marshall 27

Soil-Structure Interaction

A state variable formulation of LeBlanc's model for cyclic loading
M. E. Rasmussen, B. W. Byrne and H. J. Burd 31
An experimental framework for assessing soil reactions acting on laterally loaded monopile segments
J. M. Han, H. Burd, V. Nardelli, and M. Saberi 33
First principles approach for calculating axial and bending loads from strain measurements in laterally loaded piles
F. Van der Berg, K. Briggs, W. Powrie, and J. Smethurst 35
Investigating re-entrant corners in braced excavations
A. Chai, C. E. Augarde, W. M. Coombs and M. Ouyang 37
Numerical modelling of scour effects on pile group supported bridges
A.Al-Karawi, L. J. Prendergast and N. Thom 39
Numerical modelling and validations on artificial ground freezing under groundwater flow condition
G. Go 41

Data-Driven and AI-Based Approaches

Predicting PFAS transport through landfill composite liner using physics-informed neural networks
Y. Tan and Y. Feng 45
Applying surrogate models to predict tunnelling-induced building settlements
J. Liu, A. Tsiampousi, A. Ruiz López and D.M.G. Taborda 47
Prediction of thermo-active pile group response from single-pile surrogate models
J. Sánchez Fernández, A. Ruiz López and D.M.G. Taborda 49
GPU-accelerated 3D finite element analysis of monopile foundations with SANISAND-MS
M.R.F. Bowman, H. J. Burd and W. Armour 51

Experimental Characterisation and Site Investigation

Heat transfer in saturated sand: insights from centrifuge experiments
D.M.P.J., E.T. Bowman and T.A.V. Gaspar 55

Investigating climate-induced failure mechanisms in UK coastal cliffs
P. J. Schoeman, T. A. V. Gaspar, L. Zdravkovic, J. Standing 57

Particle crushing in glauconitic sand under cyclic CPTu loading
A. Rodríguez Piedrabuena, D. A. de Lange, M. Mento and M. Konstantinou 59

Extending the capabilities of suction monitored unconfined compression apparatus with digital image correlation
B. Nagy, G. El Mountassir and A. Tarantino 61

Numerical Methods and Computational Geomechanics

Revisiting shear history in DEM: limitations of accumulating shear displacement compared with accumulating shear force
Y. H. Leung, D. Hernández-Delfin, D. M. G. Taborda, Catherine O'Sullivan 65

Implicit sub-stepping scheme for Critical State soil models
H. Bui and J. Ninic 67

Salinity effects on the behaviour of swelling clays: a double-structure approach to Chemo-Hydro-Mechanical (CHM) coupling
H.M. Lai, L. Zdravkovic, D. M. Potts and M. Kirby 69

Automated calibration of coarse-grained DEM models for large displacement simulations.
A. Tottle, L. Cui and J. Sagaseta 71

Comparison of mualem and burdine hydraulic conductivity models in a 1-D unsaturated soil column simulation
Q.H.X. Kong, C. O'Sullivan, K. Tsiampousi and H. Wang 73

An assessment of different methods for quantifying the thermal performance of thermo-active foundations
A. Provost, P. Sapin and D. M. G. Taborda 75

Sustainability and Engineering Applications

Sustainable reuse of historic masonry as engineered fill in the fore gill bridge rebuild
C. Walker and M.L. Walker 79

Short-term structural response of a model shaft liner during shaft breakout in clay
M. Ucur, S. Divall and S.E. Stallebrass 81

Reducing Tunnel Volume Loss Using Data Processing Techniques
R. Limbu, S. Divall and S.E. Stallebrass 83

Fundamentals of Soil Behaviour

Exploring the stability of granular metamaterials for soil stabilisation applications

Sarah Irvine*[1], Vasileios Angelidakis[1]
[1] School of Natural and Built Environment, Queen's University Belfast, Stranmillis Road, Belfast, Northern Ireland, BT9 5AG
(E-mail: sirvine26@qub.ac.uk, v.angelidakis@qub.ac.uk)

Abstract

Granular Metamaterials are engineered materials composed of discrete particles, with abilities to exhibit unique mechanical properties, not typically observed in naturally occurring granular materials. One of these properties is geometric cohesion, a type of bulk-scale apparent cohesion that emerges from the intense interlocking of cohesionless, highly non-convex, engineered particle morphologies. Systems exhibiting geometric cohesion can form mechanically stable, free-standing structures with nearly vertical angles of repose, whereas natural dry granular soils typically feature repose states of lower angles, around 20-40 degrees. This presents the opportunity to use these metamaterials as additives to granular soils to enhance their mechanical response, for the purpose of soil stabilisation. This study presents numerical investigations into the behaviour of assemblies made of granular metamaterials using the Discrete Element Method (DEM), with a focus on their Angle of Repose (AoR) as a measure of bulk-scale stability.

Introduction

Achieving reliable and consistent stability of granular soils is crucial for the design of resilient infrastructure. The continuous rise in demand for infrastructure means it is becoming increasingly necessary to use areas of land previously considered too weak for building use [1]. Hence, these sites will need to be subjected to soil stabilisation. There is no single governing principle when it comes to soil stabilisation. Highly site-specific techniques are employed, which depend on a soil's unique mechanical composition. Familiar techniques include initial conditioning achieved through drainage, compaction or pre-consolidation, chemical stabilisation and mechanical stabilisation through vertical rigid inclusions and geosynthetics.

However, many of these techniques come with a significant carbon footprint, and there is now a pressing need to implement solutions which are environmentally conscious. Additionally, climate-related changes pose a growing threat to soil stability and the longevity of buried infrastructure, and this must be considered when designing the next generation of soil stabilisation techniques. For instance, environmental loading has been shown to induce cyclic stresses on soils, governing a shrink-swell behaviour [2], having detrimental impacts, and new stabilisation techniques are sought to mitigate this.

Granular metamaterials are an emerging class of artificial materials with extraordinary mechanical properties. Their usage finds interdisciplinary applications across fields studying granular mechanics, such as Physics, Mechanical Engineering, Architecture, and Material Science [3, 4], due to their unusual mechanical properties, achieved not just by material composition but by particle geometry and contact topology. This study explores the properties of granular metamaterials, with the scope to use them as a novel soil improvement technique, via mixing natural soils and granular metamaterials particles.

Methodology

The stability of systems made of granular metamaterials is explored via simulations using the Discrete Element Method (DEM) and the YADE open-source software [5]. Complex metamaterial particles are created as multipods with varying numbers of arms, as shown in Figure 1, which feature variable morphological features e.g. in terms of sphericity. These particles are simulated in YADE as flexible grids composed of sphero-cylinders. Simulations are conducted by inserting

particles periodically above a hollow cylindrical container and allowing them to settle under gravity. Following filling of the cylinder, the particle arrangement is either vibrated or compressed, with aims to densify the packing. The system constraints are then removed allowing a stable repose state to form. The final Angle of Repose (AoR) is measured as well as the evolution of interparticle forces, orientations, and contacts, over time. Here, the AoR is employed as a simplistic and repeatable test to quantitively assess the bulk stability and behavioural patterns of Granular Metamaterials, where more stable configurations feature higher AoR values.

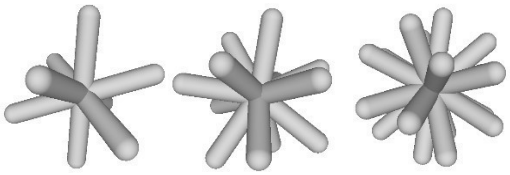


Figure 1: Granular metamaterial particles.

Results

Preliminary results indicate that particle morphology plays a dominant role in governing the macroscopic response of granular packings made of these complex particles. Figure 2 illustrates that particles with higher sphericity consistently exhibit lower AoR values, reflecting limited interlocking between particles and enhanced bulk mobility.

Insights into the underlying micromechanical behaviour are obtained through evaluation of coordination number, fabric anisotropy, mean contact force and mean normal deformation. Such parameters provide a direct link between particle-particle scale interactions and the emerging bulk response of the system; this forms a basis for shape optimization. Additionally, the system response is also strongly governed by the sample preparation protocol, which defines a granular packings history.

Conclusions and future work

Our findings indicate that interparticle friction and particle morphology dominate the emergence of geometric cohesion in AoR simulations of granular metamaterials. The results show a linear scaling of the AoR with particle sphericity, which may allow for the design of these systems in the future. More work is required to establish the dominant parameters which control the onset of this phenomenon more comprehensively.

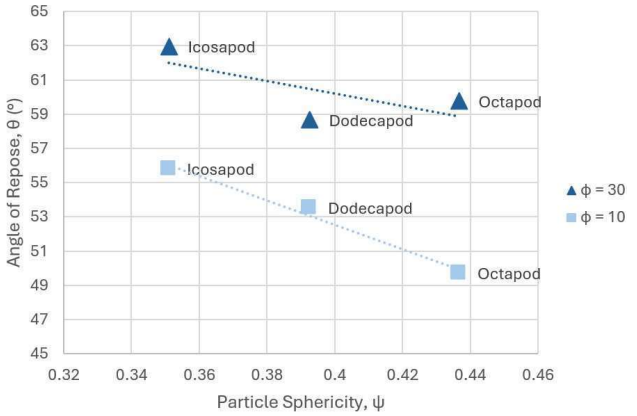


Figure 2: AoR of assemblies with varied sphericities ψ, and interparticle friction angles.

Understanding the behaviour of granular metamaterials via bridging microscale properties to macroscale response creates the basis for extending investigations to mixed assemblies of granular metamaterials with natural soils and allows for the effectiveness of these particles as mechanical additives to be systematically quantified. This creates the foundation for future numerical and experimental work to explore how engineered particles can be designed as a novel ground improvement technique.

References

[1] Obolewicz, J. and Wadolowska, E. (2019), Modern Engineering, Volume 2, pp. 94–102.

[2] Sivakumar, V. , Tan, W. C. , Murray, E. J., McKinley, J. D. (2006), Géotechnique, Volume 56(1), pp. 57–62.

[3] Dierichs, K. and Menges, A. (2016), Granular Matter, Volume 18(25).

[4] Aponte, D., Barés, J., Renouf, M., Azéma, E. and Estrada, N., (2025), Granular Matter, 27(1), p.27.

[5] Angelidakis, V., Boschi, K., Brzeziński, K., Caulk, R.A., Chareyre, B., et al. (2024), Computer Physics Communications, 304, 109293.

Rate of primary consolidation behaviour of kaolinite under chemically active pore fluids

Kabiru Adebayo*[1], Ken Vinck[2], Angela Casarella[3], and Catherine O'Sullivan[4]
[1 – 4] Department of Civil and Environmental Engineering, Imperial College London, The United Kingdom of Great Britain and Northern Ireland
(E-mail: k.adebayo24@imperial.ac.uk, ken.vinck15@imperial.ac.uk, a.casarella@imperial.ac.uk, cath.osullivan@imperial.ac.uk)

Abstract

This study examines the rate of primary consolidation of kaolinite under chemically active pore fluids using one-dimensional consolidation tests. Speswhite kaolin specimens were sedimented in NaCl solutions at concentrations of 0.1, 0.2, and 0.6 M to develop different initial fabrics. Consolidation behaviour was evaluated up to stress levels of about 900 kPa, with coefficients of consolidation determined using Taylor's square-root-of-time method. Results indicate that increasing the NaCl concentration moderately enhances the rate of primary consolidation at all the stresses.

Introduction

Consolidation of clay soils is traditionally treated as a hydro-mechanical process controlled by compressibility and permeability. However, physicochemical interactions and pore fluid chemistry can significantly influence soil fabric and drainage behaviour, particularly at low effective stresses [1,2]. Electrolyte concentration alters electrical double layer thickness and interparticle forces, affecting particle arrangement and pore structure.

Previous studies have shown that salinity can modify clay compressibility and permeability, especially in the normally consolidated stress range [3,4]. Although chemical effects on consolidation are expected to diminish with increasing stress due to fabric collapse and contact-force dominance [5], their influence on the rate of primary consolidation remains poorly understood. This study investigates how electrolyte concentration affects the primary consolidation behaviour of kaolinite and how these effects evolve with applied stress.

Methodology

One-dimensional consolidation tests were performed on Speswhite kaolin sedimented from RO water and NaCl solutions (0.1–0.6 M) to generate different initial fabrics. Specimens were then consolidated under stresses of 113–897 kPa.

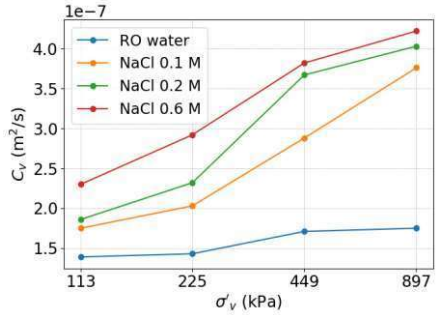
Settlement–time responses were recorded during each loading stage to evaluate primary consolidation behaviour. The coefficient of consolidation, c_v, was determined using Taylor's square-root-of-time method, expressed as $c_v = \frac{T_{90} H_d^2}{t_{90}}$ where T_{90} is the dimensionless time factor corresponding to 90% consolidation (typically 0.848), H_d is the maximum drainage path, and t_{90} is the time required to reach 90% primary consolidation.

Results

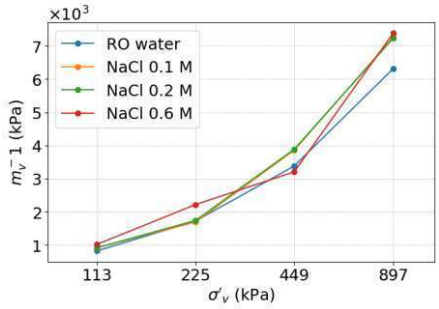
Figure 1 shows the variation of c_v and m_v^{-1} with effective vertical stress (σ_v') for Speswhite kaolin prepared with RO water and NaCl solutions. For all pore-fluid conditions, both parameters increased with stress, indicating progressive stiffening of the soil skeleton. Across the tested stress range, specimens prepared in saline solutions exhibited higher c_v values than those prepared in RO water, with c_v increasing with electrolyte concentration. This behaviour is consistent with salinity-induced fabric modification, whereby reduced double-layer repulsion promotes a more open fabric and higher permeability [3–5].

The values of m_v^{-1} were broadly similar for all pore-fluid conditions at a given stress. Since $c_v \propto k/m_v$, the higher c_v values for saline specimens suggest increased permeability resulting from salinity-induced fabric changes. The observed increase in c_v with stress

agrees with reported behaviour for low-activity clays such as kaolinite and contrasts with the decreasing c_v-stress trends often reported for montmorillonite and bentonite [6,7].



(a)



(b)

Figure 1: Variation of (a) coefficient of consolidation, c_v, and (b) constrained modulus, $m_v{}^{-1}$, with effective vertical stress, σ'_v, for Speswhite kaolin prepared in RO water and NaCl solutions.

Conclusions and future work

This study has explored the variation in both the $\boldsymbol{c_v}$ and $\boldsymbol{m_v{}^{-1}}$ by considering data from 1D oedometer tests on Speswhite kaolin consolidated with both saline pore fluids and water treated with reverse osmosis. Both $\boldsymbol{c_v}$ and $\boldsymbol{m_v{}^{-1}}$ increased with increasing $\boldsymbol{\sigma'_v}$ for all pore fluid chemistries considered. At a given $\boldsymbol{\sigma'_v}$ value, $\boldsymbol{c_v}$ increases with increasing salt concentration. As $\boldsymbol{m_v{}^{-1}}$ shows limited sensitivity to the pore fluid conditions, differences in consolidation response are inferred to be primarily controlled by permeability. Further work requires direct measurement of hydraulic conductivity, combined with microfabric characterisation, to assess the influence of electrolyte concentration on soil structure and its evolution under loading.

Acknowledgements

This research is funded by the Petroleum Technology Development Fund (PTDF), Nigeria (Award ID: 24PHD0021).

References

[1] Mitchell, J. K., & Soga, K. (2005). Fundamentals of Soil Behavior. John Wiley & Sons.

[2] Marcus, Y. (1988). Ionic radii in aqueous solutions. *Chemical Reviews*, *88*(8), 1475–1498. https://doi.org/10.1021/cr00090a003

[3] Ma, X., Xia, Z., Su, C., Cheng, Y., Yu, H., & Kang, X. (2023). Quantitative Evaluation of the Effects of Salt Concentration and pH on the Self-Assembly of Kaolin Nanoplatelets. *Langmuir*, *39*(41), 14500–14510. https://doi.org/10.1021/acs.langmuir.3c01394

[4] Yin, J., Lu, Z., Geng, W., Han, W., & Hudu, A. A. (2021). Effect of porewater salinity on compression behaviors and hydraulic conductivity of soft marine clay. *Marine Georesources & Geotechnology*, *40*(7), 813–822. https://doi.org/10.1080/1064119x.2021.1941451

[5] Pedrotti, M., & Tarantino, A. (2018). An experimental investigation into the micromechanics of non-active clays. *Géotechnique*, *68*(8), 666–683. https://doi.org/10.1680/jgeot.16.p.245

[6] Robinson, R. G. & Allam, M. M. (1998). Effect of Clay Mineralogy on Coefficient of Consolidation. *Clays and Clay Minerals*, *46*(5), 596–600. https://doi.org/10.1346/ccmn.1998.0460514

[7] Samarasinghe, A. M., Huang, Y. H., & Drnevich, V. P. (1983). Closure to " *Permeability and Consolidation of Normally Consolidated Soils* " by A. Mahinda Samarasinghe, Yang H. Huang, and Vincent P. Drnevich (June, 1982). *Journal of Geotechnical Engineering*, *109*(6), 878–882. https://doi.org/10.1061/(asce)0733-9410(1983)109:6(878)

Thermal volumetric behaviour of clays

Adhyatma Khare*[1], Truong Le[2], T. A. V. Gaspar[3] and Lidija Zdravković[4]
[1, 3, 4] Department of Civil and Environmental Engineering, Imperial College London, United Kingdom
(E-mail: a.khare24@imperial.ac.uk, t.gaspar@imperial.ac.uk, l.zdravkovic@imperial.ac.uk)
[2] Mott MacDonald, United Kingdom
(E-mail: truong.le@mottmac.com)

Abstract

Growing interest has been directed towards the thermo-hydro-mechanical behaviour of saturated soils, driven by an increasing number of geomechanical problems associated with the complex nature of heat transfer in soils. This paper presents the results from two bulk modulus tests on saturated kaolin clay specimens at 50 °C and 70 °C. These preliminary results indicate that higher temperatures induce thermal volumetric strain in kaolin clay, however, the bulk modulus may remain largely unaffected by temperature changes.

Introduction

In recent years, considerable attention has been directed towards the thermo-hydro-mechanical (THM) behaviour of saturated soils. This interest is driven by geomechanical challenges associated with increasingly complex geotechnical infrastructure involving heat transfer in the ground, key examples include ground source energy systems, high-level radioactive waste disposal, and buried high-voltage cables [1,2,3]. In such systems, thermal loading can induce significant volumetric strains. However, the magnitude and nature of these strains are governed by a range of factors, including soil mineralogy, stiffness, and thermal and mechanical loading history, making it challenging to isolate and quantify the effects of temperature.

Currently a wide range of experimental studies exists on the influence of temperature on soil behaviour providing extensive insight into strength, pore water pressure changes, consolidation, permeability, and the interactions among these factors under varying thermal conditions [3,4]. The bulk modulus of the soil is one of key parameters that is usually not evaluated in experimental studies. It is, however, an essential parameter in constitutive models used for predicting volumetric deformation in soil under mechanical and / or thermal loading. This paper presents preliminary results on the evolution of the bulk modulus in saturated kaolin clay at 50 ˚C and 70 ˚C. These experiments are part of a wider research study into the THM response of clays and sands and their mixes.

Methodology

Reconstituted kaolin specimens were prepared by mixing dry kaolin powder with deionised water to form a slurry at a moisture content of 1.25 times the liquid limit, to achieve sufficiently low viscosity to minimise entrapped air and ensure a homogeneous mixture. After mixing and allowing the sample to equilibrate for 24 hours, the slurry was consolidated in a large consolidometer for three weeks at an effective stress of 200 kPa to form a clay ‘cake’, from which 50x100mm specimens were carved for testing in a temperature controlled triaxial cell.

Advanced thermo-hydro-mechanical testing paths were adopted to investigate soil behaviour under thermo-mechanical loading, as shown in Figure 1. First, a mean effective stress of 10 kPa was applied at a temperature of 22 °C (Path 0 → 1), resulting in an overconsolidation ratio (OCR) of 20.

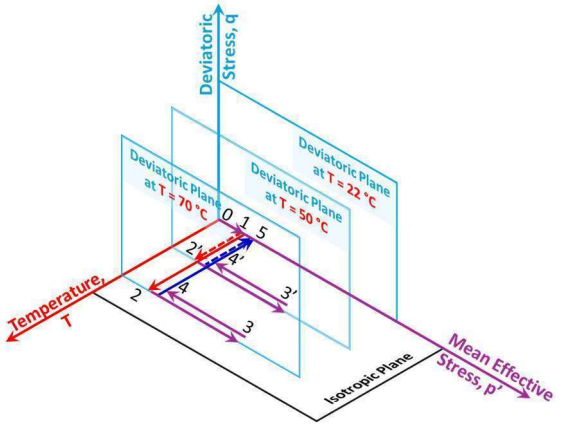


Figure 1: Thermo-hydro-mechanical testing paths

Drained isotropic heating (Paths 1 → 2 and 1 → 2') was then applied at a rate of 1 °C/h, following Chen [1], to avoid the generation of excess pore water pressure. Isotropic mechanical loading (Paths 2 → 3 and 2' → 3') and unloading was then applied at constant temperatures (Paths 3 → 4 and 3' → 4') resulting in an OCR of 1.3.

Results

Under drained conditions at constant mean effective stress (p′), an increase in temperature induces thermal volumetric strain. The results indicate that kaolin specimens exhibited thermal expansion when heated from 22-50 °C and 22-70 °C, with dilation becoming increasingly pronounced at the higher temperature, indicating strong temperature-dependency of strain development. This behaviour is attributed to the specimen's stress history [4,5].

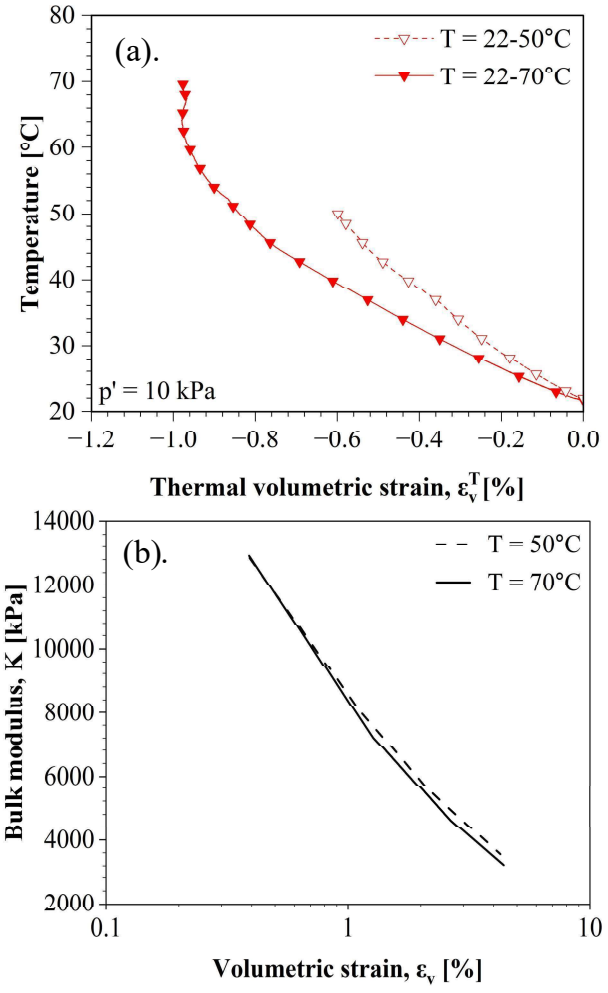


Figure 2: (a) Volumetric strain of kaolin during heating from 22 °C to 50 °C and 70 °C; (b) bulk modulus test results at 50 °C and 70 °C.

In contrast, the bulk modulus showed only minor variation with temperature, suggesting that the stiffness of the material may not be as sensitive to temperature changes.

Future work

Further planned experiments on soil mixes will contribute a broader understanding of the THM soil response.

References

[1] Chen, S., (2022). Thermo-hydro-mechanical characterisation of London clay. PhD Thesis, Imperial College London.

[2] Gawecka, K.A., (2017). Numerical Analysis of Geothermal Piles. PhD Thesis, Imperial College London.

[3] Abuel-Naga, H.M., Bergado, D.T., and Lim, B.F. (2007). Effect of Temperature on Shear Strength and Yielding Behavior of Soft Bangkok Clay, Soils and Foundation. Volume 47 (3), pp. 423–436.

[4] Cekerevac, C., and Laloui, L. (2004). Experimental study of thermal effects on the mechanical behaviour of a clay. International Journal for Numerical and Analytical Methods in Geomechanics, Volume 28 (3), pp. 209–228.

[5] Abuel-Naga, H.M., Bergado, D.T., Bouazza, A., and Ramana, G.V. (2007). Volume change behaviour of saturated clays under drained heating conditions: experimental results and constitutive modeling. Canadian Geotechnical Journal, Volume 44 (8), pp. 942–956.

Rethinking glacial till: brittle and contractive response under critical state testing

Luciano Souza*[1], Fernanda Wamser Barra[1] and Tom Shire[1]
[1] Klohn Crippen Berger, United Kingdom
(lsouza@klohn.com , fbarra@klohn.com, tshire@klohn.com)

Abstract
Glacial tills are routinely treated as competent foundations for dams on the assumption that their dense and well-graded nature excludes brittle behaviour. A comprehensive critical state programme performed on remoulded samples in a glacial till located in northern Europe, which combined triaxial and bender element testing, challenges this view. Loose specimens reveal a strongly contractive and brittle response, with rapid post-peak strength loss, while small-strain stiffness measurements place the material close to the clay domain of established global frameworks. The results suggest that, where loose pockets of the material are sufficiently extensive, they could act as a previously underappreciated trigger mechanism for deformation and flow liquefaction.

Introduction

Glacial tills are well graded, often dense, and routinely treated as competent foundations for tailings facilities. The post-Brumadinho regulatory landscape [1][2] requires operators to demonstrate that foundation materials don't present brittle behaviour. This obligation forces a closer look at materials previously considered safe.

This study discusses a glacial till which forms the foundation of an active tailings storage facility in northern Europe. It is highly heterogeneous, ranging from clay and silt through sand, gravel, cobbles and boulders, with fines content varying significantly across the foundation footprint. Although the deposit is generally dense and well graded overall, this variability suggests that loose pockets dominated by the fine matrix fraction may exist within an otherwise competent skeleton. This study presents results from a comprehensive critical state programme on a non-plastic silty sand representative of the fine matrix fraction, designed to evaluate its susceptibility to strain softening and flow liquefaction, with particular focus on the surprising brittleness identified in loose specimens and on small-strain stiffness measurements obtained from bender elements.

Methodology

A blended sample with 36% fines, representative of the average in-situ matrix gradation, was tested. Specimens were reconstituted by moist tamping using a multi-layer undercompaction technique to control initial density following the recommended procedures for critical state testing of cohesionless remoulded samples set out by [3] and [4]. The campaign comprised 14 isotropically consolidated triaxial tests (6 drained, 8 undrained) at confining stresses varying from 300 and 3000 kPa, complemented by 4 bender element tests on specimens prepared at loose, dense and very dense states. Shear-wave velocity was measured at multiple consolidation stages to characterise the small-strain stiffness over a wide range of void ratios. Index testing was carried out to support the interpretation and to bracket the range of achievable void ratios.

Results

Figure 1 presents the undrained stress response of the loose specimens tested at confining stresses up to 1000 kPa. All tests show a sharp peak at axial strains of 1 to 3%, followed by pronounced strength loss, with residual strengths collapsing towards zero at the lower confining stresses. Peak undrained strength ratios S_u/σ'_{v0} ranged from 0.24 to 0.40, with residual values as low as 0.02. This response is markedly more brittle than

typically expected for a well graded silty sand and overlaps with values reported for liquefied tailings.

Figure 2 shows the critical state line (CSL) derived from the triaxial dataset in void ratio versus mean effective stress space. A linear semi-logarithmic curve (e = 0.4251 − 0.015 ln p′) fits well with the data. A key observation is how narrow is the transition zone: a small change in void ratio, at the order of 0.02 to 0.03, is enough to move the material from contractive to dilative behaviour at a given stress level.

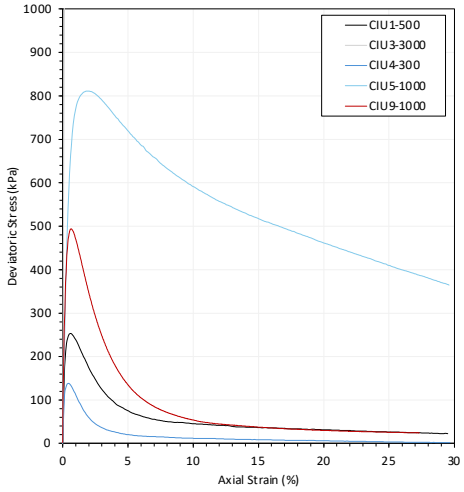


Figure 1: Undrained stress-strain response of loose specimens.

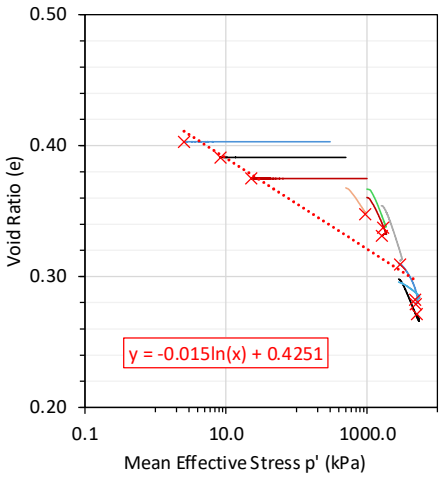


Figure 2: Critical state line in e-p' space.

The bender element programme complements the CSL plot. Four specimens prepared at loose, dense and very dense states were fitted to the empirical power law Vs = α (p′)^β. When plotted on the global dataset of [5], the fitted α values ranged from 24 to 53 m/s and β exponents from 0.31 to 0.40, close to the clay domain rather than within the typical range for clean sands, an unexpected position for a silty sand that reflects the high compressibility of the well graded material.

When analyzing all results together, it can be identified a credible failure mechanism within nominally competent till foundations. Even modest loose pockets dominated by the fine matrix fraction can behave as brittle, contractive, low residual strength material. Under rapid loading, such as seismic events or pore pressure increase, these pockets could trigger localised strength loss that propagates through neighbouring contractive zones.

Future work

Future work will integrate the laboratory dataset with in-situ testing to map loose pockets across the foundation, extend the contractive dataset to better constrain the CSL, and use mineralogical and microscopy investigations to clarify the fabric mechanisms behind the clay-like stiffness response. The calibrated critical state model will then feed deformation analyses for the TSF stability assessment.

References

[1] ICOLD (2025). Tailings dam safety guidelines (Bulletin No. 194). International Commission on Large Dams.

[2] Global Tailings Review (2020). *Global Industry Standard on Tailings Management.*

[3] Been, K., & Jefferies, M. G. (2016). Soil liquefaction: A critical state approach (2nd ed.). CRC Press.

[4] Viana da Fonseca, A., Cordeiro, D., & Molina-Gómez, F. (2021). Recommended procedures to assess critical state locus from triaxial tests in cohesionless remoulded samples. *Geotechnics*, 1(1), 95-127.

[5] Cha, M., Santamarina, J. C., Kim, H.-S., & Cho, G.-C. (2014). Small-strain stiffness, shear-wave velocity, and soil compressibility. Journal of Geotechnical and Geoenvironmental Engineering, 140(10), 06014011.

Simulating the water retention curves for hydrophobic granular soils

Tingting Zhao*[1], Melis Sutman[1] and Chris Beckett[1]
[1] Institute for Infrastructure and Environment, School of Engineering, The University of Edinburgh, United Kingdom
(E-mail: T.Zhao-30@sms.ed.ac.uk, melis.sutman@ed.ac.uk, Christopher.Beckett@ed.ac.uk)

Abstract

This study aims to investigate the water retention behaviours of hydrophobic granular soils to predict their mechanical performance in engineering applications. Numerical simulations were used to correlate water content with mechanical response by simulating the meniscus profiles under different particle shapes and surface roughnesses. The results show that hydrophobicity significantly alters the evolution of the meniscus morphology, thereby affecting the capillary forces and pressures as the volume of the water bridges changes. Future work will focus on the simulation of particle assemblies and the characterization of the water retention behaviour of hydrophobic granular soils.

Introduction

Water retention curves plays a key role in the prediction of the soil mechanical performance under changing water conditions. It connects the hydraulic behaviour with soil matric suction, which is governed by the capillary phenomena in hydrophilic materials. However, in hydrophobic granular soils, the surface wettability is altered, leading to different solid-liquid interaction. This may significantly influence capillary processes, therefore, the water retention behaviour. Such materials have been utilized in applications such as capillary barriers in slope protection and water-repellent layers in engineering, highlighting the necessity to better understand how hydrophobicity affects soil water retention behaviour.

Previous studies have investigated the hydrophobic capillary wetting experimentally and numerically [1]. Despite these advances, the effect of hydrophobicity on WRCs remains unclear, particularly in terms of the pore-scale mechanisms as previous simulation works adopt ideal sphere particle shapes and smooth surfaces. This study quantifies the hydrophobicity effect by exploring the particle shapes and surface roughness effect on water retention behaviours.

Methodology

The shape of the water bridges in mechanical equilibrium and the corresponding capillary forces and pressures acting on different shapes of particles were solved using Surface Evolver solver [2] by minimizing the interfacial free energy. For each configuration of the liquid-vapour interface with N particles, the total surface energy E_s is represented using

$$E_s = \gamma^{lv} A^{lv} + \left(\gamma^{ls} - \gamma^{vs}\right) \sum_{i=1}^{N} A_i^{ls} \quad (1)$$

where, A^{lv} is the area of the liquid-vapour interface, A^{ls} represents the area of the drop in contact with the surface, and γ^{lv}, γ^{ls} and γ^{vs} denote the liquid-vapour, liquid-solid, and vapour-solid interfacial tensions, respectively. Simulations were performed to investigate the capillary interaction between two spherical particles of diameter 1 mm. Capillary forces were also measured using a tensiometer (DCAT-25) under the same configuration to validate the simulation results.

Results

The results show that hydrophobicity alters capillary behavior, exhibiting different capillary force and pressure dynamics characteristics.

Figure 1 shows the capillary force curves corresponding to different particle spacings for given meniscus volumes. For hydrophobic (HPB) particle pairs, the capillary force undergoes a sharp transition from repulsive to attractive at small particle spacings and then approaches a negligible value as the spacing

increases further. The HPL case shows a reduction only in the attractive force regime.

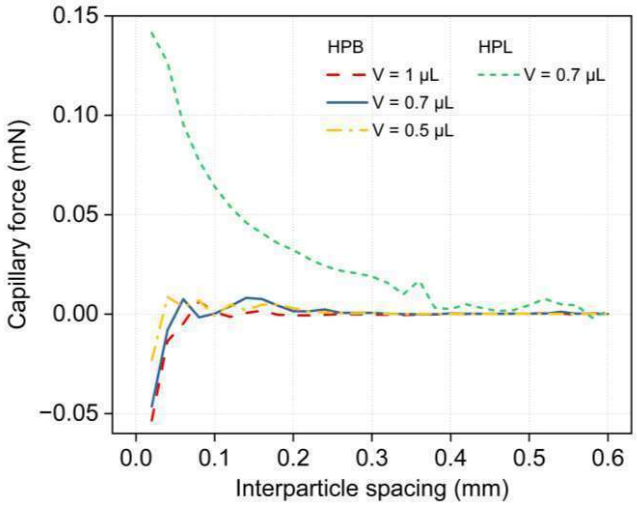


Figure 1: Capillary force versus interparticle spacing at different meniscus volumes for hydrophobic (HPB) and hydrophilic (HPL) conditions.

A particle spacing of 0.2 mm was selected to study the variation in capillary pressure with changing meniscus volume, as shown in Figure 2. For the HPB condition, the capillary pressure first reaches its maximum value then rapidly decreases to a stable pressure value. The transition from negative pressure to positive pressure corresponds to the expansion of the meniscus from concave to convex under the HPL condition [3, 4].

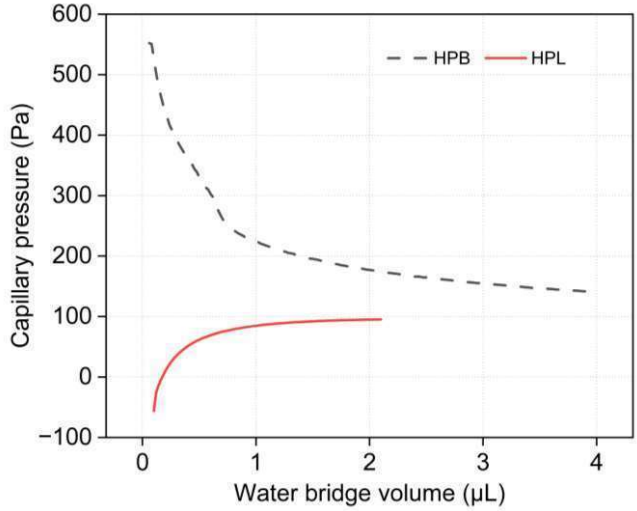


Figure 2: Capillary pressure versus water bridge volume for hydrophobic (HPB) and hydrophilic (HPL) conditions at 0.2 mm interparticle spacing.

Future work

Future work will focus on the experimental validation of the simulation results from the meniscus expansion and contraction processes. The existing model will also be extended to simulate menisci for granular particle assemblies.

This study will improve the understanding of the capillary processes for hydrophobic granular soils, and is expected to enhance the prediction of the mechanical response of such materials as water condition changes. The findings could be beneficial for industrial or agricultural application that requires capillary barriers.

Acknowledgements

The author would like to thank Prof Juan White and Prof Ken Brakke for valuable suggestions.

References

[1] Karatza, Z., Buckman, J., Medero, G.M. and Beckett, C.T.S., (2021). Evolution of meniscus structures in hydrophobic granular systems. Journal of Hydrology, Volume 603, pp. 126954. Available online at: https://doi.org/10.1016/j.jhydrol.2021.126954

[2] Brakke, K.A., (1992). The Surface Evolver. Experimental Mathematics, Volume 1(2), pp. 141–165. Available online at: https://doi.org/10.1080/10586458.1992.10504253

[3] Farmer, T.P. and Bird, J.C., (2015). Asymmetric capillary bridges between contacting spheres. Journal of Colloid and Interface Science, Volume 454, pp. 192–199.

[4] Yao, H., Liu, F., Liu, S., Miao, M., & Fan, Y. (2026). Dynamic squeezing of liquid bridge between two spherical particle surfaces. Journal of Colloid and Interface Science, 703(Pt 2), Article 139156. https://doi.org/10.1016/j.jcis.2025.139156

A low-cost automated apparatus for measuring water entry pressure

Qi Zhang*[1] and Grainne El Mountassir [2*]
[1, 2] Civil and Environmental Engineering, University of Strathclyde, United Kingdom
(E-mail: qi.zhang@strath.ac.uk, grainne.elmountassir@strath.ac.uk)

Abstract

This study presents a low-cost automated apparatus for measuring the water entry pressure (WEP) of hydrophobic porous materials. The system integrates Arduino-based motion control, moisture sensing, video recording, and MATLAB-based data acquisition to apply controlled hydraulic loading and detect water breakthrough automatically. Wax-coated glass beads were tested to demonstrate the capability of the apparatus. The results showed that the setup could capture breakthrough behaviour. The proposed apparatus provides a practical platform for WEP testing and has potential for broader application for testing chemical and biological induced hydrophobicity in soils.

Introduction

Hydrophobic porous materials can delay water infiltration and therefore have potential applications in geotechnical and geo-environmental engineering, for example in slopes, embankments, and cover systems where reduced water ingress is desirable. Their hydraulic performance is commonly characterised by the water entry pressure (WEP), defined as the pressure required for water to penetrate a hydrophobic layer [1-2]. However, existing WEP tests often rely on manual observation of breakthrough and typically provides limited information about the infiltration process through the specimen. To address these limitations, this study presents a low-cost automated apparatus for WEP measurement. The system is designed to increase hydraulic head in a controlled manner, record the breakthrough process, and terminate the test automatically once water penetration is detected. Wax-coated glass beads were used here as a reference material to demonstrate the capability of the apparatus.

Methodology

The testing system consisted of a host computer, two Arduino Uno boards, two linear actuators, moisture transducers, and a CMOS camera. MATLAB was used on the host computer for data acquisition and coordination of the test sequence. Hydraulic head was increased gradually using two linear actuators: Initially the water reservoir controlled by actuator 2 was held in a fixed position, and the specimen was lowered via actuator 1, and once its travel limit was reached, actuator 2 then raised the water reservoir to continue increasing the water head applied.

The actuators were controlled through a CNC shield mounted on Arduino 1 with TMC2209 stepper motor drivers. A T8 lead screw with 1/16 microstepping provided a linear movement resolution of 2.5 μm. In the present test, the axial actuator was operated at a constant speed of 1 mm/s.

Two moisture transducers (MD0504) were inserted at the base of the specimen to detect breakthrough. The sensor response returned to the Arduino as an analog voltage signal, which was converted by the Arduino's 10-bit analog-to-digital converter into values ranging from 0 to 1023, corresponding to 1024 discrete levels within the reference voltage range. The sensor reading typically varied from about 1023 in air to about 220 when fully submerged in water, and a threshold value of 400 was adopted to stop the test automatically. Once the threshold was reached, Arduino 2 sent a signal to Arduino 1 to terminate the system.

Wax-coated glass beads with a diameter of 2 mm were used as the proof-of-concept test material. The specimen preparation followed the procedure outlined by Bardet et al. [3], using a wax content of 6% by mass.

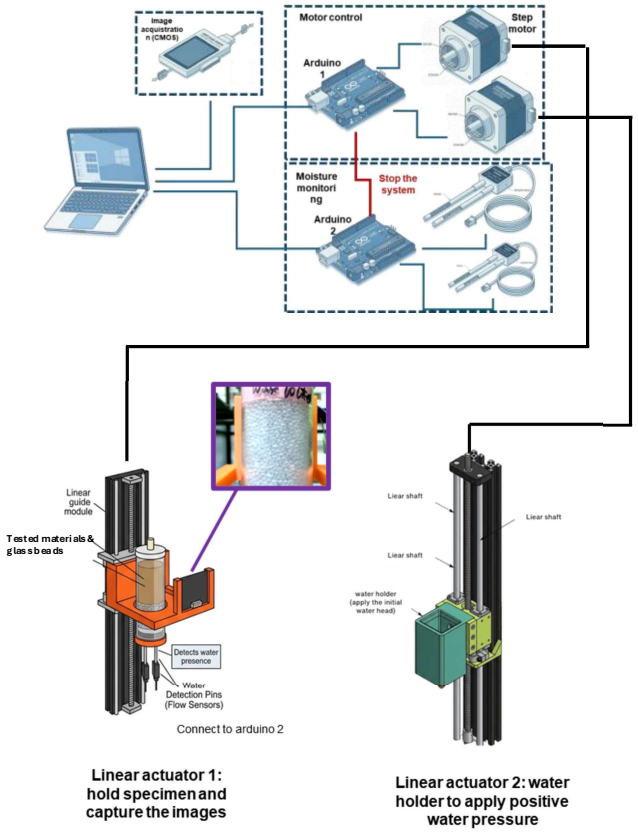


Figure 1: Sketch diagram of the system setup.

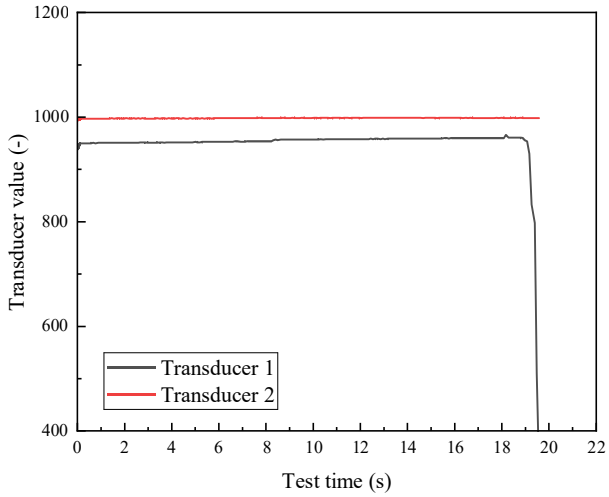


Figure 2. The variation of transducer value against test time.

Results

Figure 2 shows a representative response of the moisture transducers during testing of the wax-coated glass beads. At the beginning of the test, the sensor readings remained relatively stable, indicating that water had not yet penetrated through the specimen. As the applied hydraulic head increased, breakthrough occurred and was identified by a clear drop in transducer output. This demonstrates that the proposed system could automatically detect water penetration through the hydrophobic wax coated glass beads.

A difference was observed between the responses of the two transducers, with one sensor showing no change in transducer response. This may be related to preferential flow during breakthrough, which is plausible in hydrophobic granular materials where local wetting can be spatially non-uniform. Overall, the results confirm that the setup can capture the breakthrough event while reducing the need for continuous manual observation.

Future work

Future work will apply the system to fungal-treated porous materials to investigate how fungal growth affects both water entry pressure and infiltration behaviour. Additional repeat tests and comparison with other hydrophobic materials will also be carried out to improve the reproducibility and broader applicability of the proposed WEP testing system.

References

[1] Keatts, M.I., Daniels, J.L., Langley, W.G., Pando, M.A. and Ogunro, V.O. (2018). Apparent contact angle and water entry head measurements for organo-silane modified sand and coal fly ash. Journal of Geotechnical and Geoenvironmental Engineering, Volume 144(6), 04018030

[2] Lee, C., Yang, H.J., Yun, T.S., Choi, Y. and Yang, S. (2015). Water-entry pressure and friction angle in an artificially synthesized water-repellent silty soil. Vadose Zone Journal, Volume 14(4), vzj2014-08

[3] Bardet, J.P., Jesmani, M. and Jabbari, N. (2014). Permeability and compressibility of wax-coated sands. Géotechnique, Volume 64(5), pp. 341–350

Offshore Geotechnics

Drilled and Grouted Pile/Anchor Design for Offshore Renewable Energy: Interface Shear Behaviour from Direct Shear Box Tests

Onur Deniz*[1], Harvey Burd[2]
[1, 2] Department of Engineering Science, University of Oxford, United Kingdom
(E-mail: onur.deniz@bnc.ox.ac.uk, harvey.burd@eng.ox.ac.uk)

Abstract

This study investigates the interface shear behaviour of rock–grout systems relevant to drilled and grouted piles/anchors for offshore renewable energy applications. A staged laboratory testing programme was developed using two complementary direct shear apparatuses in Southampton and Glasgow. Initial steel–grout tests under constant normal load and constant normal stiffness boundary conditions confirmed comparable low-stress behaviour. Subsequent tests on sandstone–grout specimens provided insight into more realistic interface conditions. The results highlight the need for higher stress-level testing to characterise field-relevant behaviour, forming the basis for ongoing experimental and modelling work.

Introduction

Drilled and grouted piles and anchors are increasingly used in offshore renewable energy systems, where load transfer is typically governed by the shear behaviour of the grout–rock interface. Despite its importance, this interface remains difficult to characterise under laboratory conditions due to challenges in reproducing field-representative stress levels, boundary conditions, and surface roughness [1–2].

This study forms part of a DPhil project aimed at developing a design framework for such systems. The focus here is on the experimental investigation of interface shear behaviour using direct shear box testing. A key challenge is bridging the gap between controlled laboratory testing and the high stress levels encountered in offshore environments.

To address this, a staged laboratory programme was adopted, beginning with controlled steel–grout interfaces and extending to natural rock–grout specimens. This staged approach enables a consistent transition from controlled laboratory conditions to more realistic interface behaviour representative of offshore field conditions. The work presented here focuses on methodology development and qualitative behavioural trends rather than quantitative design outputs.

Methodology

The experimental programme employed two complementary direct shear testing systems: the GDS Direct Shear Box (Southampton), with testing conducted in Geowynd's laboratory, allowing testing under both constant normal load (CNL) and constant normal stiffness (CNS) at low stress levels, and the hand-operated portable shear rock apparatus (Glasgow), with testing conducted at the University of Glasgow soil mechanics laboratory, enabling higher normal and shear stresses under CNL conditions (Figure 1).

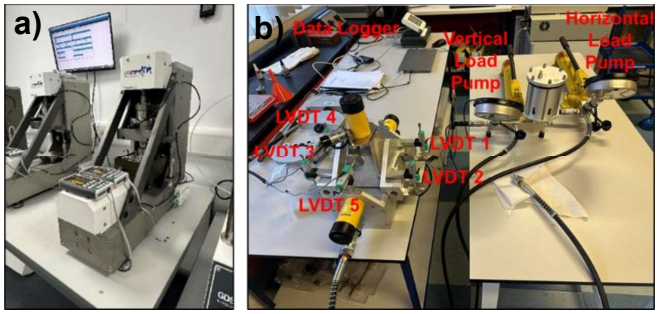


Figure 1: Direct shear testing systems: (a) Southampton, (b) Glasgow apparatus

Initial tests used steel–grout interface specimens to validate the methodology, compare CNL and CNS boundary conditions, and establish apparatus limits. The investigation was then extended to natural sandstone specimens, with sandblasted surfaces produced to introduce irregular and representative roughness (Figure 2). Due to practical limitations in machining rock with

predefined geometries, sandblasting provided a controlled method to create irregular surface profiles that better reflect field conditions. Surface roughness was quantified using 3D laser scanning and MATLAB-based processing. A staged testing programme was implemented to systematically investigate interface behaviour across different materials, boundary conditions, and stress levels (Table 1).

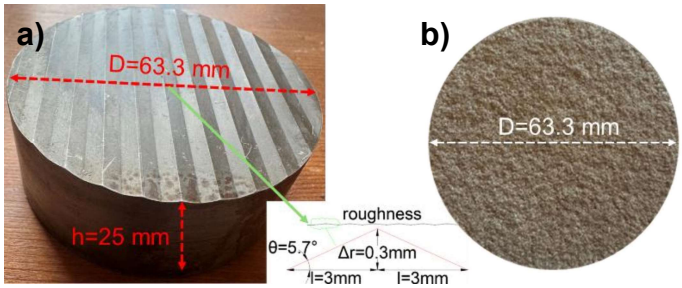


Figure 2: Specimen surfaces: (a) machined steel surface (regular), (b) sandblasted rock specimen surface (irregular)

Table 1: Summary of testing programme

Testing Stage	Interface Type	Apparatus	Boundary Condition	Stress Level
Stage 1	Steel-grout	Southampton	CNL&CNS	Low
Stage 2	Steel-grout	Glasgow	CNL	Low/High
Stage 3	Rock-grout	Southampton	CNL&CNS	Low
Stage 4	Rock-grout	Glasgow	CNL	Low/High

Results

Figure 3 shows the shear stress–normal stress response for the steel–grout interface. Steel–grout interface tests indicate that CNL and CNS conditions produce comparable shear behaviour at low stress levels. Differences in normal stress evolution and dilation were observed, but the overall shear response remained similar. Comparison between Southampton and Glasgow apparatus demonstrates consistent interface behaviour at low stresses, while the change in slope of the failure envelope with increasing stress highlights stress-dependent behaviour. These results indicate that low-stress laboratory tests alone are insufficient to fully characterise interface behaviour relevant to offshore conditions, emphasizing the need for higher stress-level testing.

Future work

Due to space constraints, detailed Stage 3 (Table 1) rock–grout test results are not presented here; however, these tests remain a key part of the experimental programme and guide the planned high-stress investigations. Future work will extend testing to higher normal stress levels using the Glasgow apparatus to better represent in-situ offshore conditions. Additional experiments will explore a wider range of surface roughness. Results will be integrated into numerical models, including interface constitutive models and simplified pile analysis frameworks, to develop a methodology linking laboratory-scale interface behaviour to full-scale drilled and grouted pile performance.

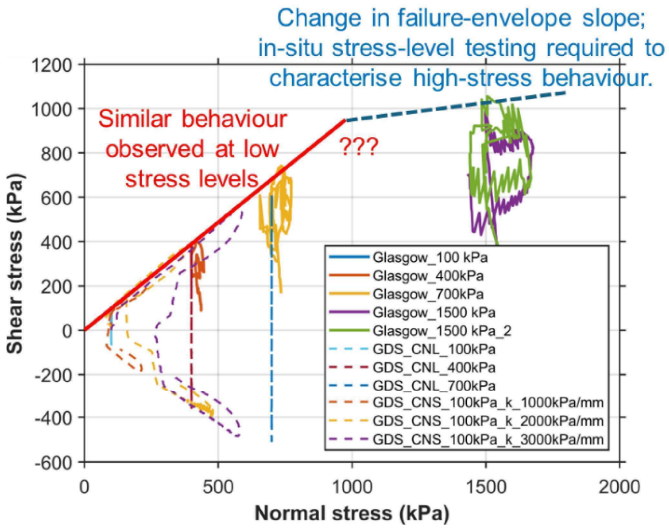


Figure 3: Shear stress–normal stress response for the steel–grout interface (Stages 1–2, Table 1).

Acknowledgements

The authors gratefully acknowledge Geowynd for access to laboratory facilities in Southampton. The authors also thank Dr Róisín Buckley for her support with the Glasgow testing.

References

[1] Seidel, J., & Haberfield, C. (2002). Laboratory testing of concrete-rock joints in constant normal stiffness direct shear. Geotechnical Testing Journal, 25(4), 391–404.

[2] Stavropoulou, E., Dano, C., & Boulon, M. (2021). Shear response of wet weak carbonate rock/grout interfaces under cyclic loading. Rock Mechanics and Rock Engineering, 54(6), 2791–2813.

Numerical Modelling of Shared Anchor Piles for Floating Offshore Wind Turbines

A.R. Bin Bahri*[1], L. Cui[1] and S. Bhattacharya[1]
[1] School of Engineering, University of Surrey, Guildford, United Kingdom
(E-mail: a.binbahri@surrey.ac.uk, l.cui@surrey.ac.uk, s.bhattacharya@surrey.ac.uk)

Abstract

This project focuses on developing a coupled numerical model to investigate the performance of shared anchor piles for floating offshore wind turbines (FOWT). A 3-mooring line model was created within ABAQUS to simulate: 1) pile installation effects, 2) pile lateral performance under multidirectional loads. The installation procedure was simulated using a coupled Eulerian-Lagrangian model (CEL). OpenFAST [1] was used to generate the wind, wave, and current (WWC) loads on the turbine, which were transferred via taut mooring lines as tensile forces to the pile. The soil domain consists of a fine sand represented by the Mohr-Coulomb (MC) constitutive model. Modelling results reveal an increase in stress from the pile toe extending to 3-4D from the outer pile wall, complemented by plastic strain along the pile driving path.

Introduction

Shared pile anchors are an extension of the single pile anchor foundation, where multiple mooring lines are connected to the anchor. Due to its axisymmetric geometry about the vertical, anchor points can be positioned in an equally spaced, radial configuration around the outer wall of the pile, facilitating numerous attachments to floating structures.

This is expected to moderate the number of anchors of a 100-turbine wind farm by 60-79%, reducing material usage and construction time [2]. Combined with the benefit of reduced mean and maximum net forces due to force cancellation effects, the shared anchor represents a promising proposition when designing large scale wind farms.

Nevertheless, this proposal is accompanied by uncertainties. These include the effects of multidirectionality and load reversals on the soil, greater vertical loads, and installation effects on the anchor behaviour among others.

Methodology

The Finite Element analysis software ABAQUS was used for both the creation of the geometric mesh and running of the analysis.

The model consists of a cylindrical soil domain with a diameter and depth of 50 m and a hollow steel pile with a 2.5 m diameter, D and 20 m length. Only half of the model was used for the installation step, given the symmetrical nature of hydraulic driving. An accelerated vertical driving rate of 5.0 m/s is prescribed to the entirety of the pile model, after which anchor tensions are transmitted (Figure 1). The tensions are generated in OpenFAST and correspond to movements produced by a 15 MW turbine with a semisubmersible platform attached to a taut 3-line mooring system spread $120°$ and inclined $45°$ from the seabed.

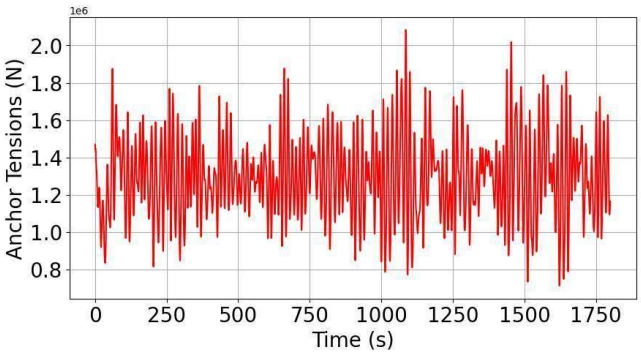


Figure 1: Anchor tensions vs time

A CEL model is used when simulating the driving action on the pile, while a Lagrangian model is used for the loading step.

The modelling timeline is as follows:

1) **Geostatic Setup – 2 seconds**
2) **Hydraulic Jacking – 4 seconds**
3) **Anchor Loading – 1800 seconds**

The properties of the sand are listed below:

Table 1: Soil properties [3]

Property	Value
Saturated Bulk Density, ρ_{sat}	2018 kg/m^3
Young's Modulus, E	90.0 MPa
Poisson's Ratio, ν	0.3
Friction Angle, ϕ'	33.1°
Dilation Angle, ψ	14.5°

The application of the MC model is preliminary in nature and destined to be replaced by a hypoplastic model with small strain to better capture the cyclical effects of offshore loading.

Results

Figures 2 and 3 display the results when the penetration reaches 12 m.

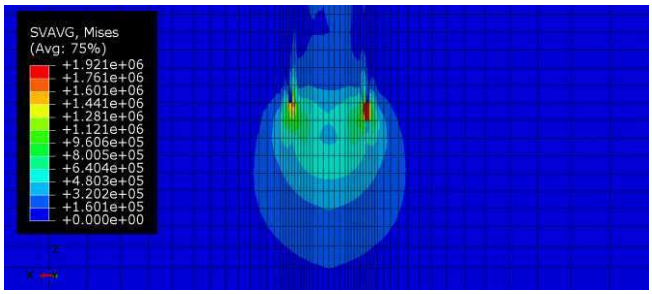


Figure 2: Stress distribution beneath pile toe

The greatest effects of pile jacking are concentrated at the pile toe, with stresses up to two orders of magnitudes greater than the surrounding geostatic stress forming right below the toe and extending to the area around the pile. However, the extent of soil truly affected by the procedure extends to between 3-4D from the pile wall.

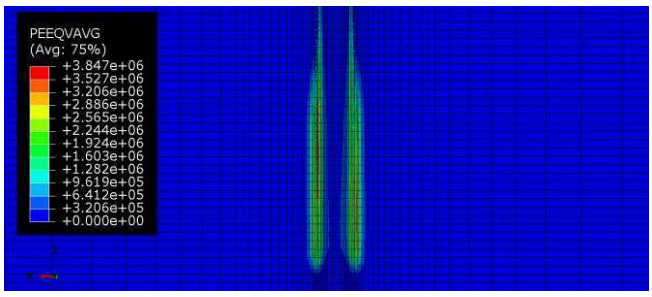


Figure 3: Plastic strain distribution along pile installation path

Similar to stress, the strain develops at the pile toe and extends along the pile displacement path. Plastic strain extends up to a 1D radius away from the outer pile wall. Soil plugging was not recorded during the installation analysis.

Preliminary loading tests were conducted using the Lagrangian loading model to assess setup accuracy. Radial stresses and strains developed especially on the side with greater anchor tensions.

Conclusion and Future Work

The numerical simulations confirm that the disturbance of soil after pile installation is significant. This may affect soil properties such as relative density which will need to be considered during the design stage.

The immediate target is to transfer the installation data as initial conditions for the loading step. This involves a postprocessing step conducted through a MATLAB subroutine which maps and linearly interpolates the state variables to the mesh of the loading regime [4,5]. This is required due to the dissimilarities between the installation and loading mesh.

References

[1] *OpenFAST/openfast: OpenFAST v4.0.0* https://github.com/OpenFAST/openfast (accessed March 23, 2026)

[2] Fontana, C. M., Hallowell, S. T., Arwade, S. R., Degroot, D. J., Landon, M. E., Aubeny, C. P., Diaz, B., Myers, A. T. & Ozmutlu, S. (2018) Multiline anchor force dynamics in floating offshore wind turbines. *Wind Energy.* 21 (11), 10.1002/we.2222.

[3] Chow, S. H., Roy, A., Herduin, M., Heins, E., King, L., Bienen, B., O'Loughlin, C., Gaudin, C. & Cassidy, M. (2019) *Characterization of UWA superfine silica sand.* doi:10.26182/5d8c185bcd366.

[4] Bienen, B., Fan, S., Schröder, M. & Randolph, M. F. (2026) *Effect of the installation process on monopile lateral response.* Emerald.

[5] Heins, E. & Grabe, J. (2017) *Class-A-prediction of lateral pile deformation with respect to vibratory and impact pile driving.* Elsevier BV.

Monotonic lateral loading of monopiles in sandy soils, considering drainage effects

R.W.L Chia*, C.M. Martin, O. Adamidis, H.J. Burd
University of Oxford, Oxford, United Kingdom
(E-mail: *ryan.chia@eng.ox.ac.uk)

Abstract

The UK aims for 50 GW of offshore wind capacity by 2030, leading to larger monopiles with diameters over 10 m. This raises concerns about the appropriateness of existing design methods that, for sandy soils, assume fully drained conditions. This research studies offshore wind monopile foundations under lateral loading in sand, focusing on drainage effects. Finite element analyses, validated by experiments, show that loading rate significantly affects lateral capacity. Monopiles exhibit lower resistance under drained conditions and higher resistance when undrained or partially drained. These findings highlight the need to consider drainage in monopile design as foundation sizes grow.

Introduction

Current design methods for offshore wind monopiles under lateral loading typically assume drained behaviour for sand and undrained behaviour for clay (Burd et al., 2020; Byrne et al., 2020). The study presents results from finite element analyses of a model monopile in Congleton Sand HST-95, validated against centrifuge findings. Various drainage conditions were examined, from undrained to fully drained, by adjusting the dimensionless loading rate V at the pile head. Load-displacement curves and excess pore pressures at different dimensionless rates are shown in the results.

Methodology

Analyses were performed using PLAXIS 3D with the SANISAND-MS model (Liu et al., 2019) to simulate soil behaviour. Soil parameters were calibrated based on triaxial tests (Fleminger, 2025). Two numerical monopile models (4.15 m and 5 m in diameter) replicated the centrifuge tests. Figure 1 illustrates a typical finite element setup used in this study. Monopiles were loaded in drained conditions using interface elements for soil-pile interaction, with the Mohr-Coulomb model applied and a friction angle equal to the critical state friction angle φ'_{cs}, representing a fully rough interaction. Thereafter, coupled consolidation analyses at different loading rates v (m/s) at the pile head for D = 5 m were carried out. A variety of drainage conditions are covered, and loading rates are presented using the dimensionless loading rate $V = vD/c_v$. Here, c_v represents the coefficient of consolidation, as defined by Equation 1. The parameter M_{oed} refers to the constrained modulus of the soil, measured at half the length of the pile. Additionally, k denotes permeability, while γ_w represents the unit weight of water. k is taken to be 1×10^{-4} m/s. A key assumption is that cavitation effects are not considered.

$$c_v = M_{oed} * k/\gamma_w \quad (1)$$

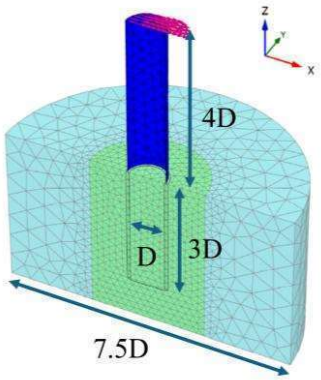


Figure 1: Finite element model

Results

Figure 2 shows the variation of normalised load against normalised ground level displacement. Where H is the reaction force in response to displacement applied at pile head, γ' is the buoyant unit weight of soil and u_x is the displacement of the pile at ground level. Taking H_{ult} at u_x of 0.1D, a 10% (approx.)

difference is consistently observed for D = 4.15 m and 5 m between centrifuge and simulated results. The assumption of a fully rough pile-soil interface might be the cause of this difference.

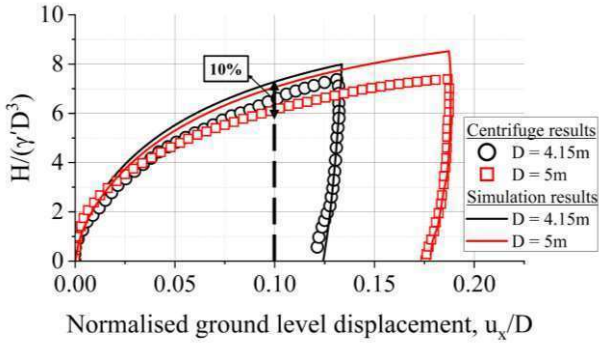


Figure 2: Load-displacement curves for D = 4.15m & 5m

Partially drained behaviour was investigated by applying loading rates v between 5×10^{-7} m/s and 100 m/s. Figure 3 shows the variation of $H/(\gamma' D^3)$ with u_x/D for different dimensionless loading rates V for which $V \rightarrow \infty$ = undrained response, $V \rightarrow 0$ = drained response. Considering an undrained response, H_{ult} taken at u_x/D = 0.1 is 8 times more than that from a drained response. A stiffer load-displacement response is also observed when transitioning from drained to undrained behaviour.

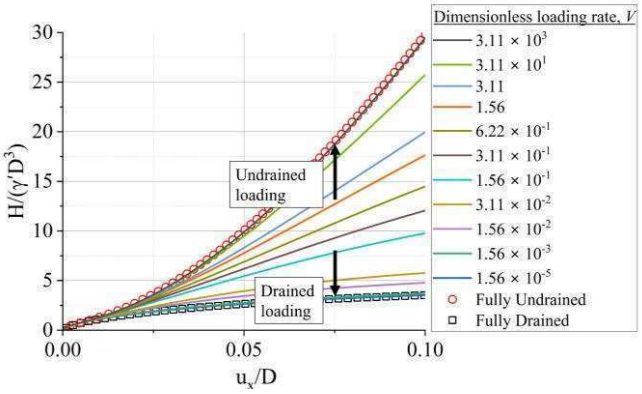


Figure 3: Load-displacement curve for varying drainage conditions

When the pile is loaded, compressive pore pressure develops in the early stages. As the soil undergoes larger strains, tensile excess pore pressure accumulates around the pile shaft and base. This suction is due to the pile pulling away from the soil, and the soil dilating during shearing. Figure 4 shows the development of excess pore pressure during undrained loading. As tensile excess pore pressure rises, effective stresses in the soil increase, leading to greater stiffness in the load-displacement curves.

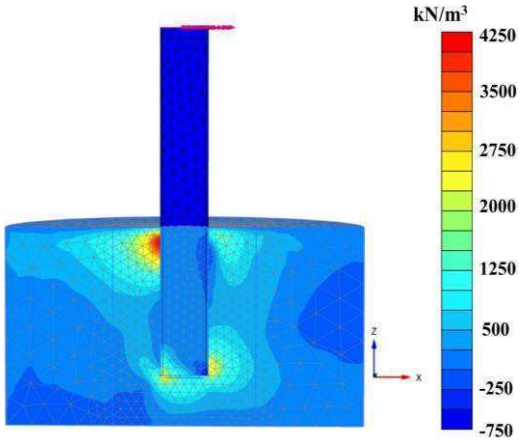


Figure 4: Excess pore pressure contour at u_x=0.1D (V = 31.1 – undrained). Negative values indicate compression, while positive values signify tension (suction)

Future work

Future work will explore how the effects of cavitation and varying monopile diameters impact the stiffness characteristics of the interaction between monopiles and surrounding soil.

References

[1] Burd, H.J. et al. (2020). *PISA design model for monopiles for offshore wind turbines: application to a marine sand.* Géotechnique, 70, 1048- 1066, https://doi.org/10.1680/jgeot.18.P.277

[2] Byrne, B. W. et al. (2020). *PISA design model for monopiles for offshore wind turbines: Application to a stiff glacial clay till.* Géotechnique, 70, 1030-1047, https://doi.org/10.1680/jgeot.18.P.255

[3] Fleminger, R. (2025). *Experimental investigation of drainage effects around monopiles in sand* (Doctoral dissertation, University of Oxford).

[4] Liu, H. Y., Abell, J. A., Diambra, A., & Pisanò, F. (2019). *Modelling the cyclic ratcheting of sands through memory-enhanced bounding surface plasticity.* Géotechnique, *69*(9), 783-800.

Development of practical geotechnical design tools for offshore wind turbine foundations subject to cyclic loads

Chun Hin Chin and Pishun Tantivangphaisal
Department of Civil and Environmental Engineering, Imperial College London, United Kingdom
(E-mail: chc222@ic.ac.uk, pt620@imperial.ac.uk)

Abstract

This study presents the calibration of a modified High-Cycle Accumulation (HCA) model for Karlsruhe fine sand using published monotonic and cyclic laboratory data. A stepwise procedure is used for the monotonic calibration and a genetic algorithm (GA) for the HCA strain accumulation parameters based on 13 drained cyclic triaxial tests. A PLAXIS 3D finite element model of a laterally loaded monopile (D = 7.5 m, L = 40 m) is developed and compared against results in the literature. This serves as a starting point to aggregate 3D FE long-term cyclic analyses of laterally loaded offshore monopiles into one-dimensional design tools.

Introduction

Currently, over 80% of offshore wind turbines are founded on monopiles. These must resist lateral cyclic loads over its design life while keeping the accumulated rotation below serviceability limits (typically 0.25–0.5°) (DNV, 2021).

The API cyclic p-y approach, the stiffness degradation method (Achmus et al, 2009), and empirical accumulation rules (LeBlanc et al., 2010) are examples of existing simplified design methods. These approaches, however, cannot adequately capture combined site-specific, geometric and loading effects.

The High-Cycle Accumulation (HCA) model addressed these limitations allowing site specific calibration using drained cyclic triaxial tests (Niemunis et al., 2005). A recent modification coupled HCA with a practical sand constitutive model (Tantivangphaisal et al, 2025). This study calibrates monotonic and cyclic parameters for Karlsruhe fine sand using laboratory data (Wichtmann and Triantafyllidis, 2015), validates monotonic and cyclic models, and compiles a parameter set for future studies to develop a simplified 1D design tool.

Methodology

Monotonic model parameters (Taborda et al., 2022) for Karlsruhe fine sand were calibrated using isotropic compression, oedometer, drained and undrained triaxial tests. The small-strain shear stiffness modulus is $G_{\max} = G_{ref}\ f(e)\ \left(\frac{p'}{p_{ref}}\right)^{m_G}$ where $G_{ref} = 157{,}300$ kPa, $m_G = 0.43$, while critical state parameters were $e_{max} = 1.054$, $\lambda = 0.0707$, $\xi = 0.2859$ and $\varphi_{cs} = 33.37$. Oedometer unloading and reloading data were used to calibrate an independent bulk stiffness $K_{max} = K_{ref}\ \frac{(a_K - e)^2}{1+e}\left(\frac{p}{p_{ref}}\right)^{m_K}$ with $K_{\mathrm{ref}} = 24{,}000$ kPa and $m_K = 0.43$. This approach avoids reliance on an unrealistic constant poisson's ratio.

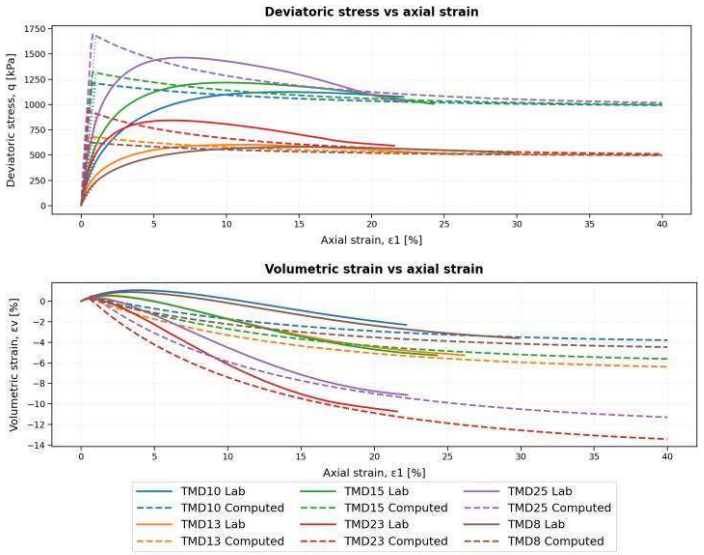


Figure 1: Predicted and measured drained triaxial response (deviatoric stress q (top), volumetric strain ε_v (bottom) vs axial strain)

A half-geometry 3D FE model was created for a monopile with L = 40 m, D = 7.5 m, t = 90 mm, and h = 20 m lever arm (Cao et al., 2023). The pile is modelled using linear elastic shell elements (E = 210 GPa, v = 0.3). The pile-soil interface is modelled using a Mohr–Coulomb

failure criterion, with interface friction angle of 23.7°. Accumulated strain is computed by the HCA model as $\frac{d\varepsilon^{acc}}{dN} = f_{ampl}\, f_e\, f_p\, f_Y\, \frac{df_N}{dN}$. 13 drained cyclic triaxial tests were used to calibrate the six accumulation model parameters, $\{C_{ampl}, C_e, C_p, C_Y, C_{N1}, C_{N2}\}$, using a two-stage genetic algorithm method.

Results

The calibrated parameter set is provided in Table 1. Figure 2 shows comparison between predicted and measured accumulated strain ε_{acc} against cycle number N for 4 selected calibration tests. The model captures the primary influences of strain amplitude, density, mean stress, and stress ratio on long-term cyclic behaviour. A leave one out analysis confirms calibration robustness, with a COV below 15% for five of six parameters.

Table 1: Calibrated high cyclic parameters

P18	C_{ampl}	1.467	**P23**	C_{N1}	1.8×10^{-4}
P19	C_e	2.545	**P24**	C_{N2}	0.235
P20	e_{ref}	1.054	**P26**	φ'_{dir}	28.79°
P21	C_p	0.294	**P27**	$K_{ref,HCA}$	120,900 kPa
P22	C_Y	2.615	**P28**	v_{HCA}	0.32

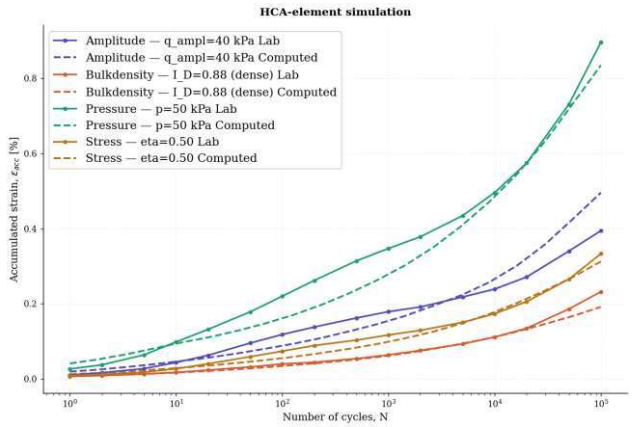


Figure 2: Comparison between measured and predicted accumulated strain, ε_{acc}, with number of cycles, N.

Future work

The calibrated parameter set will be used in parametric analyses of the monopile subjected to different lateral cyclic amplitude and directions. Distributed soil reactions will be taken from the 3D results to assess whether cyclic loading characteristics can be incorporated into the PISA framework (Burd et al., 2020). This could simplify the link between advanced constitutive modelling and routine offshore foundation design practice.

Acknowledgements

Credit to Dr P. Tantivangphaisal for supervision, and the laboratory dataset of Prof. T. Wichtmann is greatly acknowledged.

References

[1] Achmus, M., Kuo, Y.-S. & Abdel-Rahman, K. (2009). Behavior of monopile foundations under cyclic lateral load. Computers and Geotechnics, 36(5)

[2] Burd, H.J. et al. (2019). PISA design model for monopiles for offshore wind turbines: application to a marine sand. Géotechnique, 70(11), pp. 1048–1066.

[3] Cao, S., Abdel-Rahman, K. & Achmus, M. (2023). A new method for the analysis of foundation behavior in sand under drained high-cycle loading. Int. J. Numer. Anal. Methods Geomech., 47(10), pp. 1876–1893.

[4] DNV. (2021). *DNV-ST-0126: Support structures for wind turbines*.

[5] LeBlanc, C., Houlsby, G.T. & Byrne, B.W. (2010). Response of stiff piles in sand to long-term cyclic lateral loading. Géotechnique, 60(2), pp. 79–90.

[6] Niemunis, A., Wichtmann, T. & Triantafyllidis, Th. (2005). A high-cycle accumulation model for sand. Computers and Geotechnics, 32(4), pp. 245–263.

[7] Taborda, D.M.G., Pedro, A.M.G. & Pirrone, A.I. (2022). A state parameter-dependent constitutive model for sands. Computers and Geotechnics, 148, 104811.

[8] Tantivangphaisal et al. (2025). Numerical modelling of long-term cyclic response of piles in sands using HCA. Géotechnique, 75(12), pp. 1507–1526.

[9] Wichtmann, T. and Triantafyllidis, T. (2015). An experimental database for the development, calibration and verification of constitutive models for sand with focus to cyclic loading: part I—tests with monotonic loading and stress cycles. *Acta Geotechnica*, 11(4), pp.739–761.

Calibration of Low-Cost Soil Moisture Sensors for Accurate Measurement of Water Content in High Plasticity Clay

X. Z. Wu*[1], Joel A. Smethurst[2] and Kevin M. Briggs[3]
[1, 2, 3] School of Engineering, Faculty of Engineering and Physical Sciences, University of Southampton, UK.
(E-mail: XZ.Wu@soton.ac.uk, J.A.SMETHURST@soton.ac.uk, K.Briggs@soton.ac.uk)

Abstract

Resistive and capacitive soil moisture sensors are simple and cost-effective. Although previous studies have shown that low-cost sensors can be used to measure soil water content in sandy soils, their applicability to high plasticity clay is unclear due to its dense structure, strong water retention, and pronounced shrink–swell behaviour. In this study, low-cost resistive and capacitive sensors were calibrated for high plasticity clay. By optimising specimen size and sensor installation, embedding the capacitive sensor during compaction enabled calibration for soil gravimetric water content.

Introduction

Soil water content is a key parameter for the hydraulic and mechanical behaviour of soils (Briggs *et al.*, 2017). Its continuous monitoring relies on soil moisture sensors, including high-accuracy time-domain reflectometry (TDR) and frequency-domain reflectometry (FDR) sensors, as well as low-cost resistive and capacitive sensors.

High-accuracy sensors provide reliable measurements of soil water content, but their high cost limits wider application (Mittelbach *et al.*, 2012). Resistive and capacitive sensors are simple and inexpensive; however, their measurements are strongly influenced by soil type (Adla *et al.*, 2020). Previous studies have shown that low-cost capacitive sensors can monitor water content in sandy soils (Schwamback *et al.* 2023), although reliable results require soil-specific calibration (Placidi *et al.*, 2020).

High plasticity clay has a denser structure, greater water absorption and retention capacity, and more pronounced shrink–swell behaviour. These characteristics affect low-cost sensor performance. This study calibrated low-cost moisture sensors using weathered London Clay under controlled laboratory conditions to evaluate their applicability to high plasticity clay.

Methodology

Weathered London Clay passing a 2 mm sieve and prepared at an initial gravimetric water content of 30% was used to establish quantitative relationships between the output of low-cost soil moisture sensors and soil gravimetric water content. Soil moisture was measured using resistive (SEN0114) and capacitive (SEN0193) soil moisture sensors manufactured by DFRobot.

All sensors were tested under controlled drying conditions, with the laboratory temperature maintained at 20±2 °C. For the resistive sensor, 100 mm high specimens were used, and the sensor was inserted horizontally into the specimen centre after compaction. For the capacitive sensor, specimen height was reduced to 30 mm to minimise response lag, and two installation methods were adopted: lateral insertion into demoulded specimens and embedding during compaction. All specimens were compacted in acrylic tubes to a dry density of 1.48 g/cm³.

During testing, specimen mass was continuously monitored with an electronic balance, and sensor voltage was recorded every 15 min using a data logger until gravimetric water content fell below 15%. The data were then used to analyse sensor response and derive calibration equations.

Results

The resistive sensor could capture the overall drying trend of weathered London Clay; however, electrode corrosion occurred during testing, resulting in unstable output and poor repeatability (Figure 1).

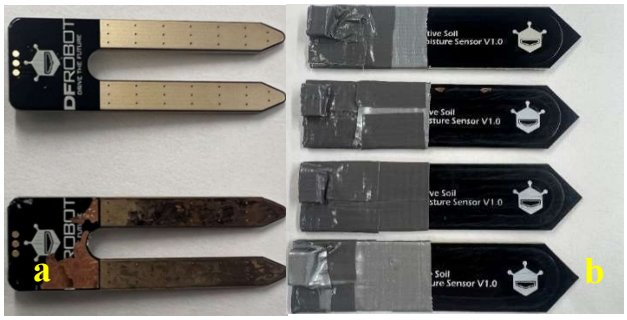


Figure 1: (a) SEN0114 resistive soil moisture sensor, with the new sensor at the top and the used sensor at the bottom; (b) SEN0193 capacitive soil moisture sensor, with the new sensor at the top and used sensors below

The capacitive sensor showed markedly better durability and measurement stability. After repeated tests, no corrosion was observed, with only slight mechanical wear (Figure 1). Embedding the capacitive sensor during compaction improved sensor–soil contact and reduced variability between specimens. As gravimetric water content decreased, sensor output changed continuously and monotonically, and the calibration curves from repeated tests showed good consistency. An output range of 1200–1700 mV corresponded to a gravimetric water content range of approximately 15%–28% (Figure 2).

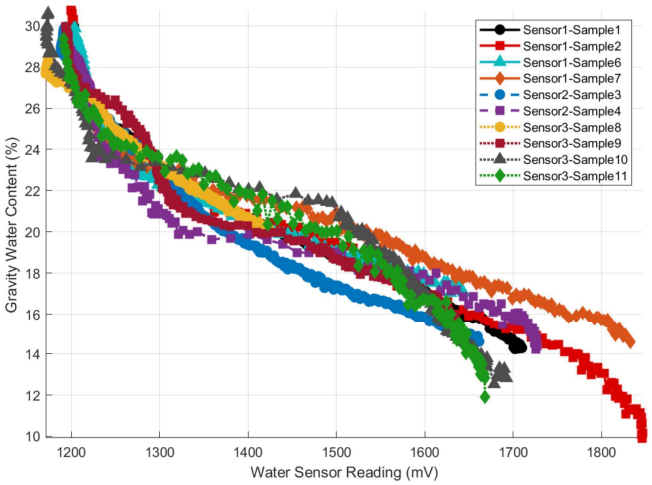


Figure 2: Calibration results for SEN0193 capacitive soil moisture sensor

Future work

Future work will apply the present calibration results to measure changes in the gravimetric water content of willow-planted weathered London Clay under the same laboratory conditions.The calibration range will also be extended to a wider range of conditions, including different temperatures, densities, initial water contents, and soil types, to improve the general applicability of the sensor model. In addition, more sensors and repeated tests should be used to strengthen the robustness of a unified calibration equation and to assess its long-term reliability for monitoring of high plasticity clay.

References

[1] Adla, S., Rai, N.K., Karumanchi, S.H., Tripathi, S., Disse, M. and Pande, S. (2020). *Laboratory Calibration and Performance Evaluation of Low-Cost Capacitive and Very Low-Cost Resistive Soil Moisture Sensors*. Sensors, 20(2), 363. Available online at: https://doi.org/10.3390/s20020363

[2] Briggs, K., Loveridge, F.A. and Glendinning, S. (2017). *Failures in transport infrastructure embankments*. Engineering Geology, 219, pp. 107–117. Available online at: https://doi.org/10.1016/j.enggeo.2016.07.016

[3] Mittelbach, H., Lehner, I. and Seneviratne, S.I. (2012). *Comparison of four soil moisture sensor types under field conditions in Switzerland*. Journal of Hydrology, 430–431, pp. 39–49. Available online at: https://doi.org/10.1016/j.jhydrol.2012.01.041

[4] Placidi, P., Gasperini, L., Grassi, A., Cecconi, M. and Scorzoni, A. (2020). *Characterization of Low-Cost Capacitive Soil Moisture Sensors for IoT Networks*. Sensors, 20(12), 3585. Available online at: https://doi.org/10.3390/s20123585

[5] Schwamback, D., Persson, M., Berndtsson, R., Bertotto, L.E., Kobayashi, A.N.A. and Wendland, E.C. (2023). *Automated Low-Cost Soil Moisture Sensors: Trade-Off between Cost and Accuracy*. Sensors, 23(5), 2451. Available online at: https://doi.org/10.3390/s23052451

Long-term deformation mechanisms of monopile foundation in sand under cyclic lateral loading of different symmetries

L.L.K. Hung-Lo-Sang*[1], J. Wang[2], C.M. Heron[3], A. Pettey[4] and A.M. Marshall[5]
[1, 2] Department of Civil Engineering, Advanced Energy and Environmental Materials & Technologies Research Centre, University of Nottingham Ningbo China, China
(E-mail: liam.hunglosang@nottingham.edu.cn, juan.wang@nottingham.edu.cn)
[1, 3, 4] Department of Civil Engineering, Centre for Geomechanics, University of Nottingham, UK
(E-mail: charles.heron@nottingham.ac.uk, angus.pettey1@nottingham.ac.uk)
[5] Formerly Department of Civil Engineering, University of Nottingham, UK

Abstract
Monopiles supporting offshore wind turbines are subjected to cyclic lateral loads. This study investigates the role of load symmetry on monopile–soil interaction in sand using physical modelling and digital image correlation over 20,000 load cycles. Results show that, at identical load amplitudes, load symmetry governs the transition between shakedown and ratcheting behaviour. Balanced loading leads to stabilised, distributed deformation, whereas unbalanced loading induces localised shear and progressive displacement accumulation. These findings demonstrate that neglecting load symmetry may lead to unconservative predictions of long-term performance, highlighting the need for symmetry-dependent design approaches.

Introduction

Monopile foundations are widely used to support offshore wind turbines. During their service life, the monopiles must resist lateral cyclic loads from waves, winds, and tides. However, the soil deformation mechanisms responsible for displacement accumulation, ratcheting, and shakedown behaviour under cyclic lateral loading remain insufficiently understood. Previously, Frick and Achmus [1] attempted to track soil particles around a pile under lateral cyclic loading. However, the analysis was limited to 25 cycles due to computational limitations. This study extends the method and analyses images for 20,000 cycles at different symmetries.

Methodology

A servo-motor actuator, shown in Figure 1, was used to apply lateral cyclic loads to a rigid model monopile. The model was scaled from a prototype typically used in the offshore wind industry. The sand was poured around the monopile using an automated sand pluviation device described in Hung-Lo-Sang *et al.* [2]. During the loading tests, a high-resolution camera was used to record soil displacement around the monopile. Post-testing digital image correlation by GeoPIV-RG was then utilised to analyse the pile-soil interaction.

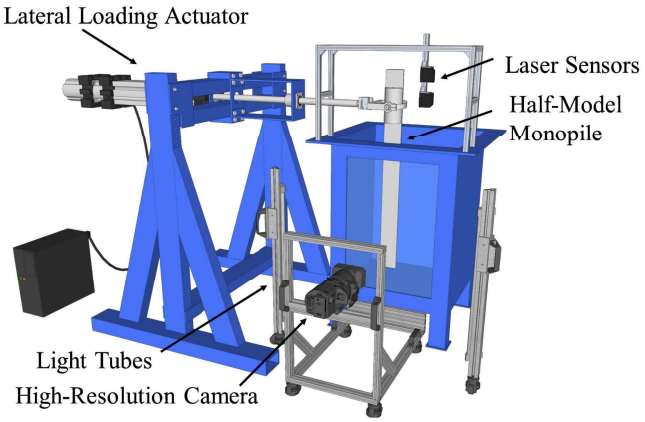


Figure 1: Experimental set-up

Table 1: Test schedule

Symmetry	ξ_c	H_{max} (N)	H_{min} (N)	N	f (Hz)
One-Way	0	31.6	0	20000	0.5
Unbalanced	-0.5	31.6	-15.8	20000	0.5
Balanced	-1	31.6	-31.6	20000	0.5

Table 2: Monopile properties

Property		Prototype	1-g
Ratio	-	1	50
Diameter	D	4 m	80 mm
Wall Thickness	t	180 mm	7 mm
Embedment Depth	L_{em}	18 m	360 mm
Load Eccentricity	e	21.5 m	430 mm

Table 3: Sand properties

Property	Specification	
Relative Density	26.7	%
ϕ'_{cr}	36.5	Degrees
D_{10}, D_{50}, D_{60}	0.43, 0.50, 0.56	mm
e_{min}, e_{max}	0.729, 1.054	-
G_s	2.6	-

Results

Figure 2(a) shows the load histories for the tests conducted. Although the maximum load amplitude was set same, the accumulated displacement increased systematically when the load applied is more asymmetric.

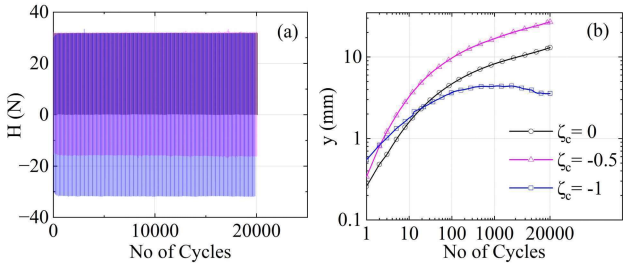


Figure 2: (a). Load histories and (b). pile displacement accumulation Vs. No of cycles

After 20,000 cycles, the accumulated pile displacement was 10.4 mm, 11.8 mm and 3.2 mm for the one-way, unbalanced and balanced loading cases respectively. The pile displacement trends correspond closely with observed soil deformation patterns shown in Figure 3. Under balanced loading, deformation was distributed more symmetrically around the monopile, promoting cyclic dilation–contraction and a tendency towards shakedown behaviour. In contrast, one-way and unbalanced loading generated localised shear zones and directional strain accumulation, resulting in progressive ratcheting and continued displacement growth throughout the test. These highlight a critical limitation of conventional monopile design methods, which focus on pile capacity and load amplitude, while neglecting load symmetry, despite its effects on the soil response mechanism. At equal load magnitude, load symmetry governs the transition between localised, unidirectional shear banding and distributed cyclic shearing in monopile–soil systems.

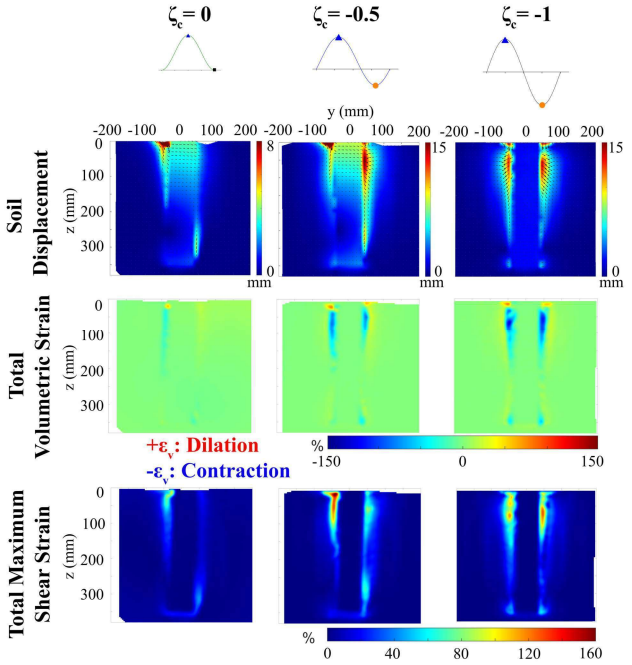


Figure 3: Soil displacement, volumetric and shear strains at the 20,000th load cycle

Future work

Future work should focus on quantifying the transition from shakedown to ratcheting as a function of load magnitude, symmetry, and high-cycle loading. Validation at a larger scale through centrifuge testing is also needed to confirm the observed mechanisms and support implementation in design guidelines.

Acknowledgements

The authors are grateful for the financial support provided by the Zhejiang Natural Science Foundation (LY22E080018).

References

[1] Frick, D. and Achmus, M. (2020). *An experimental study on the parameters affecting the cyclic lateral response of monopiles for offshore wind turbines in sand*, *Soils and Foundations,* 60(6), pp. 1570-1587.

[2] Hung-Lo-Sang, L. L. K., Wang, J., Heron, C. M., Pettey, A. and Marshall, A. M. (2026). *An automatic sand pourer for the preparation of loose and dense samples for physical modelling*. *Proceedings of the 11th International Conference on Physical Modelling in Geotechnics*, Zurich, Switzerland.

Soil-Structure Interaction

A State Variable Formulation of LeBlanc's Model for Cyclic Loading

Magne E. Rasmussen*[1], Byron W. Byrne[2] and Harvey J. Burd[3]
[1, 2,3] University of Oxford, Department of Engineering Science, Parks Road, Oxford OX1 3PJ, UK
(E-mail: magne.rasmussen@eng.ox.ac.uk)

Abstract

Monopile foundations supporting offshore structures are subjected to long-term, biased lateral cyclic loading from wind and waves. The irregular loading histories can cause progressive accumulation of rotation and may govern serviceability performance. In modelling pile response under cyclic loading, these histories are reduced to bins of sinusoidal cycles through cycle-counting methods. The widely used LeBlanc model for pile design adopts this approach, with the drawback that no unique simplification of the load time history exists. This work reformulates the LeBlanc model by replacing its explicit dependence on cycle counting with a single state variable, enabling extension to arbitrary loading histories.

Introduction

Over their operational lifetime, offshore wind turbine monopiles are subjected to millions of lateral load cycles. The cumulative effects of cyclic loading are critical for pile design, yet the problem, by its nature, is not as well-defined as monotonic lateral loading problems. The term cyclic loading is typically used by industry to describe rather complex problems. In the laboratories, the term is conceived differently and refers to regular sinusoidal load cycles (Houlsby et al. 2020). Common design methods are based on low-fidelity theoretical models calibrated against regular load-cycle responses from laboratory tests, since these tests can be easily characterised (Fig. 1). Such tests bear little resemblance to the pseudo-random loading experienced in the field. Efficient design methods are needed that can [a] be calibrated using laboratory tests, but [b] generalise to the complexity of the field loading. The LeBlanc et al. (2010a) model is well-suited for problems of type [a]. This work seeks, through reformulation, to generalise the model to accommodate [b].

Methodology

To predict accumulated rotation, LeBlanc et al. (2010a) introduced a functional relationship relating the stress magnitude, asymmetry and number of cycles to the accumulated rotation:

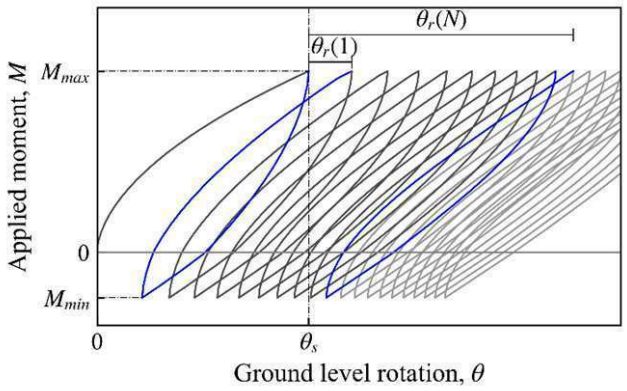


Figure 1: Characterising observed behaviour of a monopile subjected to cyclic loading.

$$\frac{\theta_r}{\theta_s} = T_b T_c N^{m_\alpha} \quad (1)$$

in which θ_r is the accumulated rotation and θ_s is the strain under monotonic loading up to the peak cyclic stress. T_b is a function of the normalised peak cycle magnitude, while T_c is a function of the normalised cycle asymmetry. N is the number of cycles applied, while m_α is an exponent found to be around 0.3.

LeBlanc et al. (2010b) extended Eq. (1) to a cycle-counting design model that accounted for sinusoidal loading packages through an iterative strain superposition procedure.

Inverting Eq. (1) yields an equivalent cycle count for the current accumulated rotation:

$$N = \left[\frac{\theta_r}{\theta_s T_b T_c}\right]^{\frac{1}{m_\alpha}} \quad (2)$$

Where N is the number of sinusoidal cycles of a specific type that have produced the current accumulated rotation. Differentiating Eq. (1) by the cycle number, N, and substituting N with the equivalent cycle count from Eq. (2) defines an incremental LeBlanc version that eliminates dependence on cycle number, N:

$$\frac{d\theta_r}{dN} = [\theta_s T_b T_c]^{\frac{1}{m_\alpha}} \; m_\alpha \; [\theta_r]^{\frac{m_\alpha - 1}{m_\alpha}} \qquad (3)$$

Results

The key finding of this work is that the LeBlanc model possesses a state-variable structure. Eq. (3) shows that the rate of accumulation depends only on the current rotation, θ_r. Thus, the accumulated rotation serves as a single state variable fully characterising the effects of prior history in the LeBlanc model. Practically, two piles with identical accumulated rotations are indistinguishable, no matter their previous loading history.

As a separable differential equation, Eq. (3) also admits a linearisation that simplifies the procedure of strain superposition.

An example of the implications of Eq. (3) is presented in Tab. 1 and Fig. 2. Sequences of tested loading regimes from LeBlanc et al. (2010b) are modelled, where the regimes are applied in increasing and decreasing order. Fig. (2) shows that the final accumulated rotation is unaffected by the loading order, in agreement with the test results reported in LeBlanc et al. (2010b). When a subsequent loading regime C is applied at the end, the response is independent of preceding loading.

Table 1: Modelled load regimes A, B and C.

Regime	N	T_b	T_c	$\theta_s\ (rad)$
A	10^4	0.055	1	0.45×10^{-3}
B	10^2	0.091	1	0.90×10^{-3}
C	10	0.135	1	1.60×10^{-3}

Future work

Eq. (3) is still dependent on cyclic knowledge, since θ_s, T_b and T_c can only be characterised with full knowledge of the current load cycle. Ongoing work aims to identify a continuous function g, dependent on the applied moment M and the plastic strain rate $\dot{\theta}_p$, which obeys:

$$\int_0^{t_N} g(M, \dot{\theta}_p)\, dt = [\theta_s T_b T_c]^{\frac{1}{m_\alpha}} \qquad (4)$$

for any single cycle, where t_N is the period. Eqs. (3) & (4) form an intrinsic LeBlanc model:

$$\frac{d\theta_r}{dt} = m_\alpha \; g(M, \dot{\theta}_p) \; [\theta_r]^{\frac{m_\alpha - 1}{m_\alpha}} \qquad (5)$$

which is a first-order differential equation in time that generalises the LeBlanc model to arbitrary random loading history inputs.

References

[1] Houlsby et al. (2020). *Methods of Numerical Analysis of Monopiles under Pseudo-Random Lateral Loading, in Proceedings of the 4th International Symposium on Frontiers in Offshore Geotechnics (ISFOG 2020), Austin,* Texas, 2020

[2] LeBlanc et al. (2010a). *Response of stiff piles in sand to long-term cyclic lateral loading, Geotechnique, Vol. 60*

[3] LeBlanc et al. (2010b). *Response of stiff piles to random two-way lateral loading, Geotechnique, Vol. 60*

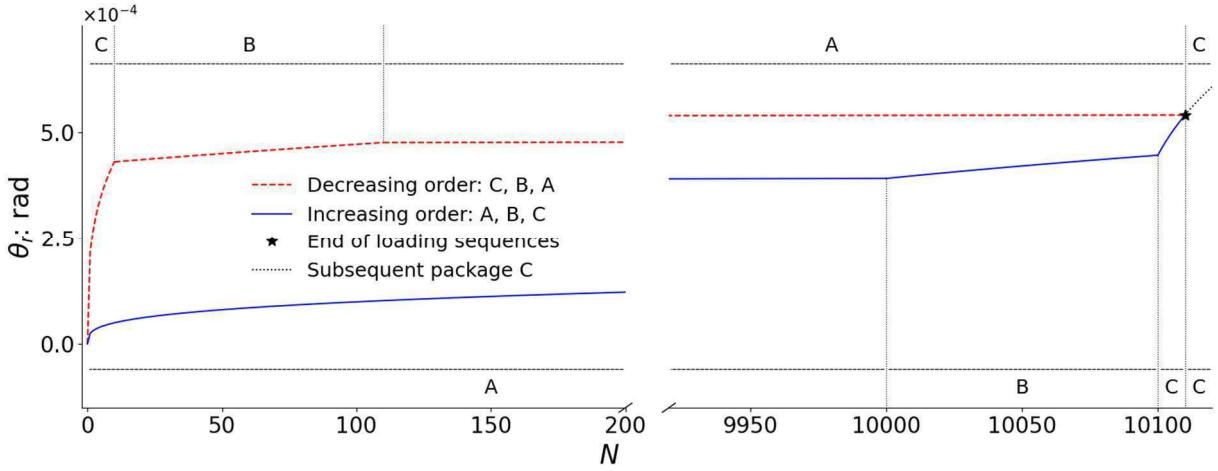


Figure 2: Envelopes of modelled pile rotation using Eq. (3) with $m_\alpha = 0.3$ plotted against the cycle number for an increasing and equivalent decreasing load sequence.

An Experimental Framework for Assessing Soil Reactions Acting on Laterally Loaded Monopile Segments

Jayne M. Han*[1], Harvey Burd[2], Vincenzo Nardelli[3], and Miad Saberi[4]
[1, 2, 3, 4] Department of Engineering Science, University of Oxford, United Kingdom
(E-mail: jayne.han@eng.ox.ac.uk, harvey.burd@eng.ox.ac.uk, vincenzo.nardelli@eng.ox.ac.uk, miad.saberi@eng.ox.ac.uk)

Abstract

This paper presents an experimental framework, which was developed for directly obtaining the soil reactions acting on a laterally loaded monopile, using the novel model testing device ("pile segment testing device") that was recently developed at the University of Oxford. A numerical study was carried out to assess the feasibility of the proposed framework and the testing device. The results of the numerical study demonstrated that the testing device is capable of yielding soil reaction curves, which can be implemented in a 1D finite element (OxPile) model to produce accurate predictions of the monotonic lateral load-displacement curves of full-scale monopiles.

Introduction

Monopile foundations of offshore wind turbines are subjected to a large number of lateral loading cycles over their design lifetime. Various experimental studies have explored the behaviour of monopiles under long-term lateral cyclic loading, but mostly with small-scale models in 1*g* conditions. Due to this, there is limited understanding of monopile behaviour under in situ stress conditions, which is crucial for the calibration of cyclic monopile design models.

To address this, a novel pile segment testing device was developed by Malhotra and Byrne [1] at the University of Oxford. The device was designed to measure the soil reactions acting on laterally loaded monopiles under in situ stress conditions. As shown in Figure 1, the device consists of a 50 mm diameter pile model embedded in soil inside a pressure chamber, an air cushion that applies vertical pressure to the soil, and actuators that apply displacements to the pile ends. The pile model represents a portion of a prototype monopile at a given depth, corresponding to the stress level applied in the device. A portion of a monopile is referred to as a "segment" in the following descriptions.

This paper presents an experimental framework for directly obtaining a full set of Soil Reaction Curves (SRCs) from the device, which can be used to predict the lateral load-displacement behaviour of full-scale monopiles. The framework is validated through a numerical study on the device. The current paper is concerned with monotonic loading conditions only.

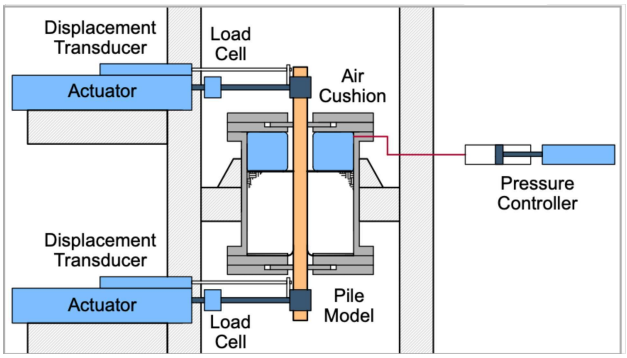


Figure 1: Pile segment testing device

Methodology

2.1 Proposed Experimental Framework

A full-scale monopile of interest can be analysed by first dividing it into multiple segments of equal length (Figure 2a). Each full-scale segment is taken to correspond to a segment of the pile model in the testing device with the same depth-to-diameter ratio *z*/*D*. Considering this, the device can be used to obtain the soil reactions acting on each (i^{th}) segment of the full-scale monopile, following the procedures outlined below.

(1) Apply the vertical stress $\sigma'_{v0,app}$ to the soil

in the testing device (Figure 2b) that is equal to the initial effective overburden stress at the mid-point of the corresponding full-scale segment ($\sigma'_{v0,i}$; Figure 2a).

(2) Apply displacements to the pile model, consistent with the average displacement (v_i) and rotation (ψ_i) of the full-scale segment.

(3) Extract and normalise the SRCs from the i^{th} segment of the pile model.

(4) Repeat steps (1) – (3) for all segments, and input the normalised SRCs to the 1D finite element (OxPile) model to estimate the monotonic lateral load-displacement curve of the full-scale monopile.

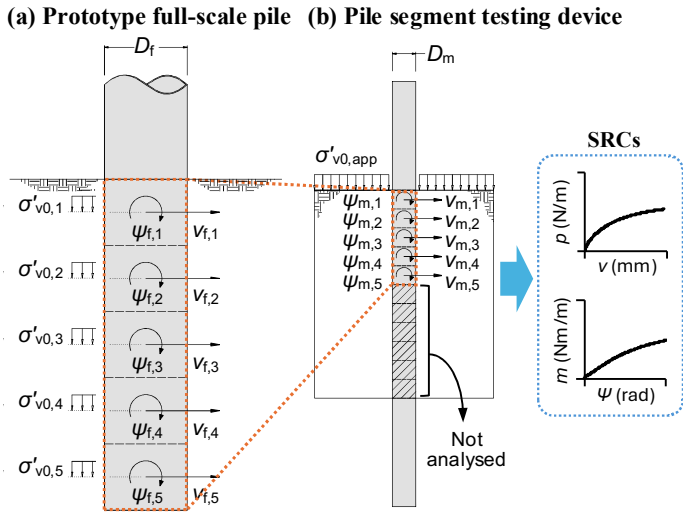


Figure 2: Framework for obtaining the SRCs of each full-scale pile segment from the pile segment testing device (5 segments).

2.2 Example Numerical Study

A numerical study was conducted using PLAXIS 3D to explore the feasibility of the proposed experimental framework. The study considers an example prototype monopile design with a diameter of D = 8.75 m and an embedment ratio of L/D = 3 (D2 monopile [2]), installed in Dunkirk sand with the relative density of D_r = 75%. The hardening soil model with small-strain stiffness (HSsmall model) [3] was adopted.

Two numerical models were constructed: (1) Model of the prototype monopile to obtain benchmark results for the load-displacement curve; (2) Model of the testing device to obtain SRCs using the proposed framework, and therefore predict the load-displacement curve of the prototype monopile.

Results

The load-displacement curve, which was estimated using the SRCs from the testing device model and the proposed framework, closely approximates the curve that was directly extracted from the numerical model of the full-scale monopile. This suggests that the use of the SRCs from the pile segment testing device is feasible for accurately predicting the full-scale pile behaviour.

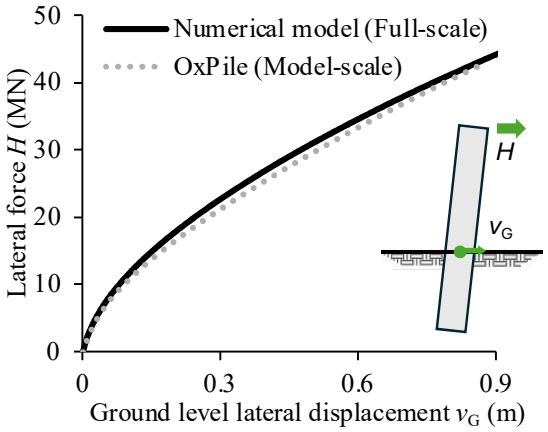


Figure 3: Estimated lateral load-displacement curves of the prototype monopile.

Future work

An instrumented monopile model, equipped with Fibre Bragg Grating (FBG) sensors, will be developed to enable direct measurements of the soil reactions. A series of model tests will then be conducted on the instrumented pile and in situ soil, using the testing device following the proposed experimental framework, to predict the behaviour of full-scale monopiles tested under field conditions.

References

[1] Malhotra, S. & Byrne, B.W. (2024). *Cyclic lateral load testing of model pile segments in sand: Equipment development and early results.* In: Geo-Congress 2024. Vancouver, Canada: American Society of Civil Engineers.

[2] Burd, H.J., et al. (2020). *PISA design model for monopiles for offshore wind turbines: Application to a marine sand.* Géotechnique, Vol. 70, pp. 1048-1066.

[3] Benz, T. (2007). *Small-strain stiffness of soils and its numerical consequences.* Ph.D. Thesis, University of Stuttgart.

First principles approach for calculating axial and bending loads from strain measurements in laterally loaded piles

F. Van der Berg[1], K. Briggs[2], W. Powrie[3], and J. Smethurst[4]

[1, 2, 3, 4] Department of Civil, Maritime and Environmental Engineering, University of Southampton, United Kingdom

(E-mail: F.A.VAN-DER-BERG@soton.ac.uk)

Abstract

The generalised moment-curvature relationship can be used to calculate bending moments from strain measurements of a pair of strain gauges in a laterally loaded pile, but this method has several shortcomings. A first principles approach allows moments and axial forces to be calculated and load profiles to be plotted, while also considering non-linear material behaviour and concrete cracking. This allows much more insight into the behaviour of the materials in the cross section, giving designers the opportunity to optimise future designs.

Introduction

Understanding the behavioural mechanism of geotechnical infrastructure is essential for optimised, cost-effective and practical design[1]. Instrumented infrastructure is an essential part of understanding these behavioural mechanisms. Earth Retaining structures instrumented with pairs of strain gauges can be used to calculate the loads in the structure[2-5].

The general moment curvature relationship can be used to calculate bending moments from a pair of strain gauges, but this has several shortcomings, including axial loads not being calculated, linear material behaviour, concrete cracking not being accounted for and load profiles not being plotted. Using a first principles approach addresses all these shortcomings of using the general moment-curvature relationship to analyse strain results in the cross-section of a laterally loaded pile.

Methodology

A pair of strain gauges were installed at opposite sides of a reinforced concrete laterally loaded pile. The strain gauge results gave two distinct strain measurements which were used to calculate the gradient of strain across the cross section (known as curvature) as well as the y-intercept (known as the neutral axis). The general moment-curvature relationship (equation 1) was not used due to the shortcomings discussed above, but rather a first principles method was used, discussed below.

$$\boldsymbol{M = EI * \kappa} \quad (1)$$

The cross section was divided into distinct horizontal slices, differentiating between concrete and steel. Each distinct area was assigned a strain value based on the curvature and proximity to the neutral axis. The strain was converted to stress using material models for concrete and steel were taken as those proposed by BS 8110[6]. Force could then be calculated using the slice areas, and moments taken about the centroid of the cross section.

Results

Figure 1 shows the calculated profiles of strain, stress, force and moment. The force

and moment profiles were summed across the entire cross section to get the total force and moment across the cross-section.

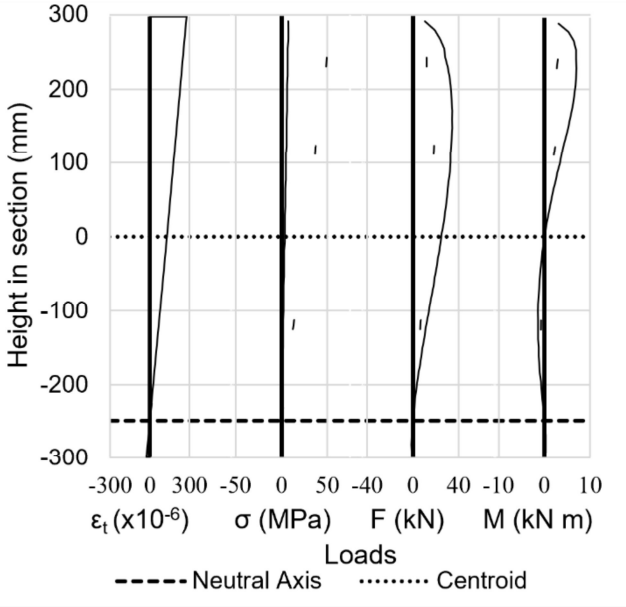


Figure 1: Strain, stress, force and moment profile in the cross-section of a reinforced concrete laterally loaded pile.

The conversion from strain to stress using a function rather than a fixed modulus of elasticity (*E*) allowed non-linear material behaviour to be considered, and taking moments about the centroid rather than using a fixed second moment of area (I) allowed changes in cross sectional area (due to concrete cracking). The addition of axial forces to the analysis of strain measurements and the plotting of the force and moment profiles gave additional insight into the behavioural mechanism of the pile.

Future work

Using this method for analysing strain measurements in geotechnical retaining structures will give additional valuable information about the behavioural mechanism of the structure, allowing design optimisations for future projects.

Acknowledgements

To the University of Southampton and Mott Macdonald for funding this research.

References

[1] W. Powrie, "The role of behavioural mechanisms and observed performance in affordable, resilient geotechnical infrastructure," in *The 64th Rankine Lecture*, London, 2026.

[2] J. A. Smethurst and W. Powrie, "Monitoring and analysis of the bending behaviour of discrete piles used to stabilise a railway embankment," *Géotechnique,* vol. 57, no. 8, pp. 663–677, 2007, doi: 10.1680/geot.2007.57.8.663.

[3] J. A. Smethurst, N. Bicocchi, W. Powrie, and A. S. O'Brien, "Behaviour of discrete piles used to stabilise a tree-covered railway embankment," *Géotechnique,* vol. 70, no. 9, pp. 774–790, 2020, doi: 10.1680/jgeot.18.P.150.

[4] N. Bicocchi, "Structural and geotechnical interpretation of strain gauge data from laterally loaded reinforced concrete piles.," Doctoral Thesis, School of civil engineering and the environment, University of Southampton, 2011. [Online]. Available: https://eprints.soton.ac.uk/210949/

[5] C. W. W. Ng, M. L. Lings, and D. F. T. Nash, "Back-analysing the bending moment in a concrete diaphragm wall," *The Structural Engineer,* vol. 70, pp. 421–426, 1992.

[6] *Structural Use of Concrete.*, BSI, Milton Keynes, 1985.

Investigating Re-entrant Corners in Braced Excavations

Arthur Chai*[1], Charles E. Augarde[2], William M. Coombs[3] and Mao Ouyang[4]
[1, 2, 3, 4] Department of Engineering, Durham University, United Kingdom
(E-mail: arthur.chai@durham.ac.uk)

Abstract

Re-entrant (convex) corners in braced excavations for basement construction lack detailed design guidance despite their ubiquity, leading to conservative designs or the use of computationally expensive finite element (FE) analyses. This study investigates strength and stiffness behaviour at re-entrant corners utilising analytical and numerical models to support more efficient designs for multi-stage braced excavations that include a re-entrant corner.

Introduction

Aside from preventing failure of soils or support systems in braced excavations, limiting wall deflections to ensure compliance with serviceability requirements set by standards such as those in Eurocode 7 [1] are important to the geotechnical engineer.

While guidance exists for simple excavation geometries, real excavations frequently contain re-entrant (convex) corners due to spatial constraints, such as in urban environments where existing structures lie close to and can be affected by the excavation, intensifying the challenge of controlling deflections. Yet, design guidance for re-entrant corners is limited [2, 3], leading to the adoption of conservative support measures or computationally expensive FE modelling, often without assessing whether such measures are necessary to begin with.

This study therefore aims to investigate deflection behaviour at re-entrant corners in braced excavations and evaluate potential strategies that are more efficient than simply defaulting to full-scale numerical simulations. The work will focus on typical multi-stage braced excavations and will combine analytical and numerical models to quantify and interpret movements.

The study is linked to a PhD the first author started at Durham University in October 2025, and much of what is written below is planned rather than completed work.

Methodology

2.1 Analytical Modelling

Analytical models are being developed using upper bound limit analysis [4] to assess strength at re-entrant corners. As corner behaviour is inherently three-dimensional, out-of-plane corner stiffness effects are incorporated instead of assuming plane strain, and the model focuses on a single re-entrant corner with semi-infinite adjoining walls and a uniform excavation depth.

For the analytical approach, soil is modelled using the Mohr-Coulomb constitutive model under small-deformation assumptions, and the output of the analytical model is the maximum surcharge that can be applied within close proximity to the re-entrant corner.

2.2 Numerical Modelling

A numerical model is under development based on an in-house, bespoke FE code written in the language Julia. Soil is represented by tetrahedral continuum elements with parameters typical to London Clay, while the retaining wall is modelled using wedge elements. Soil in the FE modelling is described using a combined Small Strain Overlay [5] and Drucker-Prager model to capture its non-linear elastic and plastic behaviour. Emphasis is placed on pre-failure deformations, as these are most relevant to serviceability limit states, whereas post-failure deformations are excluded as

they do not represent acceptable design conditions.

A geostatic state is initialised using a simplified K_0 approach (Chapters 8 and 24 of [6]), and non-linear equilibrium for each excavation stage is obtained using a Newton-Raphson scheme (maximum 40 iterations, tolerance 1×10^{-5}). Boundary conditions consist of roller restraints on the vertical faces, a fully fixed base, and a free top surface. Excavation staging is represented by the sequential removal of soil layers within the excavated region and the activation of bracing levels in the corresponding layer, with struts modelled as axial springs and installed with their initial preloads.

Mesh dependency checks are performed by progressively refining the mesh until the difference between current and preceding wall deflection profile fall below 5%, through the use of point-wise differences across the profiles. The influence of the corner-boundary proximity is assessed similarly. The numerical model will then be verified by reproducing published deflection curves for concave (<180°) corners, before being extended to 90° re-entrant corners and compared against available data.

2.3 Parametric studies and evaluation strategies

A structured parametric study will be conducted to identify the conditions under which the analytical predictions remain reliable. Considered parameters include re-entrant corner angle, bracing spacing and arrangement, and the relative position of the corner within the excavation plan. Again, the resulting deformation profiles of these analyses will be compared against published data from real-world excavations to further assess the robustness of the numerical models.

Future work

The numerical models could be extended to include multiple re-entrant corner geometries, which are common in typical excavation layouts. An additional extension would be the incorporation of an optimisation framework to automate parameter selection and improve design efficiency, potentially integrating modern techniques such as machine learning.

Acknowledgements

The author gratefully acknowledges funding from the Engineering and Physical Sciences Research Council (EPSRC) for this project.

References

[1] British Standards Institution, (2013). BS EN 1997-1:2004+A1:2013 – Eurocode 7: Geotechnical Design – Part 1: General Rules. London: BSI Standards Limited.

[2] Construction Industry Research and Information Association, (2003). CIRIA C580: Embedded Retaining Walls – Guidance for Economic Design. London: CIRIA.

[3] Crossrail Ltd., (2010). CR-STD-303-9: Civil Engineering Design Standards – Part 9: Temporary Works. London: Crossrail Ltd. Version 5.0.

[4] Davis, R.O. and Selvadurai, A.P.S., (2002). Plasticity and Geomechanics. Cambridge: Cambridge University Press.

[5] Benz, T., Vermeer, P.A. and Schwab, R., (2009). A small-strain overlay model. International Journal for Numerical and Analytical Methods in Geomechanics, 33(1), pp. 25–44. https://doi.org/10.1002/nag.701

[6] Atkinson, J.H., (2007). The Mechanics of Soils and Foundations. 2nd Edition. London: Taylor & Francis.

Numerical modelling of scour effects on pile group supported bridges

Ansam Al-Karawi*[1], Luke J. Prendergast[2] and Nick Thom[3]
[1, 2, 3] Department of Civil Engineering, Faculty of Engineering, Civil Engineering Department, School of Engineering, University of Nottingham, United Kingdom
(E-mail alyaa48@nottingham.ac.uk, Luke.Prendergast@nottingham.ac.uk, nicholas.thom@nottingham.ac.uk)

Abstract

Erosion significantly threatens structures in flowing water, such as bridge piers and abutments, by reducing foundation embedment. This can lead to excessive deformation and tilting, compromising structural stability and increasing collapse risk, thereby affecting human safety. Understanding scour and mitigating its effects remains challenging. This study examines how scour hole formation influences the lateral loading behavior of a bridge pile group. A Winkler spring-based numerical model is developed to investigate scour effects on pile lateral response under linear conditions. The presence of scour holes notably affects pile deflection and bending moments, especially when scour hole asymmetry is considered, which provides a more realistic representation of soil-pile interaction by capturing changes in overburden pressure and stiffness due to scour-induced stress reductions.

Introduction

Scour, namely the gradual erosion of soil around bridge foundations, is a leading cause of failure, often with sudden, costly consequences [1,2]. While extensive research exists on uniform scour around single piles or groups [3], real-world scour is frequently non-uniform, creating asymmetric scour holes around pile groups due to flow interference, jetting, and sheltering effects. This asymmetry can induce differential settlements, uneven foundation stiffness, and unexpected torsional behavior, significantly affecting global bridge stability. However, most existing studies simplify pile groups as equivalent single piles or assume uniform scour [4], neglecting the full three-dimensional behavior and overburden soil distribution after scouring. Few investigations have addressed non-uniform scour in whole-bridge models [5], especially under 3D conditions. To fill this gap, this study develops a high-fidelity 3D numerical model in MATLAB to simulate non-uniform scour evolution around pile-group foundations, incorporating post-scour over burden soil pressure.

Methodology

An idealized two-span concrete box-girder bridge (30 m total length, 12 m width, 1.2 m thickness) is modeled, featuring an 8 m tall pier (diameter 1 m) resting on a 2×2 pile group foundation (four drilled shafts of 0.85 m diameter and 12 m length) in medium dense sandy soil (relative density 50%, bulk unit weight 18.5 kN/m³). All structural components are assigned a Young's modulus of 2 × 10¹⁰ N/m². The bridge is discretized using six-degree-of-freedom Euler-Bernoulli frame elements, with the global static equilibrium equation $[K]_{global} \cdot \{d\} = \{F\}$; $[K]_{global}$ is global stiffness matrix, $\{d\}$ is nodal displacement, and $\{F\}$ is applied force solved for nodal displacements. Roller supports are applied at both deck ends, and the model is validated against SAP2000 simulations. Soil-structure interaction is incorporated via horizontal Winkler springs (linear *p-y* curves) at 1 m discretized pile segments, where spring stiffness is derived from CPT-based calculations including small-strain shear modulus (G_0) and Young's modulus (E_0), following established subgrade reaction modulus equations. Scour effects are simulated by eliminating springs at specified depths ($1D$, $2D$, and $3D$, where $D = 0.85$ m), with upstream piles experiencing deeper scour than downstream piles to capture differential erosion patterns. Two overburden stress-history cases are evaluated for each scenario: Case 1 recalculates vertical stress from the new riverbed level (accounting for scour effects), while Case 2 maintains the original no-scour stress distribution (ignoring scour effects). The water level is 2 m below the top of the pier. The study also examined

seven different scours scenarios. Test 1 was the no-scour baseline. Tests 2–4 involved uniform scour (equal depths of 1, 2, and 3 m at both front and rear piles). Tests 5–7 involved non-uniform scour, with front depths always greater than rear depths.

Results

This study investigates the influence of scour depth (both uniform and non-uniform) on the lateral response and bending moments of a bridge pile group in medium dense sandy soil, under combined off-center wind and debris loads. Two cases of overburden stress are considered: Case 1 (post-scour stress reduction) and Case 2 (unchanged stress). Results show that lateral deflections (Figure 1) and bending moments (Figure 2) increase with scour depth, with front piles deflecting more than rear piles under non-uniform scour. Case 1 consistently produces greater deflections and moments than Case 2, highlighting the importance of accounting for stress history effects after scouring to avoid underestimating pile deformations.

Future work

Future work aims to understand the dynamic response of a bridge to scour under different scour hole geometries, considering the remaining soil surrounding the scour hole under random excitation loads.

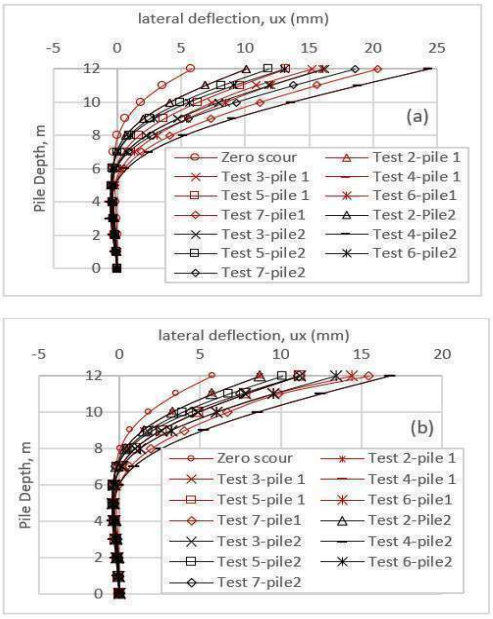


Figure 1 Lateral pile deflection profile responses of front and rear piles (a) Case 1 and (b) Case2.

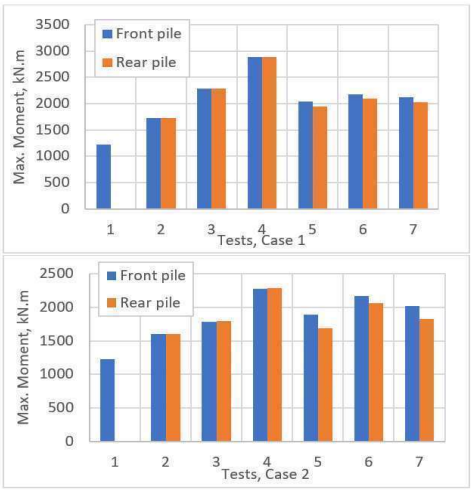


Figure 2 Maximum bending moment for different tests and a) Case 1, b) Case 2.

Acknowledgements

The author (Ansam Al-Karawi) gratefully acknowledges the contribution of Schlumberger Foundation which awarded the author with a fellowship supporting her PhD study through Faculty for the Future Program.

References

[1] Fagundes, D.F., Pimpão, C.Y. and Servi, S.P., 2024. Mechanical behaviour of dredging waste in the port of Rio Grande by adding stabilizing agents. International Journal of Geotechnical Engineering, 18(4), pp.433-443.

[2] Hamidifar, H., Mohammad Ali Nezhadian, D. and Carnacina, I., 2022. Experimental study of debris-induced scour around a slotted bridge pier. Acta Geophysica, 70(5), pp.2325-2339.

[3] Arneson, L.A., Zevenbergen, L.W., Lagasse, P.F. and Clopper, P.E., 2012. Evaluating scour at bridges (No. FHWA-HIF-12-003). National Highway Institute (US).

[4] Prendergast, L.J., Hester, D. and Gavin, K., 2016. Determining the presence of scour around bridge foundations using vehicle-induced vibrations. Journal of Bridge Engineering, 21(10), p.04016065.

[5] Fioklou, A. and Alipour, A., 2019. Significance of non-uniform scour on the seismic performance of bridges. Structure and Infrastructure Engineering, 15(6), pp.822-836

Numerical modelling and validations on artificial ground freezing under groundwater flow condition

Gyu-Hyun Go*[1]
[1] School of Architecture, Civil and Environmental Engineering, Kumoh National Institute of Technology, Republic of Korea
(E-mail:gyuhyungo@kumoh.ac.kr)

Abstract

Artificial Ground Freezing (AGF) has been extensively employed in underground projects for soft ground reinforcement and groundwater cutoff. This study developed an artificial freezing experimental facility based on an indoor soil tank that simulates groundwater flow conditions and conducted artificial freezing experiments under groundwater flow velocity conditions. The soil temperature distribution within the tank was measured following the operation of the freezing system and compared with the results of numerical analysis performed under the same conditions.

Introduction

Artificial Ground Freezing (AGF) is a construction method that freezes soft ground to increase ground stiffness and simultaneously ensure waterproofing and excavation stability(Sres, 2009); it is being actively applied in major developed countries such as Europe and the United States. The construction efficiency of AGF depends on the formation of continuous frozen walls. However, actual excavation sites always face uncertainty in the wall formation process due to the interaction of ground environmental conditions, soil properties, and spatial variability. In particular, groundwater flow has a highly sensitive impact on changes in the shape of frozen walls due to convective heat transfer and cold heat loss effects.

To investigate these issues, this study developed an artificial freezing experimental facility based on an indoor soil tank that simulates groundwater flow conditions and conducted artificial freezing experiments under groundwater flow velocity conditions. The soil temperature distribution within the tank was measured following the operation of the freezing system and compared with the results of numerical analysis performed under the same conditions.

Methodology

The constructed soil tank freezing system consisted of a flow control device, a constant temperature water tank, a refrigeration chiller, and high-performance monitoring equipment. Multiple temperature sensors were installed inside the soil tank to monitor temperature changes by time and space during the freezing process (Fig. 1).

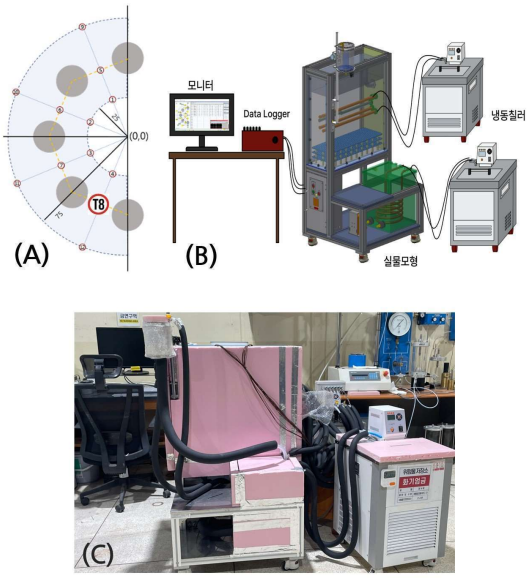


Figure 1: Experiment setup

The model soil tank was constructed in the shape of a rectangular prism with dimensions of 0.205 m (W) × 0.600 m (L) × 0.290 m (H), and was designed to allow a constant flow rate of temperature-treated water to be uniformly injected from the bottom of the tank. Additionally, experiments were conducted under conditions of groundwater flow velocity and no flow velocity, and the formation of frozen walls and soil temperature distribution characteristics were compared under each condition. The parameters according to each experimental condition are summarized in Table 1.

Table 1: AGF testing condition

Groundwater Velocity	Hydraulic gradient	Initial soil temperature
0 m/day	0	4 ℃
1.5 m/day	0.74	

Results and discussions

Fig. 2 shows the results of comparing the frozen walls in the experiment and numerical analysis at the end of the freezing process. In the experiment without groundwater flow, the shape of the frozen wall developed into a relatively uniform form, whereas in the experiment with groundwater flow, the wall shape was thin at the bottom and asymmetrically thick at the top. Furthermore, the experiment and numerical analysis showed a high degree of agreement overall across the two different experimental conditions. This numerical analysis technique is expected to be utilized for evaluating the formation of frozen walls by linking field temperature monitoring data with numerical analysis when applying artificial freezing methods in future underground excavation projects in urban areas.

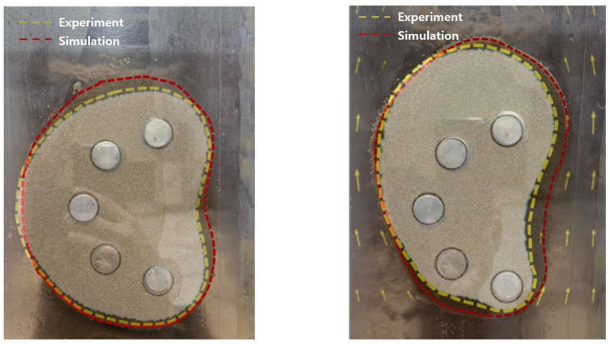


Fig. 2. Comparison of Freezing Wall Boundary by Groundwater Flow Velocity (Experiment vs. Numerical Analysis)

Acknowledgements

This work was supported by the National Research Foundation of Korea(NRF) grant funded by the Korea government(MSIT) (No. 2022R1C1C1006507).

References

[1] Sres, A., 2009. Theoretische und experimentelle Untersuchungen zur Künstlichen Bodenvereisung im Stromenden ¨ Grundwasser [Ph.D. thesis]. ETH Zürich.

Data-Driven and AI-Based Approaches

Predicting PFAS transport through landfill composite liner using physics-informed neural networks

Yu Tan[1] and Yuan Feng*[2]
[1] Department of Civil Engineering, Shanghai University, Shanghai, China
(E-mail: yutan@shu.edu.cn)
[2] Department of Civil and Environmental Engineering, University of Maryland-College Park, MD, USA
(E-mail: yfeng6@umd.edu)

Abstract

A physics-informed neural network (PINN) was developed to predict per- and polyfluoroalkyl substances (PFAS) transport through landfill composite liners (a compacted clay liner overlaid by a geomembrane). The developed model was validated using the PFAS breakthrough and elution curve from a constant-flow column test with R^2 = 0.996. The PINN prediction shows that PFAS concentrations below the composite liner with a geomembrane defect are lower than the maximum contaminant level of PFAS within 100 years, i.e., <0.14 vs. 4 ng/L. The developed open-access PINN model can be used for evaluating potential PFAS leakage through landfill liners.

Introduction

Per- and polyfluoroalkyl substances (PFAS) have been extensively used in consumer products for decades worldwide. Many of these products is disposed in municipal solid waste landfills, accumulating thousands ng/L PFAS in landfill leachates. PFAS concentrations in landfill leachates are higher than PFAS maximum contaminant levels (MCLs) in drinking water in the US (4~10 ng/L), raising concerns about PFAS leakage through landfill composite liners (e.g., a clay liner overlaid by a geomembrane). To assess the potential leakage, a tool to predict PFAS transport through liners is highly desired.

Physics-informed neural networks (PINNs) have been emerging as a powerful tool for predicting contaminant transport, which incorporates partial differential equations (PDEs) to solve forward and inverse problems. PINNs evaluate the loss functions not only for observations but also for the derivatives from PDEs using NNs to effectively utilize data [1].

This work trained a PINN model using the PFOS transport data from a column test [2] and applied the model for predicting PFAS transport through landfill composite liners.

Methodology

2.1 Computational model

Advection-diffusion equation is used to describe PFAS transport in porous media, including clay liner and subgrade:

$$\varepsilon\frac{\partial C_l}{\partial t} + (1-\varepsilon)\rho_s\frac{\partial C_s}{\partial t} + v\nabla C_l - D\nabla^2 C_l = 0 \qquad (1)$$

where C_l is the PFAS concentration in the aqueous phase, C_s is the amount of PFAS adsorbed to the solid phase, ε is the porosity when the porous media is saturated, ρ_s is the density of the solid phase, t is elapsed time, D is the PFAS diffusion coefficient, and v is the Darcy velocity. The adsorption of PFAS to solid phase can be described using the nonlinear Freundlich isotherm. Pure diffusion is applied to describe PFAS transport through geomembranes (GM) based on Tan [3].

2.2 PINN

A PINN model was built to solve the PDEs as described above along with the specific boundary and initial conditions. The neural network was constructed with a series of weight matrices and bias vectors generated from the PDEs. The neural network was trained to minimize the loss functions that quantified the differences between the predicted values and the observations or the derivatives. More details about PINN implementation can be found in Feng et al. [4].

Results

3.1 Model Validation

The developed PINN model was used to predict PFAS transport through a saturated

sand column. The sand was pumped with 0.27 mg/L PFOA solution, followed by a PFAS-free solution to elute the PFOA, all at a constant flow rate, by Garza-Rubalcava [2].

PINN predicted PFOA concentrations in the effluents are shown in Fig. 1. The predicted concentrations are in good agreement with the measurements (R^2 = 0.996). A finite-element modeling (FEM) was also conducted to predict the PFOA transport, with a R^2 of 0.991. PINN shows a better prediction than FEM between 1000 and 1800 min.

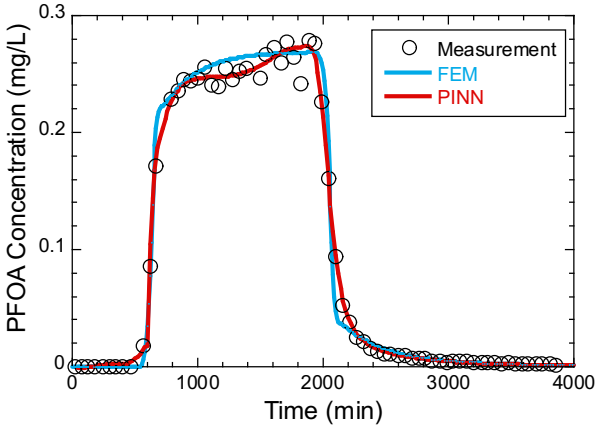


Figure 1: Predicted PFOA concentrations in the effluents of the column test

3.2 PFAS transport through composite liner

The validated PINN model was extended to a 10-m-wide landfill composite liner with a GM defect at the left side of the GM edge. An axisymmetric boundary was applied to the left side of the domain. Three layers of components were simulated, including a GM with a defect, a saturated compacted clay liner (CCL), and an unsaturated subgrade. Groundwater table (GWT) was included in the subgrade, which was set at 1.5 m below the CCL. PFAS concentration in landfill leachate was 1000 ng/L, and leachate head was 0.3 m. The geometry of the domain and transport parameters can be found in Tan [3,5].

The predicted PFAS concentration distribution at the GWT after the service of 100 years are shown in Fig. 2. The PFAS concentration below the defect is elevated but sharply decreases away from the defect. At 100 years, PFAS at the GWT accumulate to the maximum concentration, which is still lower than the MCL, i.e., <0.14 vs. 4 ng/L. The prediction suggests that landfill composite liners are effective in containing PFAS.

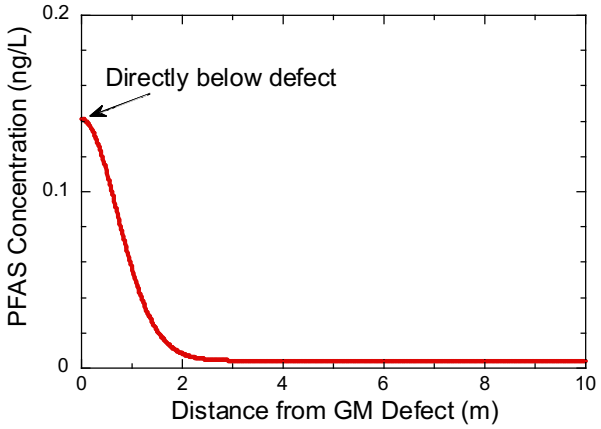


Figure 2: PINN predicted PFAS concentrations at the GWT at 100 years

Future work

In the future, the developed PINN model will be trained using different liner material properties and boundary conditions. The trained model will be used as an open-access tool for the industry to estimate the potential PFAS leakage risk of landfills.

References

[1] Raissi, M., Perdikaris, P., Karniadakis, G., (2019). Physics-informed neural networks: A deep learning framework for solving forward and inverse problems involving nonlinear partial differential equations. *J. Comput. Phys.*, Volume 378, pp. 686-707.

[2] Garza-Rubalcava, U., Klevan, C., Pennell, D., Abriola, L., (2025). Transport and competitive interfacial adsorption of PFOA and PFOS in unsaturated porous media: Experiments and modeling. *Water Res.*, Volume 268, pp. 122728.

[3] Tan, Y., (2024). Effectiveness of Landfill Composite Liners in Containing per-and Polyfluoroalkyl Substances. PhD Thesis, UW-Madison, WI, USA.

[4] Feng, Y., Eun, J., Kim, S., Kim, Y., (2025). Application of physics-informed neural networks solution to coupled thermal and hydraulic processes in silty sands. *Int. J. Geo-Eng.*, Volume 16(1), pp. 3.

[5] Tan, Y., Bradshaw, S., Edil, T., Benson, C., (2026). Hydraulic conductivity of geosynthetic clay liners and compacted clays to leachate with PFAS. *J. Geotech. Geoenviron. Eng.* In press.

Applying surrogate models to predict tunnelling-induced building settlements

J. Liu*[1], A. Tsiampousi[2], A. Ruiz López[3] and D.M.G. Taborda[4]
[1,2,3,4] Department of Civil and Environmental Engineering, Imperial College London, UK
(E-mail: j.liu22@imperial.ac.uk, aikaterini.tsiampousi05@imperial.ac.uk, agustin.ruizlopez@seequent.com, d.taborda@imperial.ac.uk)
[3]Seequent – The Bentley Subsurface Company, Delft, The Netherlands

Abstract

Tunnel excavation can induce ground movements that deform adjacent buildings, with the interaction influenced by soil conditions, tunnel geometry, and structural stiffness, requiring advanced numerical methods to consider these factors simultaneously. This study proposes an alternative approach, developing a surrogate model using an artificial neural network (ANN) to enable quick estimates of building settlement profiles caused by tunneling. The model is trained on numerical simulation data, and its performance is evaluated systematically. The ANN shows strong agreement with the reference finite element (FE) results, demonstrating its potential as a fast and reliable tool for preliminary assessment of tunnel-induced building settlement.

Introduction

Building–tunnel interaction has been widely studied with finite element (FE) analysis [1-2]. However, traditional analyses restrict the range and combination of variables that can be evaluated. Key factors such as soil stratigraphy, stiffness variation, and tunnel-induced volume loss are often simplified due to high computational demands. Surrogate modelling offers an efficient alternative by accommodating extensive parameter combinations and capturing nonlinear soil–structure relationships. Once trained, such models can rapidly predict tunnel-induced building settlement profiles, reducing reliance on repeated FE simulations and supporting fast, reliable preliminary assessments. This study develops and evaluates an artificial neural network (ANN) surrogate model trained on 2,000 numerical cases to predict building settlement profiles induced by tunnelling.

Methodology

The reference model adopted a typical London stratigraphy with Made Ground (MG), River Terrace Deposits (RTD), London Clay (LC), Lambeth Group Clay (LGC), Lambeth Group Sand (LGS), and Thanet Sand (TS). The pore water pressure profile adopted hydrostatic condition with water table set to be at the top of LC. Variations in 10 parameters were considered in the database, their adopted variation ranges are shown in Table 1. The tunnel depth was varied using a variable R to apply realistic constraints associated with tunnelling in London. The relationship between tunnel depth Z_0 and R is:

$$Z_0 = H_{max} + D/2 + R \cdot H_R \quad (1)$$

$$H_{max} = \max\{\mathrm{H} + 0.5, 8\} \quad (2)$$

$$H_R = H + 27.3 - H_{max} - D - 0.5 \quad (3)$$

The Latin Hypercube Sampling (LHS) method was adopted to generate 2000 space filling samples. The synthetic dataset was divided into training (70%), testing (20%) and validation (10%) datasets. Settlement troughs of the building from the end of tunnel excavation were extracted from FE analysis results with 401 equally spaced points taken from each trough. The validation dataset was employed to assess the performance of the ANN model during training. The testing dataset was used after training to evaluate the model's final configuration.

A feed-forward ANN, constructed with the package *Keras,* was trained to predict building displacement given the relative position x/B within the building (where x is the distance from the point on the left end of the building and B is the building width) and the ten inputs

listed in Table 1. The ANN adopted the Adam optimizer, ReLU activation for all hidden layers and linear activation for output layer. The architecture (layers and neurons) and the learning rate were tuned through an extensive search of hyperparameter combinations. To prevent overfitting, early stopping was applied such that training stopped after 10 epochs without improvement on the validation loss.

Table 1: Varying parameters and ranges

	Lower bound	Upper bound
SD thickness, H	2 m	14 m
MG relative thickness, H_1/H	0	1
MG stiffness, E'_{ref}	3 MPa	25 MPa
RTG stiffness, G_{ref}	41939 kPa	87352 kPa
Tunnel diameter, D	2 m	12 m
Tunnel depth variable, R	0	1
Relative eccentricity, e/B	0	1
Building width, B	16 m	120 m
Tunnel volume loss, V_L	0.5 %	3.3 %
Building stories, m	1	10

Results

Figure 1 illustrates regression plots where the displacement predicted by the surrogate model is plotted in the vertical axis against the numerical results for the testing dataset. The data points generally plot in a narrow band around the solid black line, which represents a perfect match, signifying a good overall performance of the surrogate model. The mean absolute error (MAE) of the surrogate prediction was calculated for the whole settlement trough of each of the cases in the testing dataset. These 400 MAE values were ranked from high to low, and different percentile cases were picked out, in which the predicted building settlement troughs were plotted against the numerical results in Figure 2. The predicted troughs shape and magnitude exhibit a close agreement with the numerical results which further demonstrates the generalization ability of the trained surrogate.

Future work

Future work will extend this study to building deformation influenced by tunnels in the presence of deep foundations, such as piles. These systems involve more complex soil–structure interaction and require more advanced modelling strategies.

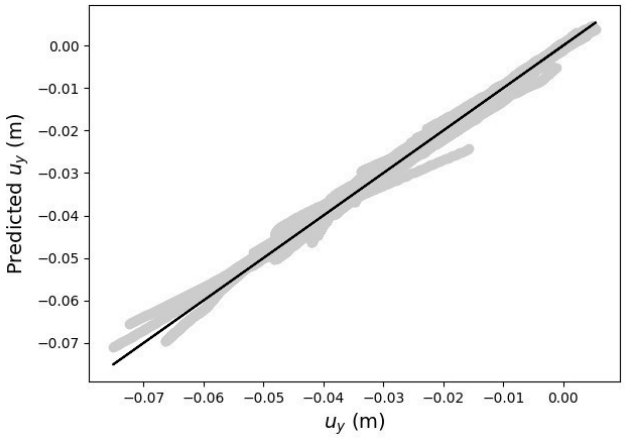


Figure 1: Regression plot of testing dataset

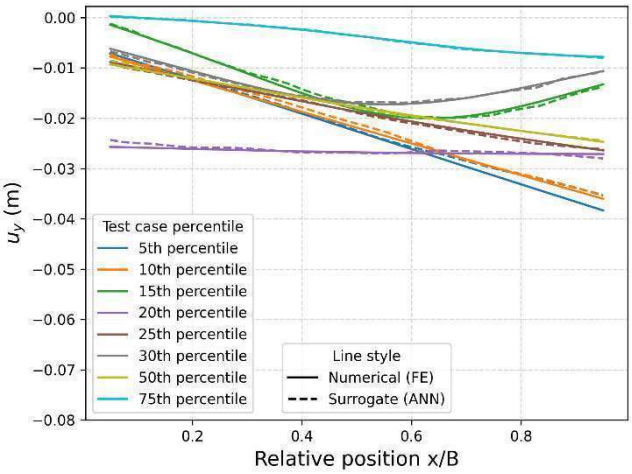


Figure 2: Numerical vs surrogate predicted building settlement trough of different MAE percentiles for testing dataset

References

[1] Potts, D. M., Addenbrooke, T. I., (1997). *A structure's influence on tunnelling induced ground movements*. Proc. Inst. Civ. Eng. Geotech. Eng., Volume 125(2), pp. 109-125

[2] Franzius, J. N., Potts, D. M., Burland, J. B., (2006). *The response of surface structures to tunnel construction*. Proc. Inst. Civ. Eng. Geotech. Eng., Volume 159(1), pp. 3-17

Prediction of thermo-active pile group response from single-pile surrogate models

J. Sánchez Fernández*[1], A. Ruiz López[2] and D.M.G. Taborda[3]
[1,2,3] Department of Civil and Environmental Engineering, Imperial College London, London, UK
(E-mail: javier.sanchez-fernandez18@imperial.ac.uk, agustin.ruizlopez@seequent.com, d.taborda@imperial.ac.uk)
[1] Science and Solutions for a Changing Planet DTP, Grantham Institute, Imperial College London, UK
[2] Seequent – The Bentley Subsurface Company, Delft, The Netherlands

Abstract

This work presents a surrogate-based framework for predicting the thermal behaviour of thermo-active pile groups by combining predictions from two single-pile surrogate models within the interaction formulation from Liu & Taborda [1]. The approach reconstructs group-scale power output and thermal response without requiring direct pile-group surrogate training. Results show good agreement with reference numerical data for corner, edge, and centre piles, capturing the main interaction effects. The methodology provides a computationally efficient alternative to full numerical simulations while preserving physical consistency, demonstrating potential for practical design and assessment of thermo-active pile groups.

Introduction

Thermo-active structures are increasingly used in low-carbon urban infrastructure by integrating heat-exchange systems within foundation elements such as piles or walls, enabling buildings to utilise the ground as a heat source or sink. In practice, thermo-active piles are typically installed in groups, where thermal interaction between neighbouring elements leads to overlapping temperature fields. Consequently, the behaviour of a pile group cannot be inferred directly from that of a single pile without accounting for these interaction effects [2]. A practical methodology for addressing this problem has been proposed [1], where pile-group response is obtained from single-pile thermal quantities using interaction factors and temporal superposition. In the present study, the objective is to evaluate whether surrogate-derived responses can reproduce group behaviour with accuracy, providing a computationally efficient alternative for group-scale thermal assessment.

Methodology

A 900 mm diameter pile is considered in a 3 × 3 group with a spacing factor of 4 (i.e. 3600 mm between pile axes). Each pile is 20 m long and equipped with a double U-loop heat exchanger formed of 26.2 mm diameter pipes. The soil and concrete thermal conductivities are 1.8 W/mK and 2.3 W/mK, respectively, the initial ground temperature is 20 °C, and the fluid velocity is 0.19 m/s. The inlet temperature is transient, combining annual and monthly cycles and is defined as $T_{\mathrm{in}}(t) = 20 + 20\sin(2\pi t_a) + 10\sin(2\pi t_m)$ [°C] where $t_a = t/360$ and $t_m = t/30$.

The proposed workflow begins with the single-pile power response, P_{si}, obtained from the power output surrogate. Since the surrogate is trained under constant inlet temperature differences, its output is interpreted as the response to a step change in thermal loading. To account for a time-varying inlet temperature, the signal is discretised into a sequence of incremental changes. Each increment is treated as a small step in thermal loading, generating a delayed power response with the same shape as the surrogate prediction. The transient single-pile response is then reconstructed by summing the contributions of all increments over time, following Duhamel superposition. The group power, $P_{i,\mathrm{gr}}$, is subsequently computed using the thermal interaction factor for power (TIF_P) to each increment and combining the contributions through temporal superposition. The second surrogate provides the single-pile wall g-function, Φ_{si}. The group g-function is obtained using the interaction factor for g-functions (TIF_G). Finally, the group power and

g-function are combined to compute the average pile wall temperature change for each pile category in the 3 × 3 group:

$$\Delta T_w(t_n) = \sum_{k=1}^{n} \frac{P(t_k)}{2\pi k_{soil}} [\Phi_g(t_n - t_{k-1}) - \Phi_g(t_n - t_k)] \quad (1)$$

Results

The surrogate-based framework reproduces the pile-group response with good agreement with reference numerical data. Figure 1 shows the predicted power histories for the corner, centre and edge piles. The agreement remains strong over the full-time range, including short-period oscillations and seasonal trends.

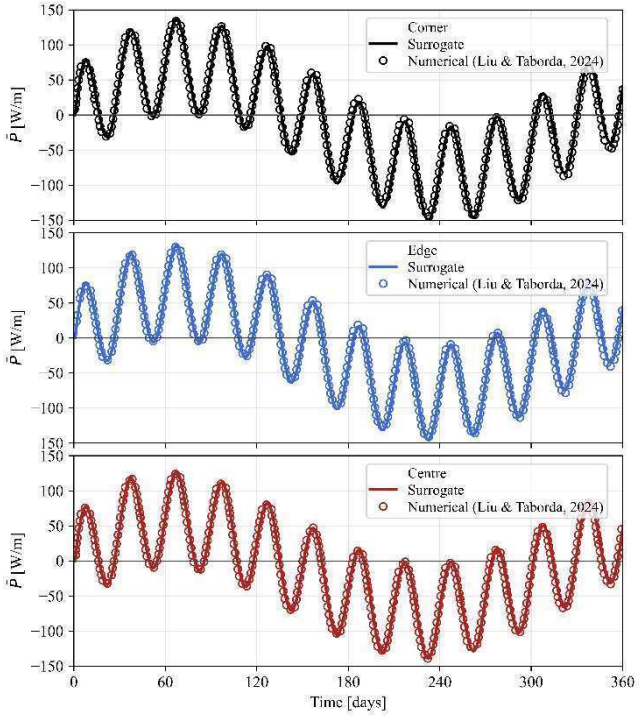


Figure 1: Surrogate-estimated and numerical power output for piles of the 3x3 group.

Figure 2 shows the resulting pile wall temperature changes obtained by combining the surrogate-derived power and g-function through temporal superposition. The predicted responses reproduce well both the amplitude and phase of the numerical trends across all pile positions. Minor deviations are observed at later times, particularly during periods of maximum heating and cooling. The overall agreement remains strong, showing that the surrogate framework provides a reliable prediction of the full thermal response.

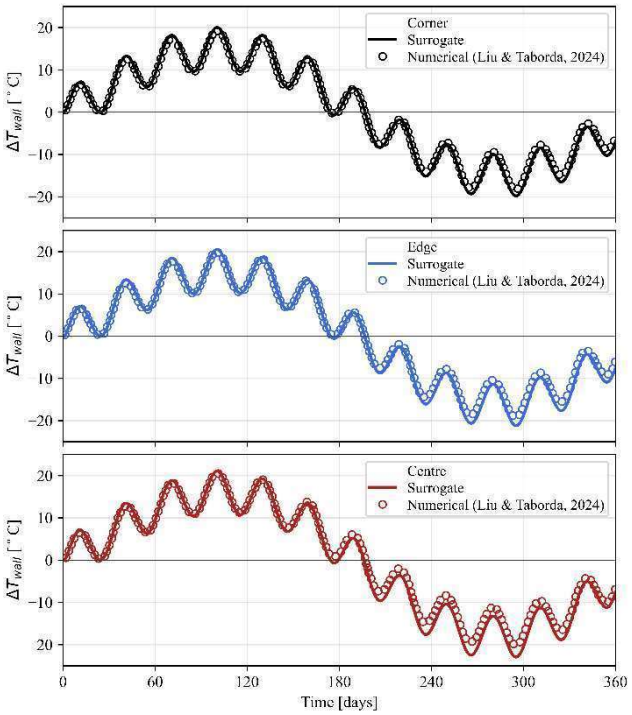


Figure 2: Wall temperature increase estimation for all pile locations in 3x3 group.

Future work

Future work may focus on developing surrogate models for other heat exchanging structures.

Acknowledgements

This work was supported by NERC under grant NE/S007415/1 and by SaFEGround, a project funded by EPSRC (EP/V042149/1).

References

[1] Liu, R. Y. W., & Taborda, D. M. G. (2024a). A methodology for incorporating thermal interference in the design of thermo-active pile groups. Geomechanics for Energy and the Environment, 39(October 2023), 100575. https://doi.org/10.1016/j.gete.2024.100575

[2] Liu, R. Y. W., & Taborda, D. M. G. (2024b). The effects of thermal interference on the thermal performance of thermo-active pile groups. Renewable Energy, 225(March), 120357. https://doi.org/10.1016/j.renene.2024.12035

GPU-accelerated 3D finite element analysis of monopile foundations with the SANISAND-MS constitutive model

Max R.F. Bowman*[1], Harvey J. Burd[2] and Wes Armour[3]
[1, 2, 3] Department of Engineering Science, University of Oxford, UK
(E-mail: max.bowman@eng.ox.ac.uk, harvey.burd@eng.ox.ac.uk, wes.armour@oerc.ox.ac.uk)

Abstract

The current work investigates the use of graphics processing units and high-performance computing to expedite the 3D finite element analysis of monopile foundations for offshore wind turbines. The SANISAND-MS constitutive model is employed as a representative advanced soil model. Computational performance is benchmarked against the commercial software PLAXIS 3D. A speed-up of 54x is achieved using high-performance hardware, challenging the prevailing view that 3D finite element analysis necessarily requires lengthy runtimes.

Introduction

Monopiles, comprising a hollow steel tube driven into the seabed, are the most common foundation type for offshore wind turbines. Properly calibrated 3D finite element analysis (3DFEA) is widely regarded as the most accurate method for analysing monopile foundations under static monotonic loading. 3DFEA is routinely used for design verification and to calibrate simplified models. Its primary limitations are computational expense and the complexity required to produce and interpret a well-calibrated analysis.

The current work investigates expediting 3DFEA using graphics processing units (GPUs) and high-performance computing (HPC). Expedited 3DFEA could reduce reliance on simplified models and streamline design workflows.

Methodology

An implicit modified Newton-Raphson scheme is employed. The governing computational costs arise from global stiffness matrix assembly, linear system solution, and constitutive model integration.

The stiffness matrix is stored in sparse format. The structure of the sparse matrix is mapped in the pre-processing stage, meaning the values can be efficiently updated throughout the analysis. NVIDIA's cuDSS library is used to directly solve the sparse global system of equations.

The SANISAND-MS [1] constitutive model is employed, representing a computationally demanding soil model. GPUs are optimised for performing many tasks in parallel; constitutive model integration is therefore well suited to GPUs as the updates carried out at each Gauss point are entirely independent. A small number of Gauss points (e.g. with stresses near the apex of the yield surface) require many sub-steps during the integration process; these Gauss points are offloaded to the CPU, which is better suited for performing a small number of complex sequential tasks.

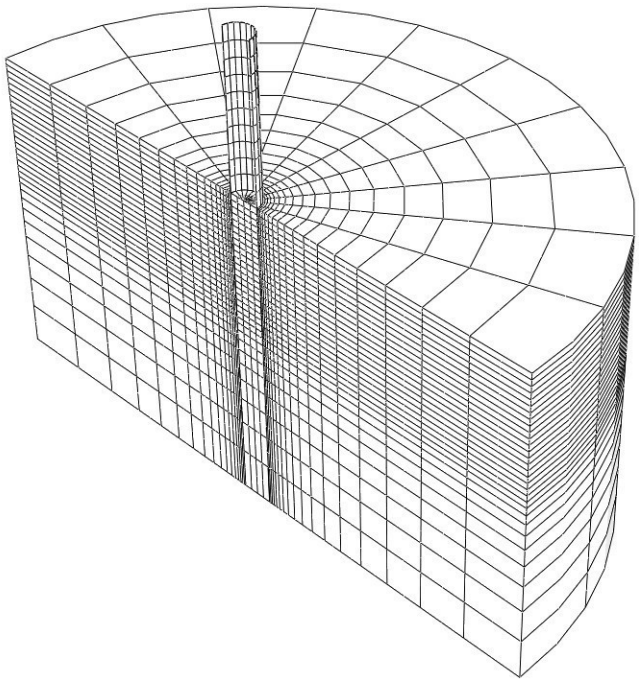


Figure 1: Typical finite element mesh for a monopile foundation

A typical finite element model of a monopile foundation is shown in Figure 1. The base of the domain is fully fixed, and the radial boundaries are horizontally restrained. Symmetry is exploited to halve the modelled domain. The pile extends above the seabed to enable application of lateral loading at an eccentricity that is representative of offshore conditions. The pile geometry in this work is D=10m, L/D=4, D/t=110 and h/D=5, where D is the external diameter, L is the embedded length, t is the wall thickness, and h is the height of the lateral load above the seabed. SANISAND-MS parameters calibrated for Dunkirk Sand are employed [2]. The pile-soil interface is modelled as fully tied.

The software (hereafter referred to as GPU-3DFEA) is compared to PLAXIS 3D 2025.1. Mesh properties adopted following a convergence study are summarised in Table 1. The current work employs 20-noded solid hexahedral elements for the pile and the soil. PLAXIS uses 10-noded solid tetrahedral elements for the soil and 6-noded shell elements for the pile. It is expected that the number of soil gauss points will govern the runtime; effort is made to ensure these are similar for both analyses.

Table 1: Mesh characteristics. Soil element and Gauss point counts are in brackets.

Software	Elements (soil)	Nodes	Gauss points (soil)
PLAXIS	10950 (10351)	15840	43201 (41404)
GPU-3DFEA	5340 (5050)	23973	42970 (40650)

Results

Close agreement between the load-displacement response of PLAXIS and GPU-3DFEA is shown in Figure 2.

Run times are compared in Table 2 for a range of hardware. Desktop hardware comprises an Intel i7-14700 CPU and an NVIDIA RTX 4060 GPU (not used by PLAXIS). HPC hardware comprises an Intel Gold 6342 CPU (using 16 cores) and an NVIDIA H100 GPU. On comparable hardware the GPU-accelerated software achieves a 21.6x speed-up relative to PLAXIS. The total speed-up using HPC hardware is 54.0x.

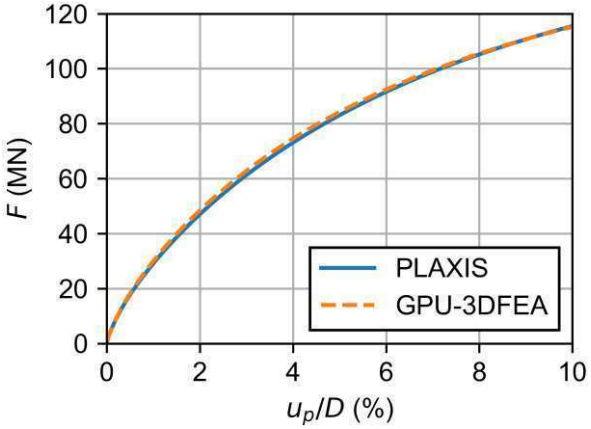


Figure 2: Comparison of the lateral load - pile head displacement response

Table 2: Run times for the software and hardware combinations

Soft-ware	Hard-ware	Asse-mbly (s)	Solve (s)	Const. model (s)	Total (s)
PLAXIS	Desktop	-	199	3953	4536
GPU-3DFEA	Desktop	9	61	137	210
GPU-3DFEA	HPC	1	5	76	84

Future work

Additional constitutive models and interface elements will be added to the GPU-3DFEA software. Application to farm-wide design will be demonstrated with representative layered soil profiles. Currently, 3DFEA of cyclically loaded monopiles is limited to approximately 100 load cycles; strategies to extend this will be investigated. Use of HPC hardware may require performing 3DFEA in the cloud; methodology to enable this will be developed.

References

[1] Liu, H.Y., Abell, J.A., Diambra, A., Pisanò, F. (2019). *Modelling the cyclic ratcheting of sands through memory-enhanced bounding surface plasticity*. Géotechnique Volume 69, pp 783-800

[2] Pisanò, F., Del Brocco, I., Ho, H.M., Brasile, S. (2024). *3D FE simulation of PISA monopile field tests at Dunkirk using SANISAND-MS*. Géotechnique letters Volume 14, pp 35-45

Experimental Characterisation and Site Investigation

Heat Transfer in Saturated Sand: Insights from Centrifuge Experiments

Dayana M.P.J.*[1], Bowman E.T. [2] and Gaspar T.A.V.[3]
[1, 2] Department of Mechanical, Aerospace and Civil Engineering, University of Sheffield, UK
(E-mail: mdpj1@sheffield.ac.uk, e.bowman@sheffield.ac.uk)
[3] Department of Civil and Environmental Engineering, Imperial College London, UK
(E-mail: t.gaspar@imperial.ac.uk)

Abstract

This study investigates heat migration in sand under radiative heating using centrifuge modelling. Tests were conducted at 20g and 40g to replicate prototype stress conditions and investigate associated heat transfer behaviour. A sand column instrumented with thermocouples was subjected to cyclic infrared heating. Results show a decrease in temperature with depth, with strong near-surface gradients. Soil temperatures were consistently higher at 20g than at 40g, despite higher air temperatures at 40g. This is attributed to differences in heat input scaling. The findings suggest that while N² thermal diffusion scaling is appropriate for the soil mass, it may not fully capture air temperature response under radiative heating.

Introduction

Understanding heat transfer in soils is essential for applications such as energy geostructures, buried infrastructure, and environmental geotechnics. However, in reduced-scale physical models, testing at 1g cannot reproduce prototype stress conditions with a soil mass. Centrifuge modelling overcomes this limitation by applying elevated acceleration to a scaled model, thereby replicating prototype stress levels. It also enables time-dependent physical behaviour to be investigated over compressed model timescales, allowing longer prototype response periods to be studied within practical test durations.

Previous studies have predominantly examined conduction-dominated heat transfer, with comparatively little attention given to centrifuge tests involving radiative surface heating. This study investigates the thermal response in saturated sand subjected to radiative heating in a geotechnical centrifuge. The analysis focuses on how acceleration level affects temperature distribution and on whether the resulting thermal response follows established centrifuge scaling laws for thermal processes.

Methodology

The experimental setup consisted of two acrylic tubes 87 mm diameter and 200 mm high. The columns were filled with sand at 75% relative density. The sand had an average grain size of 148 µm, with maximum and minimum dry densities of 1710 kg/m³ and 1350 kg/m³, respectively. In this study, only results from sand column 2 are discussed. Seven thermocouples were positioned along the column's centreline at vertical positions of 5, 10, 20, 30, 50, 100, and 195 mm beneath the soil surface, with an additional thermocouple located above the column. A 150 W infrared lamp provided radiative heating to the top surface, ensuring predominantly one-dimensional heat transfer. The lamp was cycled on and off at predetermined intervals to simulate seasonal temperature fluctuations. The system was enclosed within a strongbox with a top plate to eliminate airflow effects, as shown in Figure 1.

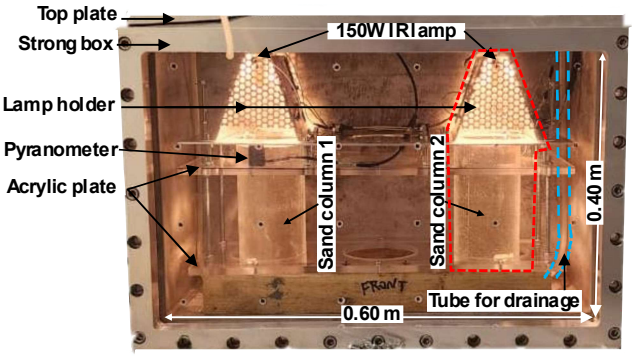


Figure 1: Sand column centrifuge test set-up

The sand column was saturated by circulating water from the bottom to the top through a drainage valve located at the base. Tests were

conducted at 20g and 40g. The 20g test was run for 108 minutes, simulating 30 days at prototype scale, with the lamp cycled on and off every 108 seconds to represent diurnal variation. The 40g test ran for 27 minutes, also simulating 30 days, with heating cycles of 27 seconds. For data interpretation, established scaling laws were used, with length and diffusion time being scaled by 1/N and 1/N² respectively [1,2].

Results

Air and soil temperature variations with time are shown in Figure 2. The results indicate a diurnal air temperature fluctuation of approximately 13 °C for both tests. Over the 30-day prototype period, the 40g test shows a sharper increase in average air temperature compared to the 20g test, suggesting that the assumed time-diffusion scaling may not fully capture the air temperature response above the soil surface in this system.

Within the soil, temperature increases are most pronounced near the surface and attenuate with depth over the 30-day prototype period. At a depth of approximately 0.2 m, the overall temperature increase is around 20 °C and 15 °C in 20g and 40g tests, lower than that observed in the air. While at depths greater than 2 m, temperature changes remain less than 5 °C.

To compare the spatial temperature distributions for the two tests, Figure 3 presents the temperature as a function of depth at different time steps. The results show that, while trends of temperature variation with depth are similar in both tests, temperatures in the 20g case are consistently higher than those at 40g, despite higher air temperatures at 40g. This discrepancy may be due to identical heat input being applied in both tests. Previous studies suggest that heat input should be scaled by N, which would likely increase air temperature differences (Figure 2a) but produce more comparable soil temperature profiles.

The results presented in this paper indicate that, while the N² scaling law for thermal diffusion provides a reasonable description of heat transfer within the soil mass, it does not fully capture the air temperature response, particularly under radiative heating conditions.

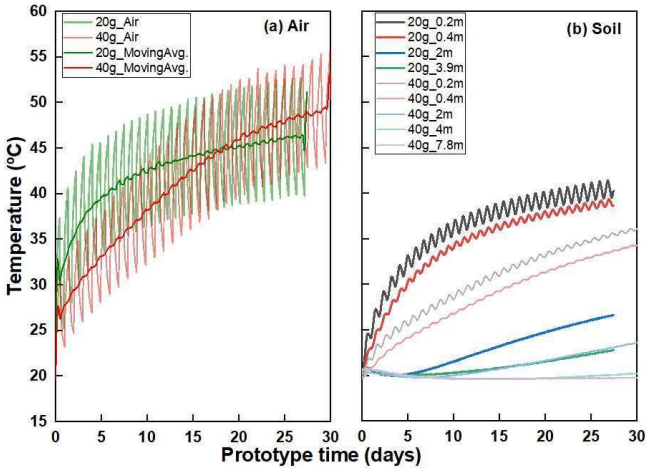


Figure 2. Temperature variation with time

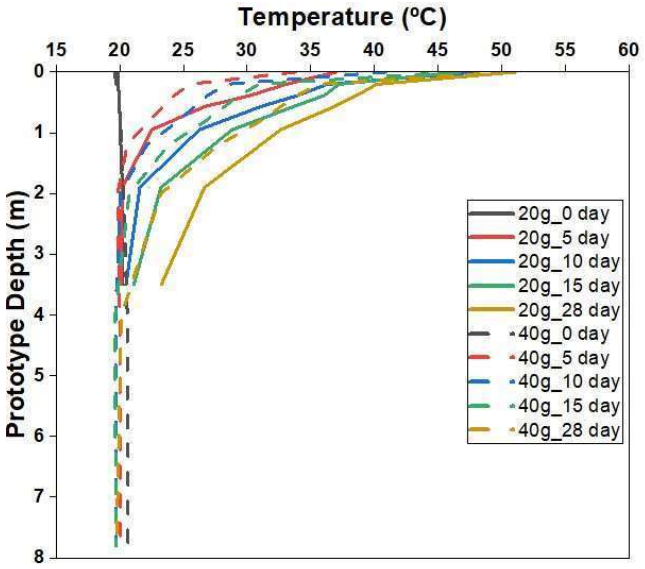


Figure 3. Temperature variation with depth

Future Work

Future research should focus on scaling heat input to ensure accurate simulation of thermal processes in centrifuge modelling.

References

[1] Madabhushi, G., (2017). *Centrifuge Modelling for Civil Engineers*. 1st edn. CRC Press. https://doi.org/10.1201/9781315272863

[2] Krishnaiah, S., Singh, D.N., (2004). *Centrifuge modelling of heat migration in soils.* International Journal of Physical Modelling in Geotechnics, Volume 4(3), pp. 39-47.

Investigating Climate-Induced Failure Mechanisms in UK Coastal Cliffs

P. J. Schoeman*[1], T. A. V. Gaspar[2], L. Zdravkovic[3], J. Standing[4]
[1,2,3,4] Department of Civil and Environmental Engineering, Imperial College London, UK
(E-mail: p.schoeman26@imperial.ac.uk, t.gaspar@imperial.ac.uk, l.zdravkovic@imperial.ac.uk, j.standing@imperial.ac.uk)

Abstract

Coastal cliff instability is an escalating geohazard along England and Wales, with climate change introducing failure mechanisms beyond conventional wave action, including thermally driven strength reduction, desiccation cracking, and instability induced by cyclic suction changes. This study aims to combine advanced numerical modelling using ICFEP with bespoke thermo-hydro-mechanical constitutive models, non-invasive muon tomography for internal cliff characterisation, and advanced element testing across varying temperatures and saturations. Anticipated outcomes include quantification of climate-driven strength degradation and identification of dominant failure mechanisms, providing a geotechnical-based framework for updated coastal risk assessment.

Introduction

Coastal cliff instability is a widespread and escalating geohazard along the coastline of England and Wales. Of the estimated 6,251 km of coastline, approximately 53% comprise cliffs that are actively subject to coastal erosion and subsequent instability [1], with some locations among the fastest retreating in Europe.

This coastline includes historical failures such as the Folkestone Warren landslide and its effects on the main Folkestone to Dover railway line. This landslide has caused numerous railway disruptions, most notably during the slips of 1877, 1896, and 1915. Stabilisation techniques, including lowering the phreatic surface and erosion protection, failed to stabilise the 1.5 million m^3 of unstable soil [2]. Additionally, the Ventnor landslide complex on the Isle of Wight highlights the scale of the problem. In 2023, significant ground movements involving approximately 14 million m^3 were recorded following a period of prolonged wet weather and stormy seas. [3].

Historically, coastal cliff instability has been studied primarily in relation to wave-driven erosion during large storms, which causes undercutting at the cliff toe, removal of basal support, and subsequent mass failure. However, this is increasingly recognised to be part of the problem. Recently, the focus has shifted to climate change as a dominant driver of future failure risk. The National Coastal Erosion Risk Mapping (NCERM) projects that up to 100,000 properties could be in at-risk areas by the end of this century. [4].

These changes in climatic conditions affect soil behaviour in several important ways. Elevated temperatures can alter the apparent pre-consolidation pressure of the soil, as shown by [5] (Fig. 1), thereby influencing its strength. Repeated drying and wetting cycles also affect soil suction, which can contribute to instability, particularly under more extreme temperature conditions. In addition, desiccation cracking creates further pathways for deterioration and can promote failure mechanisms within the soil mass [6].

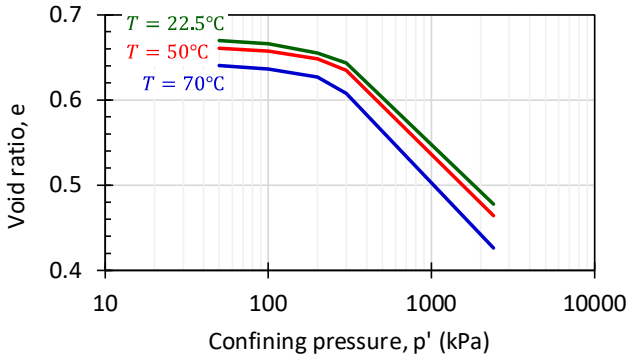


Figure 1: Clay pre-consolidation pressure decreases with increasing temperature [5].

This research aims to investigate the stability of these coastal structures using specialised investigation tools.

Methodology

To expand the understanding of the stability of these coastal structures, two investigation methods will be used.

Conventional constitutive models do not fully capture the coupled thermo-hydro-mechanical behaviour of partially saturated cliff materials under cyclic climatic loading. To address this, numerical modelling will be performed in the Imperial College Finite Element Program (ICFEP) using bespoke constitutive models developed for unsaturated, thermally sensitive, and cyclically loaded behaviour [7].

In addition, conventional site investigation methods (such as boreholes and CPTu testing) are unsafe on metastable coastal cliffs, leaving the internal structure of the most hazardous sites uncharacterised. Therefore, muon tomography will be deployed as a non-invasive site characterisation tool. Cosmic-ray muons penetrate deep into geological materials and are attenuated in proportion to density [8], potentially enabling the reconstruction of the internal cliff structure.

These investigation methods will be complimented by advanced element testing investigating the behaviour of the coastal cliff material at various saturations and temperatures.

Anticipated Results

While the project is at an early stage, the combined methodology should yield several key outcomes. Numerical analyses under current and projected climate scenarios will help identify the dominant failure mechanisms affecting UK cliff lithologies, including rainfall-induced, thermally driven, and wave-driven processes. Laboratory testing will quantify strength reduction as a function of temperature and saturation cycles, complementing the numerical analyses. Muon tomography surveys at target cliff sites will also assess the feasibility of the technique for non-invasive internal characterisation of metastable slopes, including the identification of density variations that are not detectable in surface surveys. Together, these outputs will provide an evidence base for updated risk assessment frameworks that account for the full spectrum of climate-driven failure mechanisms, a capability currently absent from UK coastal management practice.

References

[1] Moore, R., Davis, G., (2015). Cliff instability and erosion management in England and Wales, J. Coast. Cons., 19, pp. 771-784.

[2] Warren, C.D., (2022). The Folkestone Warren Landslide.

[3] Manteth, T., (2024). Isle of Wight on alert for further ground movement after biggest landslide in 20 years, New Civil Engineer.

[4] Env. Agency, (2025). National Assessment of Flood and Coastal Erosion Risk in England, Gov.uk.

[5] Kirkham, A., Tsiampousi, A., Potts, D.M., (2021). Thermo-mechanical behaviour of a kaolin-based clay soil, Géotechnique, 74, pp. 1742-1751.

[6] Wang, Y., Zhang, Q., Zhang, S., Zhong, H., Ng, C.W.W., (2025). Investigation of temperature effects on slope serviceability and subsequent rainfall-induced instability, Acta Geotech., 20, pp. 4199-4212.

[7] Pico, M., Mašín, D., Fuentes, W., (2024). Coupled hydro-mechanical hypoplastic model for partially saturated soils under monotonic and cyclic loading, Acta Geotech., 19, pp. 7049-7073.

[8] Bressler, M., Goodwin, L., Kryemadhi, A., (2017). Cosmic-ray topography, Am. J. Phys., 85 pp. 840-843.

Particle Crushing in Glauconitic Sand Under Cyclic CPTu Loading

A. Rodríguez Piedrabuena*[1], D. A. de Lange[2], M. Mento[3] and M. Konstantinou[4]
[1, 2, 4] Energy and Underground Infrastructure, Deltares, the Netherlands
(E-mail: Alba.RodriguezPiedrabuena@deltares.nl, Dirk.deLange@deltaresn.nl, maria.konstantinou@deltares.nl)
[3] Geotechnical Engineering, IQIP, the Netherlands
(E-mail: mento@iqip.com)

Abstract

This study investigates particle crushing during displacement-controlled cyclic penetration in glauconitic sand (13% glauconite content) using calibration chamber tests conducted at two loading frequencies. The aim is to evaluate the spatial extent of crushing and to examine the possible mechanism governing its propagation beyond conventional influence zones by linking the cyclic penetration response to the observed geometry and characteristics of the recovered crushed soil bulb.

Introduction

Research on jacked penetrometers in calibration chamber tests on silica sands indicates that particle crushing is typically localised near the penetrometer tip where extreme normal and shear stresses develop during penetration [1,2,3]. This crushing changes the soil grain-size distribution, with direct implications for tip resistance mobilisation and overall foundation performance [2,3]. During jacking, sand particle contraction resulting from crushing, leads to stress relaxation and potentially reducing structural resistance [1,2]. Advanced image methods used during jacking of penetrometers show that crushing is often confined to narrow shear bands immediately beneath the tip [4]. Under high-amplitude cyclic loading, the affected zone in silica sands is typically limited to about 0.4 penetrometer diameters below the tip [4]. In contrast, the present study identifies crushed glauconitic sand at depths up to 3.1 cone diameters after displacement-controlled cyclic loading of a penetrometer and explores a possible crushing mechanism to account for the deep propagation of crushed material.

Methodology

The sand fraction of glauconitic sand from the Kattendijk formation (~13% glauconite content) was tested in fully saturated samples at 75 % relative density [5]. A CPTu test with a 16 mm diameter (D) cone was conducted under vertical and horizontal effective stresses of 200 kPa and 100 kPa. After monotonic penetration to 400 mm reaching 36 MPa, two displacement-controlled cyclic tests with half-amplitude of 5 mm (Δw_{cyclic}) were performed at 0.1 Hz (Test 1) and 1 Hz (Test 2).

Results

Cyclic loading produced a bulb-shaped zone of crushed particles beneath the cone tip, extending 50 mm (3.1D) below and 40 mm above it, fully surrounding the tip and partially the friction sleeve (Figure 1). Excavation also revealed crushed material adjacent to the probe. The increased plasticity and fines of the crushed soil (Figure 2) enabled recovery of the intact bulb comprising a 60 mm-diameter spherical section with a 35 mm-long cylindrical ‘nose’. This indicates significant radial and vertical displacements, with the crushed zone extending deeper than in silica sands, where it is confined to a triangular convex-shape beneath the cone [1,3].



Figure 1: Crushed soil at the cone tip: excavated (left) and bulb (right).

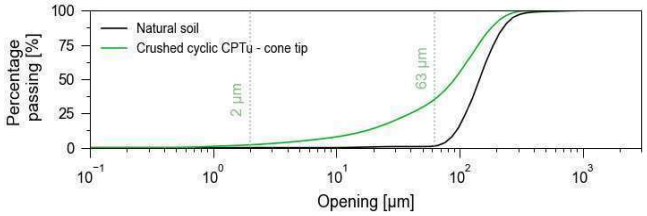


Figure 2: PSD curve natural and crushed soil.

Based on the cyclic loading regimes and recovered bulb shape, a crushing mechanism is hypothesised, although the cone resistance (q_c) and pore pressure (u_2) responses remain not yet fully understood. It comprises three phases: contact loss, suction-driven soil migration, and cumulative particle crushing. During the first 65 cycles (Test 1), $q_{c,max}$ decreases while the $q_{c,min}$ remains slightly above zero (Figure 3), indicating a gap formation beneath the tip, consistent with [4]. Concurrently, u_2 becomes increasingly negative without returning to zero during upward strokes, suggesting limited dissipation or continued suction generation. Early negative u_2 values (Test 1) indicate dilation, and/or particle crushing during the downward stroke, with decreasing q_c pointing to particle crushing. In the subsequent 100 cycles, q_c increases while u_2 becomes less negative. During Test 2, q_c stabilises between ~15–20 MPa, with minimum q_c values approaching zero and u_2 fluctuating within 5 and -20 kPa, indicating reduced suction, consistent with the formation of a finer, less permeable soil covering the u_2 filter. Downward strokes confine migrated soil, promoting crushing, progressive densification and bulb growth.

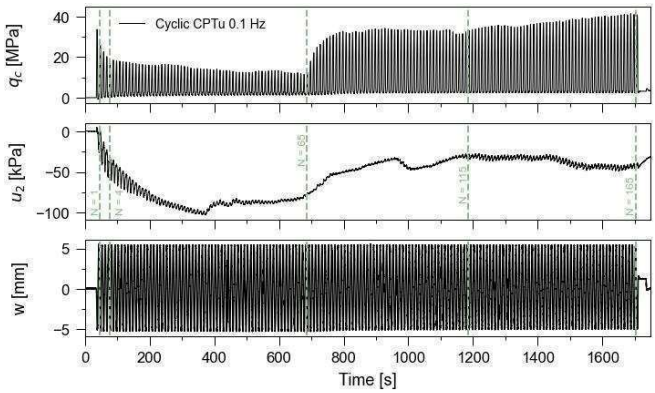


Figure 3: q_c, u_2 and w (negative downward and positive upward) over time during Test 1.

Future work

Future experimental investigations shall include half-probe penetration in a transparent glass box (~100 cm^3), with a surcharge applied at the top to reproduce initial vertical effective stress, enabling direct visualisation of soil displacements during static and cyclic half-CPT loading. This configuration allows observation of local soil response, grain crushing near the probe and migration of crushed glauconite. Complementary calibration chamber tests would improve repeatability and strengthen interpretation of the observed mechanism and CPTu response.

References

[1] Yang, Z. X., Jardine, R. J., Zhu, B. T., Foray, P., & Tsuha, C. H. C. (2010). Sand grain crushing and interface shearing during displacement pile installation in sand. Géotechnique, 60(6), 469–482. https://doi.org/10.1680/geot.2010.60.6.469

[2] Ganju, Eshan & Han, Fei & Prezzi, Monica & Salgado, Rodrigo & Pereira, Juliana. (2019). Quantification of displacement and particle crushing around a penetrometer tip. Geoscience Frontiers. 11. 10.1016/j.gsf.2019.05.007.

[3] Tovar-Valencia, R.D., Galvis-Castro, A., Salgado, R. *et al.* Experimental measurement of particle crushing around model piles jacked in a calibration chamber. *Acta Geotech.* 18, 1331–1351 (2023). https://doi.org/10.1007/s11440-022-01681-8

[4] Galvis-Castro, A. C., Tovar-Valencia, R. D., Prezzi, M., & Salgado, R. (2025, June). Experimental Study of the Effects of Cyclic Loading on Base Resistance Mobilization of Piles Using a Calibration Chamber. 5th International Symposium on Frontiers in Offshore Geotechnics (ISFOG 2025). https://doi.org/https://doi.org/10.53243/ISFOG2025-630

[5] Rodríguez Piedrabuena, A., Mento, M., de Lange, D. A., & Flessati, L. (2024, October 2). How to deal with glauconite sands in physical models. 5th European Conference on Physical Modelling in Geotechnics (ECPMG 2024). https://doi.org/https://doi.org/10.53243/ECPMG2024-20

Extending the Capabilities of Suction Monitored Unconfined Compression Apparatus with Digital Image Correlation

Benedek Nagy[1], Grainne El Mountassir[2] and Alessandro Tarantino[3]
[1, 2, 3] Civil and Environmental Engineering, University of Strathclyde, United Kingdom
(E-mail: benedek.nagy.2018@uni.strath.ac.uk, grainne.elmountassir@strath.ac.uk, alessandro.tarantino@strath.ac.uk)

Abstract

This study extends a previously developed suction-monitored unconfined compression (UC) apparatus by investigating the feasibility of applying Digital Image Correlation (DIC). While DIC is traditionally applied to planar surfaces, its use on cylindrical soil specimens introduces geometric and optical uncertainties, limiting quantitative accuracy. Nonetheless, qualitative strain field analysis was performed at axial strain rates of 1%/min, 0.1%/min, and 0.01%/min. The results demonstrate that DIC can successfully capture deformation patterns and strain localisation, providing additional insight into failure mechanisms and complementing suction and volumetric strain measurements.

Introduction

Investigating the shear strength of low density, unsaturated soils under low stress typical of near surface conditions is critical for applications such as shallow landslides. The authors previously developed a suction-monitored Unconfined Compression (UC) apparatus enabling simultaneous measurement of suction and monitoring of volumetric strain, widening possibilities of the traditional UC test [1]. However, while global measurements provide valuable insight, they do not fully capture spatial deformation patterns or strain localization. Digital Image Correlation (DIC) offers a non-contact method for obtaining full field displacement and strain data and has been widely adopted in experimental mechanics [2]. Its application in geotechnical testing is increasing, particularly for investigating localisation phenomena [3]. However, DIC is reliable on planar surfaces, whereas UC specimens are cylindrical, introducing projection errors and out of plane displacement effects [2]. This study explores the feasibility of integrating DIC into the existing suction monitored UC apparatus without any hardware modification. The objective is not to obtain precise quantitative strain values, but to assess whether meaningful qualitative deformation patterns can be extracted and used to deepen understanding of suction evolution and strain rate effects.

Methodology

The experimental configuration follows the suction monitored UC apparatus previously developed in [1]: axial deformation control, suction measurement using a METER Group T5x tensiometer, and image-based global volumetric strain monitoring. Cylindrical silty sand specimens (D=32mm L=72mm) consisting of 26% silt and 74% sand fractions were compacted to 1200kg/m^3 and tested at axial strain rates of 1%/min, 0.1%/min, and 0.01%/min following BS EN ISO 17892-7:2018. For DIC analysis, 8MP images captured during testing were processed using a Python based workflow. No artificial speckle pattern was applied; instead, the natural soil surface texture was used for correlation. The DIC parameters were: subset size of 21 pixels, subset spacing of 5 pixels, and search radius of 30 pixels. A normalized cross correlation threshold of 0.5 was selected to allow tracking under large deformations, accepting reduced correlation quality. The DIC outputs are presented in fig. 1 as displacement and strain maps arranged from left to right in decreasing strain rate (A 1%, B 0.1%, C 0.01%/min).

Results

The DIC results successfully captured the spatial evolution of deformation across all strain rates. The raw images in fig 1, show that at post -peak deviator stress, at approximately 1.17% axial strain, no visible macroscopic failure is observed (row 1), yet the derived

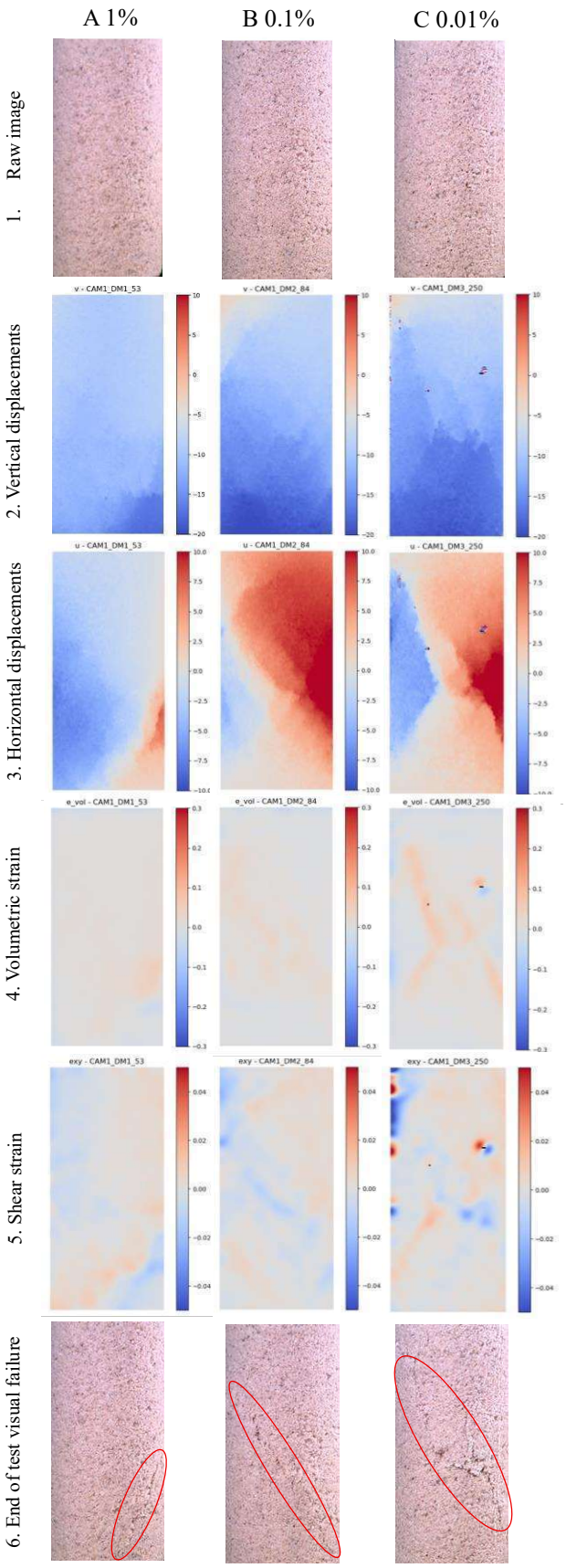


Figure 1: 1. Raw DIC input image at axial strain of 1.17% (post -peak deviator stress), 2. vertical displacement, 3. horizontal displacement, 4. volumetric strain, 5. shear strain fields and 6. raw image from the end of the test with visible failure.

strain fields reveal early-stage localisation in the volumetric and shear strain fields (rows 4 and 5). As the specimens were open to ambient air, the test ran at 0.01% strain rate resulting in the specimen drying out which led to an increase in suction and higher peak deviator stress (q_{max}) (table 1). On the other hand, the absence of a membrane allowed tracking of the particles directly on the surface of the specimen and capturing of the different displacement mechanisms between the lower and higher suction specimens. It is important to note that absolute strain magnitudes are unreliable due to curvature induced distortion and out-of-plane effects. However, this simple low cost (total cost ~£100) method gives useful insight into the relative distribution of strain and deformation mechanisms complementing global measurements.

Table 1: Suction monitored UCS test results [1]

Strain rate (%/min)	1 (A)	0.1(B)	0.01(C)
Initial water content (w) (%)	7	7	7
Dry density (P_d) (kg/m3)	1200	1200	1200
Initial suction (s) (kpa)	8	7.8	7.4
s at q_{max} (kpa)	10.8	10.4	55.4
Peak deviator stress (q_{max})(kpa)	2.38	2.36	6.91
Final w (%)	6.2	5.8	4.6

Future work

This low-cost setup could be further optimised by using a two camera setup in order to obtain a stereoscopic 3D image of the specimen. This would eliminate the out of plane effect and allow the correlation of the surface particles in 3D [2].

Acknowledgements

This research was supported by an EPSRC DTP studentship (EP/W524670/1) and a UKRI Future Leaders Fellowship (MR/V025376/1)

References

[1] Nagy, B., Mountassir, G.E. and Tarantino, A. (2025). Suction Monitored Apparatus to Investigate Shear Strength of Unsaturated Granular Material at Low (Total) Stress. *E3S Web of Conferences*, 642, p.03025. doi:https://doi.org/10.1051/e3sconf/202564203025.

[2] Michael Albert Sutton, Jean-José Orteu and Schreier, H.W. (2009). *Image correlation for shape, motion and deformation measurements : basic concepts, theory and applications*. New York, N.Y.: Springer.

[3] Rechenmacher, A. and Finno, R. (2004) 'Digital image correlation to evaluate shear banding in dilative sands,' *Geotechnical Testing Journal*, 27(1), pp. 13–22. https://doi.org/10.1520/gtj11263j.

Numerical Methods and Computational Geomechanics

Revisiting Shear History in DEM: Limitations of accumulating shear displacement compared with accumulating shear force

Yick Hong (Eric) Leung*[1], Dariel Hernandez-Delfin[2], David M G Taborda[3], Catherine O'Sullivan[4]

[1, 2, 3, 4] Department of Civil and Environmental Engineering, Imperial College London, London SW7 2BX, UK.
(E-mail: *[1]yick.leung14@imperial.ac.uk, [2]d.hernandez-delfin@imperial.ac.uk, [3]d.taborda@imperial.ac.uk, [4]cath.osullivan@imperial.ac.uk)

Abstract

The discrete element method (DEM) provides a means to advance understanding of soil behaviour by explicitly simulating particles and their interactions. In principle, a DEM contact model should accurately describe the normal and tangential interactions. These contact models need to capture the history of the tangential (shear) interaction to determine the point of frictional sliding. Two implementations to track the shear history in DEM simulations have been documented in the literature. The first approach accumulates the shear force, while the second accumulates the shear displacement. Our mathematical analysis of the two approaches demonstrates that the displacement-accumulated model does not account for the full history of the tangential interaction. Here, we demonstrate the practical implications of this shortcoming. Firstly, we consider the sensitivity of the response of a Face Centered Cubic lattice arrangement of same-sized spheres in drained triaxial compression to the choice of shear history implementation. We show that, if the shear displacement is accumulated, the sample does not reach the peak stress ratio given by the available analytical solution. Subsequently, we present data from drained compression of an assembly of polydisperse spheres that show large differences in the volumetric strain response depending on which implementation is used.

Introduction

While DEM contact models are conceptually much simpler than the constitutive models used in continuum soil mechanics, some details in these models require careful consideration. Here, we focus on the history of the tangential interaction, a key feature of DEM contact models that can be implemented erroneously as shown by O'Sullivan and Bray (2003) [1].

Two implementations for tracking the shear history and thus calculating the tangential shear force have been implemented in DEM codes. The first (integral) approach calculates the tangential or shear force from the accumulated tangential displacement at the contact. The second (incremental) approach updates and accumulates the tangential shear force directly. The integral approach (accumulating displacement) is used in Pair Gran Hertz History in LAMMPS [2] and also in MercuryDPM [3]. The incremental (force accumulation) approach is used by PFC [4] and YADE [5].

Thornton et al. (2011) [6] showed the different responses obtained when using each of these implementations for oblique impacts and contact level studies. Here, we extend this earlier study to look at implications for the collective response of systems of particles.

Methodology

DEM simulations were carried out using a modified version of LAMMPS [2] and considering both the integral and incremental approaches to record the history of the shear force for each contact. The first study considered drained triaxial compression of 2000 spheres on a Face-Centered Cubic (FCC) lattice to simulate the scenario considered analytically in Thornton (1979) [7]. The second set of simulations considered drained triaxial compression of 20,174 polydisperse spheres. Both sets of simulations considered freely rotating spheres.

Results

As shown in Fig. 1, for the drained triaxial compression of the FCC assembly, when the integral approach is used, the peak stress ratio is lower than the analytical prediction and irregular oscillations are obtained in the post-peak response. For DEM simulations where the incremental approach is used, the peak stress ratio is very close to the analytical prediction, and the post-peak oscillations are absent.

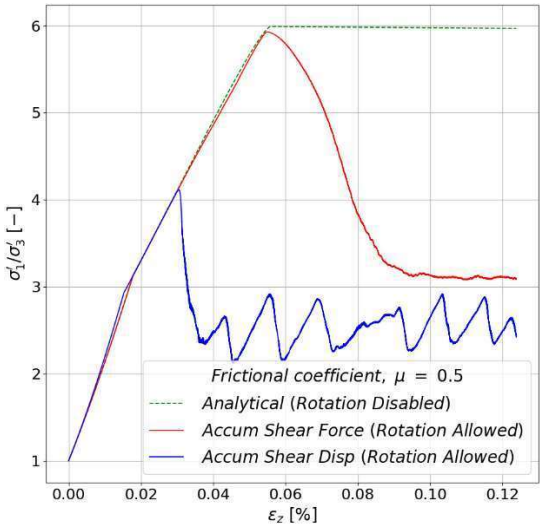


Figure 1: Stress ratio vs vertical axial strain (ε_z) for drained triaxial compression (σ'_3 and σ'_1 are minor and major principal effective stresses)

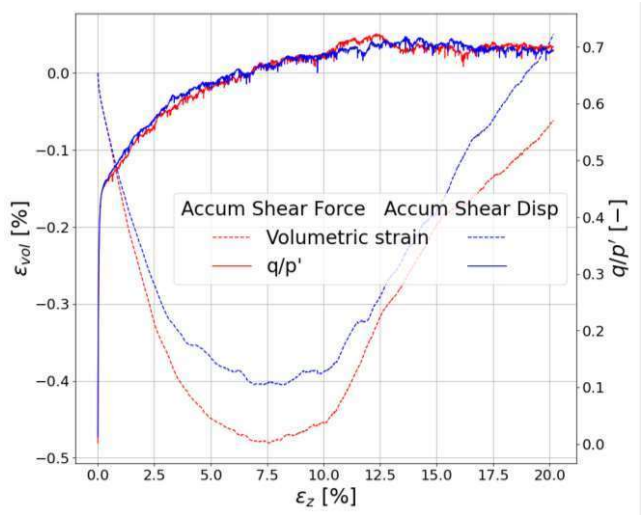


Figure 2: Volumetric strain (ε_{vol}) and q/p' vs ε_z for drained triaxial compression of polydisperse spheres (q is deviator stress and p' is mean effective stress)

For the drained triaxial compression of a polydisperse sample, the plot of volumetric strain against axial strain differs between the two approaches (see Fig. 2), despite limited differences being observed in the mobilized stresses.

In a mathematical analysis of the two approaches (not detailed here), we found that, when the integral approach is used, the calculated tangential force depends only on the normal overlap at the current timestep, with the full history of the interaction not being considered. However, this error is overcome when the incremental approach is adopted.

Future work

Ongoing supplemental work is investigating the undrained triaxial compression of a polydisperse sample and the impact of the two implementations on particles in a rotating drum.

References

[1] O'Sullivan, C., Bray, J.D., (2003). *Modified shear spring formulation for discontinuous deformation analysis of particulate media*. ASCE J. Eng. Mech, 129(7), pp. 803-834.

[2] Thompson, A. P. et al, (2022) *LAMMPS - a flexible simulation tool for particle-based materials modeling at the atomic, meso, and continuum scales.* Comp Phys Comm, 271, pp. 10817.

[3] Weinhart, T. et al., (2020). *Fast, flexible particle simulations — An introduction to MercuryDPM*. Comp Phy Comm, 249, pp. 107129.

[4] Itasca Consulting Group, Inc. (2021) *PFC — Particle Flow Code, Ver. 7.0*.

[5] Šmilauer, V. et al., (2021). *Yade Documentation 3rd ed*. The Yade Project.

[6] Thornton, C., Cummins, S.J. and Cleary, P.W., (2011). *An investigation of the comparative behaviour of alternative contact force models during elastic collisions*. Powder Technology, Volume 210(3), pp. 189–197.

[7] Thornton, C., (1979). *The conditions for failure of a face-centered cubic array of uniform rigid spheres*. Geotechnique, 29(4), pp. 441–45.

Implicit sub-stepping scheme for critical state soil models

Hoang-Giang Bui*[1] and Jelena Ninic[1]
[1] Department of Engineering, Durham University, United Kingdom
(E-mail: hoang-giang.bui@durham.ac.uk, jelena.ninic@durham.ac.uk)

Abstract

In this work, the sub-stepping scheme for critical state models is developed, taking into account the relation of void ratio with hydrostatic stress and preconsolidation. The sub-stepping scheme is shown to be robust and improve the convergence of the local nonlinear system. By deriving the consistent tangent operator for this scheme, the global Newton-Raphson iteration achieves quadratic convergence, thereby enhancing both the accuracy and robustness of the analysis. This formulation is highly efficient and can be used with problem involving arbitrary large load step, such as tunnel simulation.

Introduction

In the previous work [1], the implicit sub-stepping strategy is developed for the critical state models [2], namely the Modified Cam-Clay (MCC) [3] and Clay and Sand (CASM) [4]. This approach is highly efficient to overcome large and unpredictable load step, in particular the one stemming from stress relaxation analysis, e.g., excavation problem. For robustness, the void ratio is updated explicitly at the end of the load step [5,6]. Nevertheless, this strategy effectively invalidates the converged yield surface, leading to artificial stress development if a zero load increment is imposed. For long analysis, the accumulated error will lead to erroneous results and degrade the convergence. To remedy this drawback, the void ratio can be considered as local primal variable and solved together with the stresses and preconsolidation pressure.

Methodology

The local system adopting the nonlinear prediction of the trial stress, which has to be solved in each sub-step [1,6], reads

$$h_1 = p - p_n \exp\left(\frac{1+e}{\kappa}\Delta\varepsilon_v^e\right) = 0, \quad (1)$$

$$h_2 = q - \sqrt{\frac{3}{2}}\|\mathbf{s}_n + 2\bar{\mu}\Delta\boldsymbol{\varepsilon}_d^e\| = 0, \quad (2)$$

$$h_3 = p_c - (p_c)_n \exp(\theta\Delta\epsilon_v^p) = 0, \quad (3)$$

$$h_4 = f(p, q, p_c) = 0. \quad (4)$$

The void ratio is related to the hydrostatic pressure and preconsolidation, such as

$$e = e_0 - \lambda \log p_c - \kappa \log \frac{p}{p_c} \quad (5)$$

Following that, the local system (1)-(4) is enriched with (5) by additional residual equation

$$h_5 = e - e_0 + (\lambda - \kappa)\log p_c + \kappa \log p = 0$$

This constitutes the set of local variables $\{p, q, p_c, \Delta\phi, e\}$ to be solved by the Newton-Raphson iteration. The additional gradients necessary for the incremental update of the local variables reads

$$h_{1,5} = -\frac{p_n}{\kappa}\Delta\varepsilon_v^e \exp\left[\frac{1+e}{\kappa}\Delta\varepsilon_v^e\right],$$

$$h_{2,5} = h_{3,5} = h_{4,5} = 0,$$

$$h_{5,1} = \frac{\kappa}{p}, h_{5,2} = 0,$$

$$h_{5,3} = \frac{\lambda - \kappa}{p_c},$$

$$h_{5,4} = 0, h_{5,5} = 1.$$

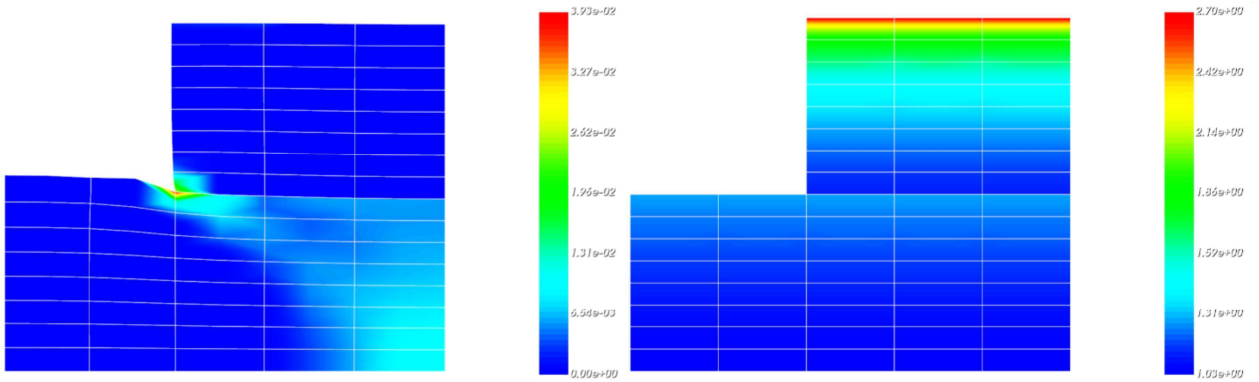


Figure 1: Simulation of soil block excavation: deformed mesh and plastic strain (Left) and void ratio distribution (Right).

Results

To verify the implementation of the modified implicit sub-stepping algorithm, the excavation simulation of a soil block with dimension 5×4 m is performed. The MCC parameters are taken as $\lambda = 0.37, \kappa = 0.054, M = 1.4, \nu = 0.35$ and $e_0 = 2.52$. The soil block is excavated in one lift (excavation domain is removed at once). The deformed mesh and corresponding void ratio distribution are visualised in Figure 1.

Conclusion

The implementation of the modified implicit sub-stepping algorithm exhibits the quadratic convergence behaviour. In the benchmark test case, the convergence is achieved with simulation involving relatively large bulk of material removal. In the future work, the MCC and CASM constitutive laws are coupled with a 3-phase element to perform simulation on partially saturated media, which takes into account the void ratio as the porosity measure. To improve the efficiency, the automatic sub-stepping shall be enabled to reduce the number of sub-steps.

Acknowledgements

The first author received funding from the Marie Curie project TwinSSI (UKRI - Project reference: EP/Z001072/1). The support is gratefully acknowledged.

References

[1] Bui, H.-G.; Ninic, J.; Meschke, G. *Implicit sub-stepping scheme for critical state soil models*. Engineering with Computers, Springer London, v. 42, n. 2, p. 76, 2026. ISSN 1435-5663.

[2] A. Gens; D.M. Potts. *Critical state models in computational geomechanics*. Engineering Computations, v. 5, n. 3, p. 178–197, 1988. ISSN 0264-4401.

[3] Roscoe, K. H.; Burland, J. B. *On the Generalized Stress-Strain Behaviour of Wet Clay*. In: Engineering Plasticity. [S.l.]: Cambridge University Press, 1968. p. 535–609.

[4] Yu, H. S. CASM: *A unified state parameter model for clay and sand*. International Journal for Numerical and Analytical Methods in Geomechanics, v. 22, n. 8, p. 621–653, 1998. ISSN 1096-9853.

[5] Borja, R. I.; Lee, S. R. *Cam-Clay plasticity, Part 1: Implicit integration of elasto-plastic constitutive relations*. Computer Methods in Applied Mechanics and Engineering, v. 78, n. 1, p. 49–72, 1990. ISSN 0045-7825.

[6] Borja, R. I. *Cam-Clay plasticity, Part II: Implicit integration of constitutive equation based on a non-linear elastic stress predictor*. Computer Methods in Applied Mechanics and Engineering, v. 88, n. 2, p. 225–240,1991. ISSN 0045-7825.

Salinity effects on the behaviour of swelling clays: A double-structure approach to Chemo-Hydro-Mechanical (CHM) coupling

Han Ming Lai*[1], Lidija Zdravkovic[2], David M. Potts[3] and Matthew Kirby[4]
[1,2,3] Department of Civil and Environmental Engineering, Imperial College London, London, United Kingdom.
(E-mail: h.lai23@imperial.ac.uk, l.zdravkovic@imperial.ac.uk , d.potts@imperial.ac.uk)
[4] Nuclear Waste Services, United Kingdom
(E-mail: matthew.kirby@nuclearwasteservices.uk)

Abstract

Compacted bentonite is widely proposed as an engineered barrier material in Geological Disposal Facilities (GDFs) for radioactive waste. However, potential exposure to saline groundwater may significantly alter its hydro-mechanical performance. This study develops a chemo-hydro-mechanical (CHM) constitutive framework incorporating salinity effects through a double-structure formulation for expansive clays. Osmotic suction is introduced as an additional stress component acting at the microstructural level. Numerical simulations using the software ICFEP reproduce experimentally observed reductions in swelling pressure and changes in microstructural behaviour with increasing salt concentration. The framework demonstrates promising capability for predicting bentonite performance under saline environments relevant to UK GDF construction.

Introduction

The expansion of the UK nuclear energy programme has intensified the need for safe long-term disposal of radioactive waste. Geological Disposal Facilities (GDFs) provide a permanent solution by isolating waste underground using multi-barrier systems. Compacted bentonite plays a critical role as an engineered barrier due to its low permeability, high swelling capacity, and self-sealing properties.

Potential UK GDF sites located near coastal regions may encounter groundwater salinity approaching 320 g/L total dissolved solids (TDS). Elevated salinity alters physico-chemical processes of bentonite at the microstructural level, by reducing diffuse double layer (DDL) thickness and interlayer hydration, leading to decreased swelling pressure and increased permeability, which may compromise barrier performance.

Experimental studies [1] have demonstrated a double-porosity structure of swelling clays, comprising macrostructural pores between clay aggregates and microstructural pores associated with clay interlayers. Double-structure constitutive models provide a physically motivated framework to represent such behaviour. This work extends an existing double-structure constitutive framework by incorporating chemical effects through osmotic suction, contributing toward a coupled hydro–mechanical–chemical model capable of predicting bentonite behaviour under saline conditions.

Methodology

Numerical analyses were conducted using the finite element (FE) code ICFEP [2]. Bentonite behaviour was simulated with the ICDSM [3] constitutive model. The microstructure is assumed to be fully saturated, elastic, and volumetric. The model characterises the microstructure via three microstructure parameters: compressibility coefficient, κ_m , void factor, VF, and interaction function, f_β.

The proposed extension of the ICDSM formulation for chemical coupling considers chemical effects through modification of the microstructural effective stress. Osmotic suction is evaluated as a function of salt concentration using the van't Hoff's Equation (1), which is subsequently converted into osmotic pressure, Equation (2)., and introduced as an additional stress component, Equation (3).

$$\pi = ic_d RT\phi \quad (1)$$

$$p_\pi = \alpha \cdot \pi \quad (2)$$

$$p' = p + s_{eq} + p_\pi \quad (3)$$

Results

Preliminary validation of the model was done by simulating the FEBEX constant volume swelling test [4]. The FE results demonstrate ability to predict the measured trend of swelling pressure reduction with increasing NaCl concentration (Figure 1). Higher salinity increases osmotic suction, generating compressive osmotic stress that suppresses clay expansion. Slight overestimation of measure swelling pressures informs further refinement in model calibration.

Microstructural analysis shows that increasing salinity, or osmotic suction, reduces the void factor (VF) (Figure 2). As VF describes the proportion of microstructure in the clay fabric, its decrease indicates decreased interlayer hydration and suppressed micro-swelling. This is consistent with physico-chemical mechanisms whereby elevated ionic concentration compresses DDL and limits interlayer water uptake, reinforcing the selected representation of chemical effects with an additional stress component in a double-structure framework.

Future work

Future developments will focus on refining the dependence of microstructural parameters on salinity to improve predictive robustness of the model. Integrating this with hydro-chemical permeability formulation will allow simultaneous modelling of salinity dependent permeability. Ultimate objective is to develop a fully coupled THM-C framework capable of supporting long-term GDF assessment.

Acknowledgements

This research receives funding from the Nuclear Waste Services UK and the Imperial College Skempton Scholarship.

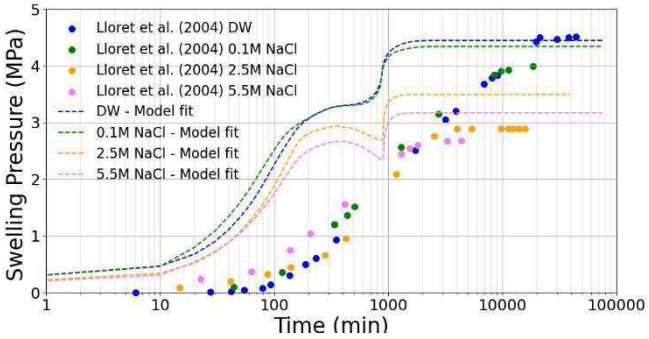


Figure 1: Measured and predicted FEBEX bentonite swelling pressures

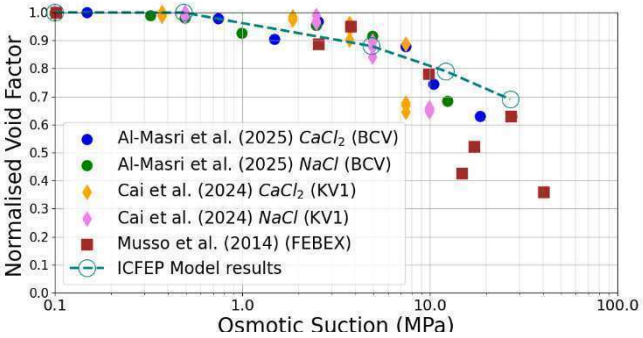


Figure 2: Normalised VF at saturation as a function of osmotic suction (salinity).

References

[1] Lloret, A. and Villar, M.V., 2007. Advances on the knowledge of the thermo-hydro-mechanical behaviour of heavily compacted "FEBEX" bentonite. Physics and Chemistry of the Earth, Parts A/B/C, 32(8-14), pp.701-715.

[2] Potts, D. M. and Zdravkovic, L., 1999. Finite element analysis in geotechnical engineering: theory. Thomas Telford Publishing, London.

[3] Ghiadistri, G.M., 2019. Constitutive modelling of compacted clays for applications in nuclear waste disposal. PhD Thesis, Imperial College London, UK.

[4] Lloret, A., Romero, E., and Villar, M. V. (2004). FEBEX II Project Final report on thermo-hydro-mechanical laboratory tests.

Automated calibration of coarse-grained DEM models for large displacement simulations.

Alister Tottle*[1], Liang Cui[2] and Juan Sagaseta[3]
[1, 2, 3] School of Engineering, University of Surrey, England
(E-mail: at01178@surrey.ac.uk)

Abstract

Sinkholes are a globally occurring geohazard caused by subsurface void collapse. The estimation of sinkhole formation probability is commonly carried out using hazard mapping techniques [1], however linking a given sinkhole hazard to structural vulnerability is underexplored. Therefore sinkhole-foundation interaction will be investigated using the discrete element method (DEM). A key challenge with this approach is producing calibrated DEM models with appropriate micro-mechanical properties. This is addressed through the development and implementation of an automated evolutionary strategy for macro to micro scale material calibration which enables the realistic replication and study of sinkhole structure interaction case-studies.

Introduction

The discrete element method is well suited to large displacement problems and has successfully been applied to sinkhole and other large displacement problems in the past [2]. However, for engineering scale simulations computational limitations necessitate that each DEM particle represents hundreds to thousands of real particles. This eliminates the possibility of direct measurement of particle-scale (micro-scale) material parameters. Therefore, it is necessary to select a micro-scale parameter set that results in macroscopic behaviour that replicates the behaviour measured through ground investigations.

Due to the relatively high cost of each parameter set evaluation and the dimensionality of the problem, simplified approaches to parameter searching, such as grid search, become prohibitively expensive. Alternatively surrogate models, such as Bayesian Optimisers, could be used to sample potential parameter combinations however this approach requires selection of a prior function which is challenging without first gaining prior understanding of the parameter space [3]. Therefore, a gradient free optimiser, the Covariance Matrix Adaptation Evolutionary Strategy (CMA-ES) algorithm [4], is adopted due to its lack of prior assumptions, robustness to noise, effective avoidance of local minima, and its efficient searching strategy [5].

Methodology

Selection of an appropriate calibration target is vital for producing a meaningfully calibrated material [3]. As the objective of this work is to replicate sinkhole ground conditions based on available data the initial stiffness and angle of friction are chosen as calibration targets. In the model both parameters are measured using three displacement-controlled triaxial tests cut from a larger soil model to preserve soil fabric. During testing, confining pressure is set to equal that measured prior to removal of non-test particles and this enables determination of a stiffness profile over depth.

The stiffness error for each parameter set is computed as the normalised RMSE between the target profile and the measured profile. The friction angle error is computed as the error between the measured and target angle. Both errors are then combined through a weighted addition to ensure that the CMA-ES algorithm does not bias one target over another.

In each CMA-ES generation 10 candidate parameter sets, sampled from a multivariate Gaussian distribution described by the covariance matrix, are evaluated with the 5 lowest error candidates used to adapt the covariance matrix and thereby steer the parameter choice towards an optimal solution. Over successive generations the covariances are reduced, or zoomed in, until the optimal solution is identified [3].

Results

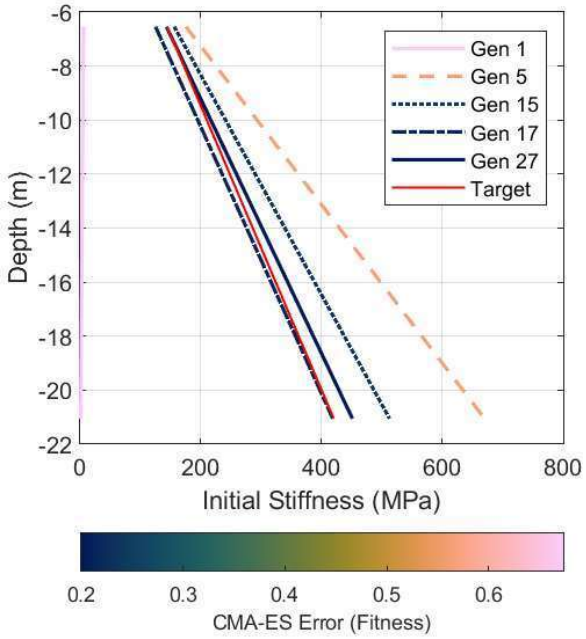


Figure 1: Best stiffness profiles from selected calibration generations with CMA-ES computed error denoted by line colour.

Initial test calibrations have been carried out against a synthetic calibration target: $\varphi = 30^{o}$ and $E_{init}(Z_{B.G.L}) = 20 + 19*Z_{B.G.L.}$ (MPa).

The micro-scale parameters controlled via the CMA-ES algorithm are: K_n (Normal Stiffness), K_s (Shear Stiffness), f_{s0} (Initial shear resistance) and m_{up} (coefficient of friction).

In this initial calibration strong agreement with the calibration target was achieved by generation 17 with marginal improvement identified by generation 27 (Figure 1). This demonstrates the feasibility of this CMA-ES framework for efficiently calibrating DEM ground models.

Future work

Initial calibration results demonstrate that the proposed methodology is a promising tool for the calibration of DEM ground models. However, further work will be required to demonstrate that the results are optimal and unique, i.e. not a local minima. This will be explored through varying the seeded "random" number generation to verify that the algorithm is able to achieve consistent calibration.

In addition, the methodology will be verified with different particle packing's, size distributions and calibration targets. Following this, breaking displacement will be incorporated as a calibration parameter, to enable the calibration of cohesive materials.

This calibration methodology will then be applied to creating a set of isotropic materials, based on ground investigation data, which can then be combined to produce a stratified ground model corresponding to investigated conditions at a sinkhole case-study: enabling its numerical investigation.

References

[1] Guerrero, J., Gutiérrez, F., Bonachea, J., Lucha, P. (2008). *A sinkhole susceptibility zonation based on paleokarst analysis along a stretch of the Madrid–Barcelona high-speed railway built over gypsum- and salt-bearing evaporites (NE Spain).* Engineering Geology 102(1-2), pp. 62-73

[2] Al-Halbouni, D., Holohan, E.P., Taheri, A., Schöpfer, M.P.J., Emam, S., Dahm, T. (2018) *Geomechanical modelling of sinkhole development using distinct elements: model verification for a single void space and application to the Dead Sea area.* Solid Earth 9(6), pp. 1341-1373

[3] Nicusan, A.L., Sykes, J.A., Seville, J., Kokalova, T., Windows-Yule, C.R.K. (2025). *ACCES: Non-Invasive Simulation Calibration via Optimisation using Evolutionary Algorithms and Metaprogramming*. Available online at: https://arxiv.org/abs/2505.02967

[4] Hansen, N. (2016). *The CMA Evolution Strategy: A Tutorial.* Available online at: https://arxiv.org/abs/1604.00772

[5] Pack, N., Machnes, S., Wilhelm, F.K. (2026). *Benchmarking Optimization Algorithms for Automated Calibration of Quantum Devices.* Available online at: https://arxiv.org/abs/2509.08555

Comparison of Mualem and Burdine Hydraulic Conductivity Models in a 1-D Unsaturated Soil Column Simulation

Q.H.X. Kong*[1], C. O'Sullivan[2], K. Tsiampousi[3], H. Wang[4]
[1, 2, 3, 4] Department of Civil and Environmental Engineering, Imperial College London, United Kingdom
(E-mail: qinghexing.kong21@ic.ac.uk, cath.osullivan@imperial.ac.uk, aikaterini.tsiampousi05@imperial.ac.uk, h.wang1@imperial.ac.uk)

Abstract

This study evaluates the influence of the expressions used to predict relative hydraulic conductivity on predictions of transient unsaturated flow by comparing the van Genuchten–Mualem (VGM) and van Genuchten–Burdine (VGB) formulations. A one-dimensional Richards-equation solver was implemented in Python to enable a controlled comparison that is not achievable in currently available software packages which typically implement only the VGM model and couple a specific pair of van Genuchten (VG) hydraulic parameters. The new implementation presented here decouples the two parameters and independently fits the tortuosity parameter so that the effect of the analytical model used to predict hydraulic conductivity can be isolated. The results show that both the expressions used to predict relative hydraulic conductivity as well as the tortuosity parameter within these expressions can significantly affect transient saturation evolution.

Introduction

Accurate prediction of relative unsaturated hydraulic conductivity (K_r) is essential to predict water transport and saturation evolution in soil. However, in most practical applications, only the van Genuchten–Mualem (VGM) expression for K_r is adopted because of its convenient closed-form structure [1, 2]. Prior research has shown that the VGM and the van Genuchten–Burdine (VGB) models can predict different responses depending on soil type, saturation range, and modelling scenario. Therefore, a systematic comparison of these two models is important. Two challenges hinder such a comparison: (1) the VGB model is rarely implemented in currently available software packages; (2) standard implementations typically enforce coupling between the VG hydraulic parameters, and this coupling relationship differs in the VGM and VGB models, inhibiting isolation of their individual effects. While the VGM model was developed from Burdine's framework [3], this historical linkage does not remove the need for an evaluation of their predictive performance.

Therefore, we developed a Python-based one-dimensional Richards-equation solver to allow full control over parameter coupling and the expression for K_r, in order to compare the use of VGM and VGB models under identical retention conditions.

Methodology

The adopted soil hydraulic parameters were obtained from UNSODA data [4]. The measured SWCC was fitted using the VG model, while measured hydraulic conductivity data were normalized by the saturated hydraulic conductivity to obtain K_r. Figure 2 compares the Mualem and Burdine $K_r - S_e$ relationships, where S_e denotes the effective saturation, and the tortuosity parameter, l, was fitted separately for each conductivity expression.

The developed Python-based solver considers vertical unsaturated flow. It can support head-controlled and flux-controlled boundaries, adaptive time stepping, and both the VGM and VGB K_r expressions. The initial and boundary conditions used here are illustrated in Figure 1. The solver was successfully benchmarked against reference numerical results obtained from PLAXIS [5] under both wetting and drying conditions (Figure 3). The column model then was used to compare VGM and VGB under identical retention parameters, geometry, and boundary conditions, the expressions for K_r

and l were varied in the sensitivity analysis.

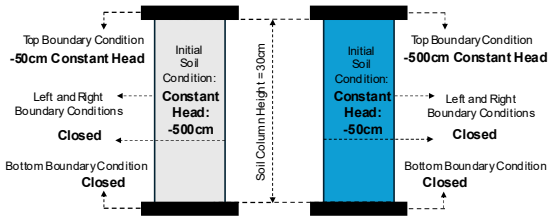


Figure 1: Column setup: Wetting Case (left) and Drying Case (right)

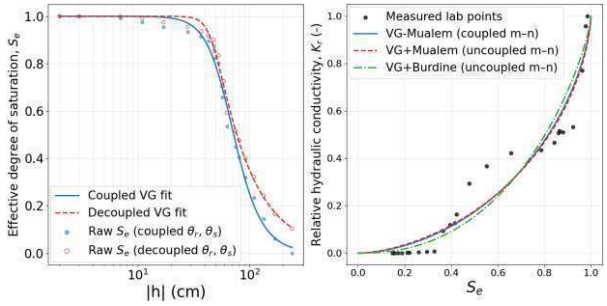


Figure 2: Fitted hydraulic functions: SWCC (left) and Relative hydraulic conductivity curve (right)

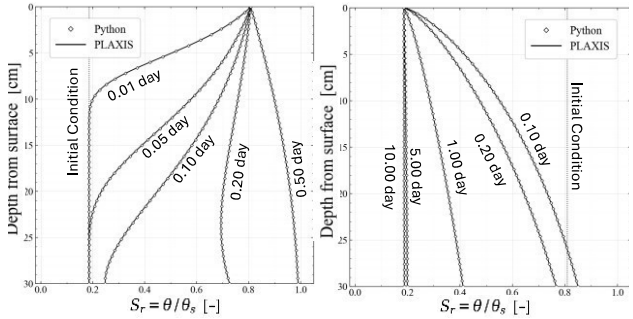


Figure 3: Model Validation: Wetting Case (left) and Drying Case (right)

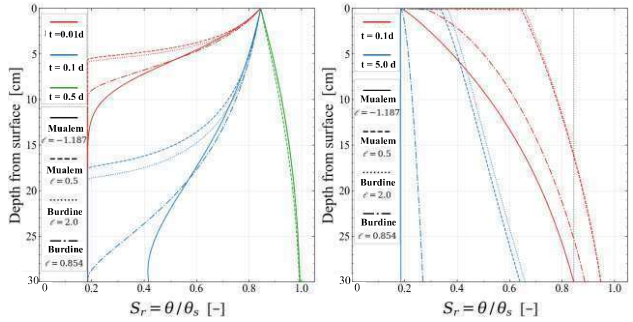


Figure 4: S_r profiles: Wetting Case (left) and Drying Case (right)

Results

The evolution of S_r was used to compare transient behavior predicted by the VGM and VGB models (Figure 4). Using the same fitted VG parameters, the VGM and VGB can produce different S_r profiles under both wetting and drying conditions. The differences are most pronounced during the transient stage, indicating that wetting and drying front propagation is strongly model-dependent. In addition, the l values can also modify the effective conductivity distribution, further affecting the temporal variation and shape of the simulated profiles. These results confirm that both the expression used to predict K_r and the choice of l significantly influence the predicted soil column response.

Future Work

Future work will extend the analysis to other configurations, including head-controlled free-drainage, flux-controlled closed-bottom, and flux-controlled free-drainage conditions, each under both wetting and drying scenarios. In addition, hysteresis will be explored through micro-scale analysis to provide a more fundamental understanding of the VGM and VGB models.

Acknowledgements

The first author gratefully acknowledges the financial support provided by the Imperial College Skempton Scholarship.

References

[1] Mualem, Y. (1976). A new model for predicting the hydraulic conductivity of unsaturated porous media. Water Resources Research, Volume 12(3), pp. 513–522.

[2] van Genuchten, M.T. (1980). A closed-form equation for predicting the hydraulic conductivity of unsaturated soils. Soil Science Society of America Journal, Volume 44(5), pp. 892–898.

[3] Burdine, N.T. (1953). Relative permeability calculations from pore-size distribution data. Transactions of the AIME, Volume 198(1), pp. 71–78.

[4] Nemes, A., Schaap, M.G., Leij, F.J., and Wösten, J.H.M. (2001). Description of the unsaturated soil hydraulic database UNSODA version 2.0. Journal of Hydrology, Volume 251(3-4), pp. 151–162.

[5] Bentley Systems. (2024). PLAXIS 2D Reference Manual. Seequent, Bentley Systems. Available online at: https://files.seequent.com/PLAXIS/Manuals/PLAXIS_2D/English/PLAXIS_2D_2_Reference%20Manual.pdf, Accessed on 23 April 2026.

An assessment of different methods for quantifying the thermal performance of thermo-active foundations

Alison Provost[1], Paul Sapin[2] and David M. G. Taborda[3]
[1,3] Department of Civil and Environmental Engineering, Imperial College London, United Kingdom
(E-mail: ali.provost21@imperial.ac.uk, d.taborda@imperial.ac.uk)
[2]Clean Energy Processes (CEP) Laboratory, Department of Chemical Engineering, Imperial College London, United Kingdom
[2]Centre for Process Systems Engineering (CPSE), Department of Chemical Engineering, Imperial College London, United Kingdom
(E-mail: p.sapin@imperial.ac.uk)

Abstract

The need to reduce carbon emissions in the built environment has led to an ever-growing focus in energy geostructures, particularly thermo-active piles, which provide both structural support and enable low-carbon heating and cooling through ground heat exchange. Traditional methods of assessing thermal performance overlook heat pump behaviour. This study compares simplified methods based on prescribed heat fluxes with a comprehensive first-law formulation that integrates the heat pump performance through explicit modelling of the heat exchanger pipework. The results of both methods are interpreted using a common model of the heat pump coefficient of performance (COP), which allows estimating the overall performance using electricity consumption. Parametric analyses show that pile length has a stronger influence on performance than diameter.

Introduction

Thermo-active foundations use embedded pipework in piles to exchange heat with the ground via electrically driven heat pumps, making system behaviour dependent on both the ground heat exchanger and heat pump operation [1]. Conventional prescribed heat flux methods treat piles as isolated conductors and overlook key operational effects such as temperature lift and electricity demand [2-4]. A new approach links fluid temperature changes directly to heat pump electricity use through the coefficient of performance (COP, [5]). This study compares these methods to assess their influence on predicted thermal performance, long term temperature field, and system efficiency.

Methodology

The conventional heat flux (HF) method represents embedded pipes as line heat sources, along which a constant linear heat rate P (W/m) is applied. Integration along the heat sources allows the estimation of the average fluid temperature, which can then be used to predict the inlet and outlet temperatures based on an assumed mass flow rate. An alternative approach, proposed and designated as the comprehensive heat pump (HP) method [5], explicitly models the fluid circuit and computes inlet/outlet temperatures. This is achieved by modelling a closed pipe circuit through which a fluid flows at constant velocity, with heat Q being transferred to one of the elements of the circuit outside the pile, mimicking the temperature jump applied by the heat pump.

For both methods, an analytical COP model can be used to estimate the electricity consumption, using:

$$COP = \sqrt{\frac{T_{\text{building}}}{T_{\text{building}} - T_{\text{outlet}}}}, \quad (1)$$

where T_{building} is the temperature required within the building (expressed in Kelvin) and T_{outlet} is the temperature of the fluid at the pile outlet (K). The annual electricity consumption can then be calculated using $E = Q \,/\, COP$, providing a direct performance indicator for the combined system comprising the pile and the heat pump.

A 3D COMSOL model simulated a 0.9 m diameter, 30 m pile embedded in a sufficiently large soil domain. HDPE pipes (26.2 mm ID)

formed a double U-loop; flow rate was 0.1 kg/s and $Q = 1.5\,kW$. Additional parametric cases considered different values of diameter (0.6 m, 0.9 m, 1.2 m), length (20 m, 30 m, 40 m), concrete cover (70mm vs 140 mm)), thermal conductivity of the pile concrete/grout (2.3 vs 0.1 W/mK), and applied power. Steady state conditions were used to assess long term behaviour.

Results

Only the effects of pile length and pile diameter are shown for brevity. Pile length (Figure 1) is seen to be the dominant geometric parameter, although the effects are generally minor: increasing length from 20 m to 40 m reduces electricity consumption for the same heat flux by $\approx 7\%$, as longer piles provide greater surface area for heat exchange. The observed trend is consistent for both HF and HP models, with $\approx 1\%$ difference between them.

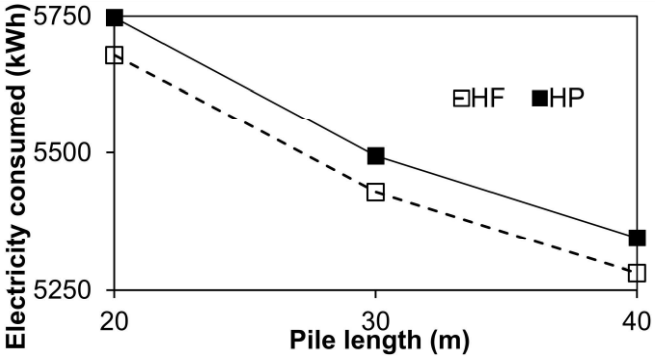


Figure 1 - Influence of pile length on electricity consumption.

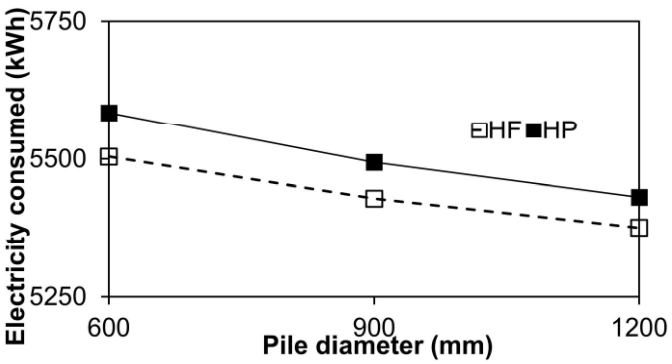


Figure 2 - Influence of pile diameter on electricity consumption.

Pile diameter (Figure 2) however, shows even smaller effects, with doubling the diameter from 0.6 m to 1.2 m (which represents doubling the concrete-soil contact area) leading only to a reduction of about 3% in electricity consumption. Similar to the previous study, the differences between HF and HP approaches are very small.

Future work

Transient analyses for long-term performance will be vital in future work. This framework can be extended to the evaluation of heat pump operational strategies to investigate seasonal ground regeneration cycles for maintaining thermal stability and mitigating capacity degradation over operational lifetimes.

Acknowledgements

This research is part of the SaFEGround project, funded by EPSRC (EP/V042149/1), while A. Provost is supported by EPSRC (EP/W524323/1).

References

[1] Brandl, H., (2006). Energy foundations and other thermo-active ground structures. Geotechnique, Volume 56 (2) pp.81–122.

[2] Eskilson, P. 1987. Thermal analysis of heat extraction boreholes. Doctoral thesis, Department of Mathematical Physics. University of Lund, Sweden.

[3] Liu R. Y. W. and Taborda, D. M. G., (2023). A simplified methodology for determining the thermal performance of thermo-active piles. Environmental Geotechnics, Volume 1 (13).

[4] Loveridge F. and Powrie, W., (2013). Temperature response functions (G-functions) for single pile heat exchangers. Energy. Volume 57, 554-564.

[5] Provost, A., Sánchez Fernández, J., Sapin, P., and Taborda, D.M.G., (2025). An approach for including heat pump performance in the design of thermo-active piles. In: International Conference on Energy Geotechnics. Paris. 17-19 Jun 2025.

Sustainability and Engineering Applications

Sustainable Reuse of Historic Masonry as Engineered Fill in the Fore Gill Bridge Rebuild

C. Walker*[1] and M.L. Walker[2]
[1, 2] The North Yorkshire Council, UK
(*E-mail: christopher.walker@northyork.gov.uk)

Abstract

The rebuild of Fore Gill Bridge in Arkengarthdale highlights the challenges which face asset owners managing aging geotechnical infrastructure amid increasing climatic and financial pressures. The partial collapse of the masonry retaining walls during Storm Gerrit in 2023 initiated the major rebuild of the structure. A circular construction approach enabled the reuse of the historic masonry to produce Class 6I fill which was incorporated into the new soil-reinforced retaining walls. This strategy reduced carbon emissions, lowered project costs through fewer vehicle movements, and demonstrated a sustainable approach to the renewal of aging infrastructure.

Introduction

Fore Gill Bridge is a prime example of the UK's aging geotechnical infrastructure, comprising of a historic masonry single span bridge and approach back-to-back retaining walls. The structure was originally constructed circa 1770 as part of the mining turnpike roads and now carries the C29 road connecting Arkengarthdale to Swaledale. Despite its age the structure still remains vital to rural communities within the Yorkshire Dales National Park.

Heavy rainfall during Storm Gerrit in December 2023 led to the partial collapse of the retaining wall approaching the bridge revealing three, previously unknown, 9m span hidden masonry arches which were unable to be inspected or maintained (Figure 1). Further deterioration of the structure also risked lengthy road closures, potentially isolating local communities. The presence of the concealed arches necessitated a full rebuild of the structure, with the solution required to maintain the original historic aesthetic.

This exemplifies the common challenges faced by asset owners due to aging asset stocks which are now further intensified by tightening budgets and rising construction costs [1, 2]. The reconstruction of Fore Gill Bridge aimed to address these challenges by incorporating the sustainable reuse of materials in the geotechnical solution.

Structure Replacement

Demolition of the existing masonry structure generated substantial quantity of stone. The selected options for the replacement structure therefore aimed to maximise the reuse of this stone and minimise the requirement for carbon intensive concrete solutions. To achieve this the 8.5m span masonry arch bridge was chosen to be reconstructed by reusing the existing arch stones, also allowing the bridge to be widened removing the pinch point in the road.



Figure 1: Retaining wall collapse December 2023

A Maccaferri MacWall Vertica soil reinforced retaining solution was selected to replace the 5m tall approach back-to-back retaining walls (Figure 2). This allowed for a circular approach by reusing the remaining stone from

the demolition as compacted fill. Furthermore, the ability of the wall system to accommodate differential settlement was also important due to challenging ground conditions at the site resulting from the presence of the Yorkshire Dales Glacial Till comprising of variable mixed soils.

Masonry Re-use

The existing structure comprised of a local quarried sandstone. To generate the Class 6I fill, excess stone was fed through an onsite Compac 700 Agri crusher, powered by an idling tractor. The resulting aggregate diameter was calibrated onsite and a series of laboratory tests were conducted to ensure compliance with Series 600 of the MCHW. The results for one of the particle size distribution tests and corresponding limits for 6I fill are shown in Figure 3. It demonstrates that the crushed material fell within the required limits for use as fill for a soil reinforced earth wall. A suite of chemical tests, shear box and Proctor compaction tests were also conducted to allow for quality control and compliance. Using this method a total of 1,500 tonnes of fill material was generated onsite in only 5 days and incorporated into the retaining structure.



Figure 2: Replacement structure comprising of traditional masonry arch and soil reinforced retaining walls

The processing of fill onsite significantly reduced vehicle movements when compared with importing equivalent aggregate, resulting in a saving of 250 tCO_2e. Furthermore, an additional 820 tonnes of masonry was reused in the new masonry bridge and facing to the retaining walls, delivering a carbon saving of approximately 140 tCO_2e compared with sourcing and importing like-for-like new materials. This circular approach to construction also brought financial benefits saving in excess of £500,000 while completely eliminating waste from the demolition of the original structure and maintaining its original aesthetic.

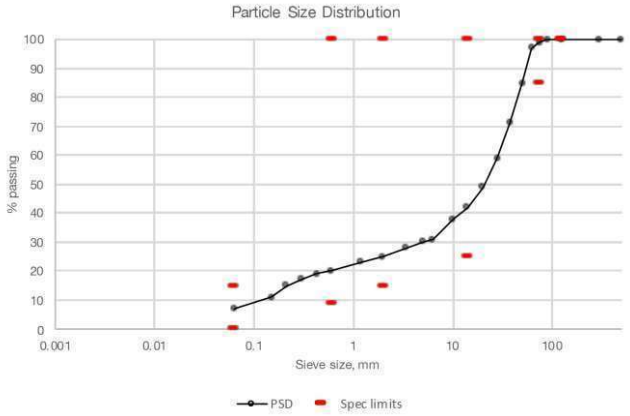


Figure 3: PSD of the crushed masonry for 6I fill

Conclusions

The circular approach to construction of the soil reinforced retaining walls demonstrates the potential for reuse of existing materials in the renewal of aging masonry infrastructure. It demonstrates that a circular approach can deliver both benefits for sustainability by reducing vehicle movements and reducing project costs by importing less new materials while maintaining the aesthetics of historic structures.

References

[1] National Engineering Policy Center (2025). *Reviving our ageing infrastructure*. Available online at: https://nepc.raeng.org.uk/media/r43jxf4l/nepc-reviving-ageing-infrastructure-final-report.pdf

[2] Walker, C., Heitor, A. and Clarke, B., (2022). *Influence of weather-driven processes on the performance of UK transport infrastructure with reference to historic geostructures*. Applied Sciences, Volume *12*(15), pp.7461 (Journal articles)

Short-term structural response of a model shaft liner during shaft breakout in clay

M. Ucur*[1], S. Divall[2] and S.E. Stallebrass[3]
[1, 2, 3] Department of Engineering, City St George's, University of London, United Kingdom,
(Email: Mayda.ucur@citystgeorges.ac.uk, sam.divall@city.ac.uk, s.e.stallebrass@city.ac.uk)

Abstract

Underground networks (i.e., tunnels and shafts) are connected by short drives known as junctions. The construction of a lateral opening at a junction is referred to as a shaft breakout. The design of a shaft breakout can be complex, often resulting in the adoption of conservative design practices. The application of reinforcement around the opening is common practice to ensure that the additional loading can be safely resisted. This paper presents results obtained from geotechnical centrifuge modelling of a simulated shaft breakout. The model shaft consists of an aluminium tube with a diameter of 101.6 mm and a depth of 254.0 mm, founded in a sample of overconsolidated Speswhite kaolin clay.

1. Introduction

Current design approaches (ICE, 1996), for the temporary support required during the construction of an opening in an existing shaft, state that there is limited understanding of the response of the shaft lining during construction of the opening. At present, theoretical solutions giving the distribution of stress around an opening in an infinite elastic plane stress plate (e.g. Spyridis, 2015) are often used in practice. In addition, finite element modelling (FEM) may be undertaken, however, even complex 3D models are unable to capture the soil-structure interaction that is critical to this scenario (Jayasiri *et al.*, 2022). Using physical modelling it is possible to create an opening in a shaft in clay whilst measuring the changes of stress in the shaft lining as the soil deforms into the shaft. This extended abstract outlines the methodology and results obtained from these tests.

2. Methodology

The geotechnical centrifuge testing has been undertaken at City St George's, University of London using the Acutronic 661 geotechnical centrifuge. This is a 40 *g*-tonne machine capable of accelerating 200 kg to 200 times Earth's gravity using a 1.8 m radius arm. The typical package used on the centrifuge has a depth of 300 mm, which when tested at 100*g* would be equivalent to 30 m of soil at prototype scale. This allowed a shaft of depth 254 mm to be inserted which according to Le *et al.* (2019) ensures that ground movements below the shaft are not affected by the base of the soil container.

2.1 Model Shaft liner

The model shaft liner (Figure 1) comprised an aluminium tube with a diameter of 101.6 mm and a wall thickness of 1.6 mm. The model liner represents a prototype continuous concrete liner with a diameter of 10 m and a depth of 25 m, having a Young's modulus of 30 GPa. The base of the model shaft liner was sealed with a brass plate and an O-ring.

2.2 Shaft breakout support mechanism

The support mechanism comprised of a double acting pneumatic actuator with a C-shaped lever supporting a curved plug. The lever arm allows the plug to collapse inwards when released. The actuator was fixed on to a U-shape channel fitted across the top of the soil container. The fixed location ensured the mechanism was centred.

2.3 Opening Dimension

Two sizes of openings have been modelled; 34 mm diameter, which is 1/3 of the shaft diameter and commonly used in practice,

and 44 mm diameter.

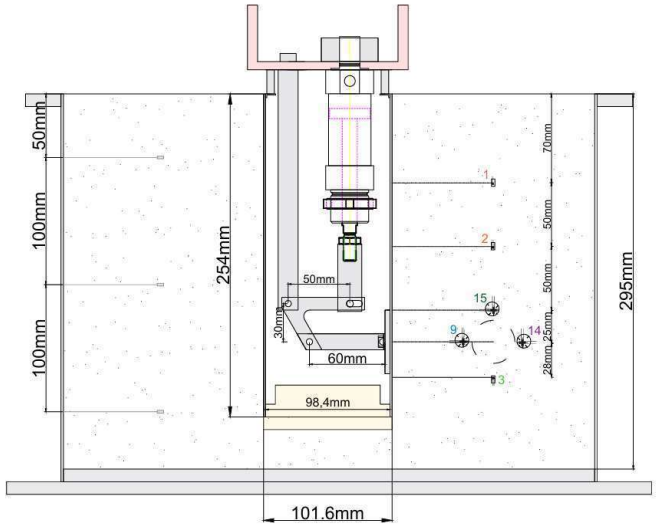


Figure 1: Cross-section of model showing the locations of the strain gauges around the opening.

2.4 Model Sample Preparation

The model shaft lining (Figure 1) was embedded in a bed of Speswhite kaolin clay. The sample was prepared in soil container with an internal diameter of 420 mm, and an internal depth of 295 mm. The soil bed was prepared from a slurry which was subjected to a vertical stress of 275 kPa applied over 9 days. 24 hours before testing, the soil sample was swelled to 175 kPa. This stress history typically results in an undrained strength at the midpoint of the opening of approximately 31 kPa following consolidation on the swing.

3. Testing

The model was accelerated to 100*g* and remained in-flight for 48 hours for the pore-water pressures to come into equilibrium. Once this was achieved, the plug was released simulating the shaft breakout. 30 minutes of consolidation time was allowed post breakout.

4. Results

Figure 2 shows an example of the variation in vertical strain with time measured by the strain gauges identified in Figure 1 during a breakout event. The greatest change in strain during the test was located at the spring lines. These changes in strain were equivalent to changes in stress of approximately 2,200 kPa and 2,800 kPa, respectively. This is approximately three times the stress predicted by the Kirsch hole in plate theory for this size of opening which was 44 mm in diameter.

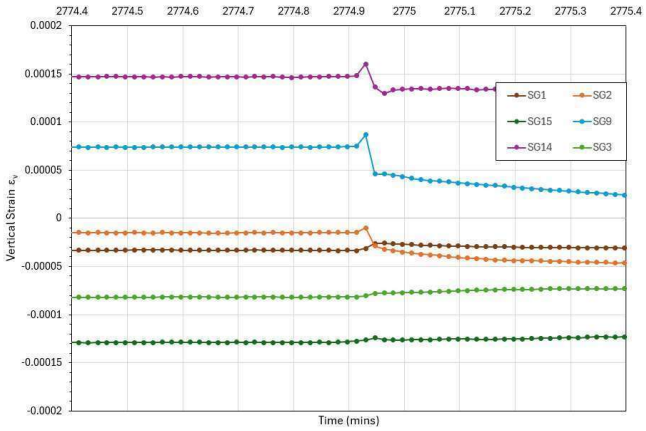


Figure 2: Vertical Strain with time. (Opening diameter 44 mm, with water table 10mm below surface.)

6. Acknowledgements

The authors are grateful for the support provided by COWI, Joseph Gallagher Ltd and the School of Science & Technology at City St George's, University of London.

7. References

[1] ICE, 1996. PRACTICE GUIDES: Sprayed concrete linings (NATM) for tunnels in soft ground. Institution of Civil Engineers, London.

[2] Jayasiri, N.S., Chao, K.C., Phien-Wej, N., Duangsano, O. & Asanprakit, A., 2022. Design and analysis of tunnel cross-passage openings: 3D finite element analysis versus 3D shell-spring approach. Innovative Infrastructure Solutions, 7(3), p.204.

[3] Spyridis, P. & Bergmeister, K., 2015. Analysis of lateral openings in tunnel linings. Tunnelling and Underground Space Technology, 50, pp.376-395.

[4] Le, B.T., Goodey, R.J. & Divall, S., 2019. Subsurface ground movements due to circular shaft construction. Soils and Foundations, 59(5), pp.1160-1171.

Reducing Tunnel Volume Loss Using Data Processing Techniques

R. limbu*[1], S. Divall[2] and S.E. Stallebrass[3]
[1, 2, 3] Department of Engineering, City St George's, University of London, UK
(E-Mail: Reshuni.Limbu@citystgeorges.ac.uk, Sam.Divall@city.ac.uk, S.E.Stallebrass@city.ac.uk)

Abstract

The development of Tunnel Boring Machines (TBMs) has improved the efficiency of tunnelling; however, uncertainty in ground response complicates the anticipation of potential risks. Therefore, an accurate prediction of ground movements also known as settlement is essential for effective mitigation before and during construction. Conventional prediction methods are often constrained by site specificity, computational demands, and simplified geological representation, which has driven the adoption of Machine Learning (ML) approaches. This study analyses monitoring data from the HS2 Project to investigate the relationship between surface settlement and TBM parameters to identify the key variables, forming a preliminary step towards a Machine Learning-based predictive framework.

Introduction

The mechanisation of tunnelling has facilitated the development of underground space for various functions including transportation. However, during the state-of-the-art report by [1] it was highlighted that the inevitable change in the stress state of soil during excavation induces settlement that may damage the surrounding infrastructures and, therefore, a reliable method of prediction is important for tunnel design.

There are multiple methods of prediction such as, Empirical [2], Analytical [3], Numerical [4] and Machine Learning (ML) methods. ML techniques have gained increasing attention for their ability to model complex non-linear relationships and generate accurate predictions, but their performance is limited by data scarcity [5].

This study used real time monitoring data from the HS2 Project to begin development of a data-driven model by analysing the relationship between TBM parameters and surface settlement. The preliminary findings from the analysis of separate and integrated datasets are presented in this paper.

Methodology

The study adopts a five-stage methodological framework comprising data collection, exploration, preparation, modelling, and evaluation. This paper focuses on the first two stages, with the results of the preliminary data analysis.

Data were collected using MissionOS and Tunnel Process Control (TPC). These platforms are remotely accessible data storage systems that record and monitor surface settlement and TBM operational parameters, respectively. Settlement data were obtained from MissionOS, while TBM parameter data were sourced from TPC. After downloading the raw data, data preparation and exploration were carried out. Data visualisation involved examining the relationship between two parameters, one from each dataset, by generating XY scatter plots. This formed the basis for analysing the link between surface settlement and TBM operations.

Results

1. The development of transverse settlement trough (*Figure 1)* follows the Gaussian curve consistent with observations reported by [6] at the Hyde Park site.

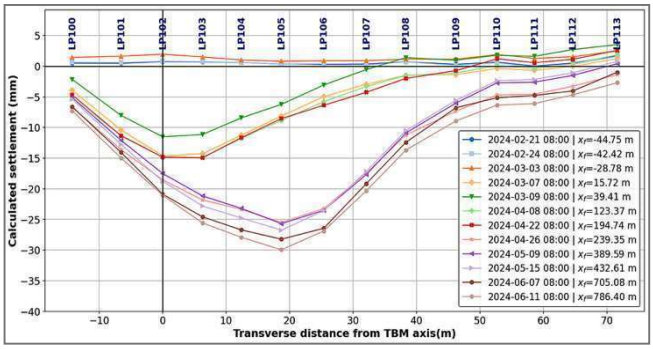


Figure 1: Development of transverse settlement during passage of TBM

2. *Figure 2* suggests a strong relationship between Face support pressure and chainage indicating that higher support pressure was required as the TBM advanced along the axis, reflecting changes in stiffness of soil and overburden.

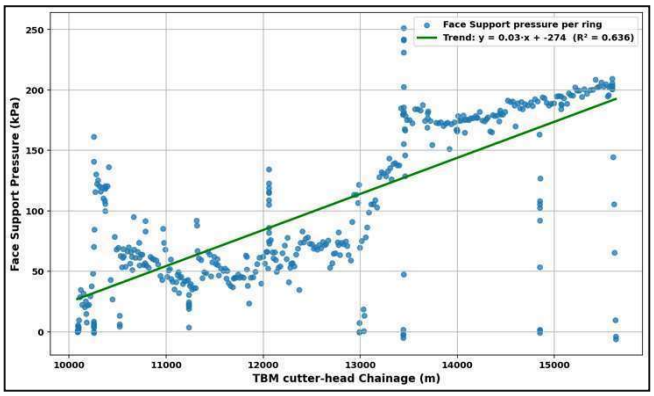


Figure 2: Variation of Face Support Pressure with TBM chainage (per ring)

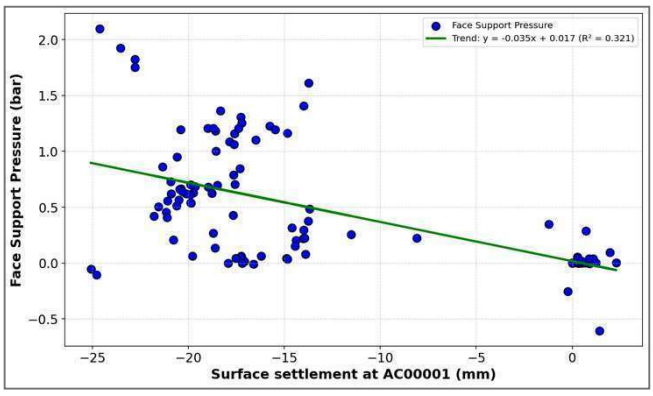


Figure 3: Correlation between Face Support Pressure and Surface Settlement

3. *Figure 3* shows a negative correlation between settlement and Face support pressure, where lower pressures associate with greater settlements. The dispersed points suggest that this parameter solely is not responsible for the settlement, suggesting contribution of other factors.

Future work

The results indicate that multivariate analysis will need to be conducted to capture the combined influence of multiple variables. Further work will include incorporating this development into a predictive ML model and evaluating its performance.

References

[1] Mair, R. J., & Taylor, R. N. (1997). *Bored tunnelling in the urban environments.* In Fourteenth International Conference on Soil Mechanics and Foundation Engineering. Proceedings International Society for Soil Mechanics and Foundation Engineering (Vol. 4).

[2] Peck, B. B. (1969). *Deep excavation and tunnelling in soft ground, State of the art volume.* In *7th ICSMFE* (Vol. 4), pp. 225-290.

[3] Loganathan, N., & Poulos, H. G. (1998). *Analytical prediction for tunnelling-induced ground movements in clays.* Journal of Geotechnical and geoenvironmental engineering, 124(9), pp. 846-856.

[4] Potts, D. M., & Vaughan, P. R. (2003). *Numerical analysis: a virtual dream or practical reality?* Géotechnique, 53(6), pp. 535-573.

[5] Niu, G., He, X., Xu, H., & Dai, S. (2024). *Tunnelling-induced ground surface settlement: A comprehensive review with particular attention to artificial intelligence technologies.* Natural Hazards Research, 4(1), pp. 148-168.

[6] Wan, M. S. P., Standing, J. R., Potts, D. M., & Burland, J. B. (2017a). *Measured short-term ground surface response to EPBM tunnelling in London Clay.* Géotechnique, 67(5), pp. 420-445.